# Simulation of 4-dimensional tumor motion and the assessment of the interplay effect in pencil beam scanning proton beam therapy

**R.B. (Ruben) van den Broek**

A clinical evaluation study as part of the graduation thesis for the Master's degree of Technical Medicine

August 2023

**Supervisors:**
**Jérémy Schiphof-Godart, PhD. Clinical physicist, HollandPTC**
**Kees Spruijt. Clinical physicist, HollandPTC**
**Michiel Kroesen, MD PhD. Radiation oncologist, HollandPTC and Erasmus MC**


HollandPTC, Delft, the Netherlands
TU Delft, Delft, the Netherlands

# Preface

This thesis is focused on investigating the interplay effect in proton therapy pencil beam scanning. The interplay effect is an inherent result of moving tumors and can have negative dosimetric effects on dose distribution and, because of that, on treatment quality. The primary goal of this thesis and internship is to evaluate the extent of the interplay effect in a group of eighteen patients.

In the first months of this thesis, my focus was on making the tumor motion simulations more elaborate by incorporating methods such as deformable registration and tracking the center of mass of the tumor. Unfortunately, none of the attempts resulted in useful and representative tumor motion. This was the first major setback, resulting in months of work and progress being moved from the Methods Section to the Appendix.

The simulations of the interplay robustness were performed using a derivative of a pre-existing and clinically validated interplay simulations script. Unfortunately, due to my own negligence, I failed to perform validation of this derivative script to make sure its results were to be relied on. This led to results that have no resemblance to clinical reality, so they are essentially obsolete. Unfortunately enough, this discovery was only made one week before my thesis deadline. I decided it would not be possible to repeat all simulations using a validated script and to analyze, interpret, and discuss the new results.

Ik wil graag als eerste Kees, Jérémy en Michiel bedanken. Ik heb erg veel van jullie alle drie geleerd, zowel op medisch en wetenschappelijk gebied als op persoonlijk en professioneel vlak. Er waren regelmatig momenten dat ik erg vastzat en niet meer wist waar ik naartoe moest met dit project. Elke keer als we een voortgangsgesprek hadden, kreeg ik weer nieuwe moed. Dankzij jullie rust en nuancering zakte de moed me niet in de schoenen toen alle methodes om beweging te simuleren niet lukten en toen bleek dat mijn resultaten onbruikbaar waren.

Daarnaast ben ik ook dankbaar dat ik in zo'n mooi instituut heb mogen werken als het Holland PTC. Tijdens de opleiding klonk het al als een magische plek. Het klinkt als keiharde science fiction, subatomaire deeltjes versnellen tot bijna de snelheid van het licht (ja, sure) en hier vervolgens daadwerkelijk kanker mee kunnen genezen. Soms geloof ik het nog steeds niet helemaal. Het was een eer om een klein radertje te mogen zijn in zo'n fantastische organisatie.

Daarnaast was ik ook erg blij met de toegankelijkheid, vriendelijkheid en behulpzaamheid van alle werknemers van het Holland PTC. Van de artsen wil ik graag nog specifiek Rutger Bartels, Niels den Haan, Sophie Bosma en Michiel Kroesen bedanken. Ik heb van jullie allemaal veel geleerd en ben jullie erg dankbaar voor het feit dat jullie mij zo actief betrokken bij patientencontact en behandelingen, zelfs als ik er niet om vroeg.

Ook wil ik Ankie, Reinoud en Ivo heel hartelijk bedanken voor de onvoorwaardelijke steun de afgelopen tien (!) jaar. Het heeft allemaal een stuk langer geduurd dat misschien nodig en wenselijk was. Toch geloofden jullie in me.

Ik wil ook graag Stephan Kieft, RA, bedanken voor zijn hulp met het zetten van de puntjes op de i van deze scriptie.

Ik ben Odin en Iris dankbaar voor de lol die ik met ze heb gehad. Het was erg leuk om met jullie ze zeëen van een materscriptie te bevaren.

A special thanks is dedicated to dr. Yibing Wang. You were extremely helpful in patiently explaining his code and helping me with a plan when the task seemed too difficult and overwhelming for me.

En als allerlaatste en belangrijkste natuurlijk Valerie. Altijd als het goed ging was je er om het te vieren. Als het even zwaar of saai werd, was jij er. Al bijna zes jaar ben je er onvoorwaardelijk voor me, en sleep je me door de goede en slechtere periodes heen. Zonder jou was ik niet de persoon geweest die ik nu ben.

# Contents

## Abstract

**Introduction** Holland PTC (Delft, The Netherlands) is an independent outpatient clinic where ten different types of cancer are treated with Pencil Beam Scanning (PBS). Some of these cancer types are situated in the thoracic region and therefore exposed to breathing motion. The interplay between the dynamic pencil beam delivered in PBS and the target motion in the thoracic region can lead to severe dose inhomogeneities. While interplay mitigation tactics, such as repainting and using larger spot sizes, are available, they can come at a dosimetric cost. Simulating the interplay effect aids in formulating clinical protocols for managing interplay-related challenges during treatment planning, as well as assessing the robustness of treatment plans both retrospectively and prospectively.

**Goals** The primary goal is to perform clinical evaluation of the treatment beams of 18 patients' treatment plans. Clinical evaluation can be achieved using an interplay simulation script. The secondary goal is to assess which patient-specific factors affect the interplay effect in these patients.

**Methods** A derivative script, based on a clinically validated interplay simulation script, has been used to perform clinical evaluation. This derivative script allowed the input of 2-dimensional tumor motion rather than only superior-inferior (SI) tumor motion. 2-dimensional tumor motion information has been extracted from 18 lung cancer, esophagus cancer, and lymphoma patients. Quality Assurance (QA) dosimetric measurements were available of all the patients' beams, 161 in total.

The static QA dose measurements are compared to the same measurements with a two-dimensional sinusoidal motion in an in-house developed interplay simulation script. Simulations of each treatment beam consisted of a number of patient-specific fractions, with 100 treatment simulations performed for each beam. Gamma acceptance criteria are set at 2% dose difference and 2mm distance to agreement.

The last fraction where a treatment plan is below the predefined robustness threshold, known as the Last Fraction below Threshold (LFBT), is the metric on which clinical evaluation is based. If the 90th percentile LFBT was equal to or below the number of prescribed treatment fractions, a treatment beam is considered robust against the interplay effect.
Near the end of thesis completion, the discovery was made that the interplay simulation script used throughout the majority of this thesis yielded results that differed notably and clinically from those generated by the validated script. Due to the work and time needed to repeat the simulations with the correct script, and the time necessary to analyze and interpret the new results, the decision was made not to repeat the simulations for all beams with the validated script. The simulations are repeated for nine out of 161 beams to compare the outcomes of both scripts.

**Results** Using the unvalidated script,tumor-type specific interplay analysis shows interplay robustness in tumors with motion amplitude of up to 9 mm in lymphomas, 5 mm in lung cancer patients, and 6 mm in esophageal cancer patients. A high correlation (up to r=0.95) between 2D tumor motion amplitude and interplay robustness was found. The clinically validated script's results show that all nine treatment beams are robust against the interplay effect, even when the amplitude is 11.22 mm in SI direction. All the

patient beams with a tumor motion amplitude greater than 8.45 mm in SI direction are not robust according to the unvalidated script. This suggests that the unvalidated script underestimated the interplay robustness of the treatment beams.

**Implications/Conclusion** Since only 9 out of 161 beams have been simulated using this script, limited general conclusions can be drawn from this data. The results of the clinically validated script suggest all beams up to 11.22 mm tumor motion amplitude are robust against the interplay.

## Outline of this report

Chapter 1 Background of this report provides all the background information deemed necessary to understand the rest of the report. This includes general information regarding proton therapy, organ motion, and the interplay effect, and an explanation of the current interplay simulation script.
The research thesis itself is divided into four parts: A general Introduction, a chapter on methods and results of Clinical Evaluation, and a chapter discussing Factors influencing the interplay effect. Next, there is a common Discussion section.
The Appendix contains background data like patient tables and data that have been gathered during the internship but are not used directly to answer the research questions. **During the last few days of writing the thesis, we discovered that the results from the script that was used throughout the majority of the thesis were different from the clinically validated interplay simulation script.** This mistake resulted in significant differences in outcome. The result is that the majority of the results and conclusions of this thesis have become obsolete. This problem will be discussed in Chapter 5 Unvalidated script.

# Chapter 1

# Background

## 1.1 Holland PTC

Holland PTC is an independent outpatient clinic located in Delft, the Netherlands. It is a collaboration of the Technical University Delft, Erasmus Medical Center, and Leiden University Medical Center. It is actively involved in treatment, research, and education. Since 2018, patients with various types of cancer have been treated at Holland PTC, with the majority being mammae, esophagus, and eye patients. In three of these cancer types, the tumor is located in the thoracic region: esophagus cancer, lung cancer, and lymphomas.


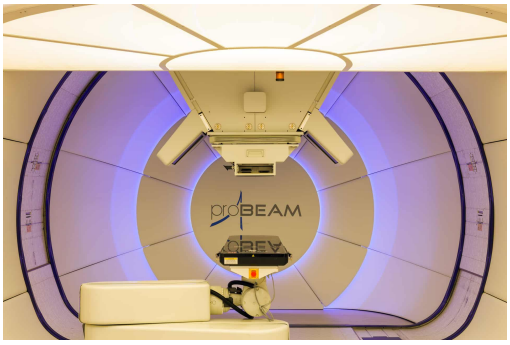


(a) **The proton beam gantry in one of the two treatment rooms of Holland PTC. The patient is positioned on the black table. The proton beam is delivered from the top structure, which can rotate 360° around the patient.**

Figure 1.1:

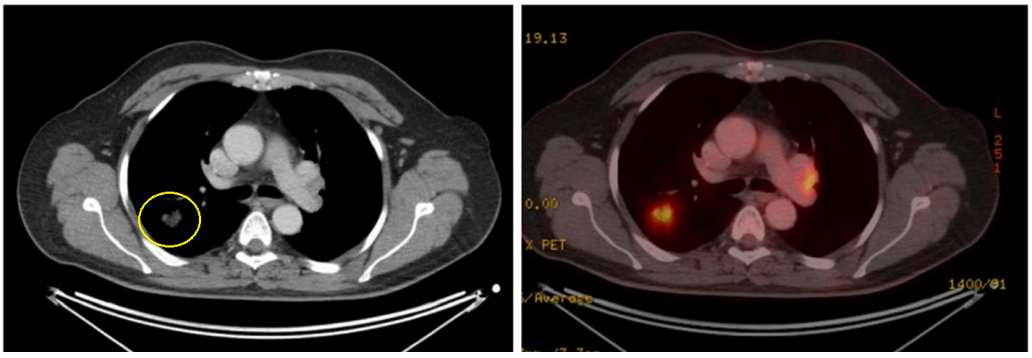


Figure 1.2: **A regular CT (left) and a PET/CT (right) of a patient with NSCLC. While the primary tumor is visible on the CT, the FDG-PET also detected contralateral affected lymph nodes.**
**Image source:** [7]

## 1.2 Lung cancer

Lung cancer is the most common type of cancer worldwide, accounting for approximately 13% of all cancer cases [1], [2]. In the Netherlands alone, 14.000 new patients are diagnosed with lung cancer each year, and both incidence and prevalence keep increasing [3]. The most important cause of lung cancer is smoking. 90% of lung cancer cases are caused by smoking. Important factors for non-smoking people with lung cancer are second-hand smoke, radon exposure, and air pollution [2], [4].

Lung cancer can be divided into multiple categories, the most common being small-cell lung carcinoma and non-small cell lung carcinoma (NSCLC). This section of the thesis specifically focuses on NSCLC since all lung cancer patients in this research have NSCLC. About 85% of newly diagnosed lung cancer cases are NSCLC, and almost all of them are regular tobacco users [1]. Half the people diagnosed with lung cancer have already reached stage IV at the moment of diagnosis [5]. Stage IV lung cancer has a 5-year survival of about 3%.

A combination of FDG-PET with diagnostic CT is the preferred method of diagnosis for patients suspected of NSCLC because it allows for more accurate staging than CT alone (figure 1.2) [5]–[7].

In patients with stage I NSCLC, a lobectomy or segmentectomy is recommended. In a lobectomy, the lung lobe containing the tumor is removed. Depending on tumor location, a segmentectomy can be performed, in which only a part of the lung lobe is removed. This section should be expanded to encompass the excision of affected lymph nodes and the consideration of adjuvant chemotherapy in cases of stage II NSCLC. Radiotherapy should be considered in stage I patients with an increased surgical risk.
For patients with stage III NSCLC, concomitant chemoradiotherapy is recommended. Patients generally receive a total dose of 60Gy in fractions of 2Gy. Locoregional radiotherapy leads to a decrease in tumor size, with a decrease in symptoms as a result [6].

For some patients, proton therapy can be beneficial as compared to photon therapy. In the Netherlands, this decision is based on the national indication protocol proton therapy (*Landelijk Indicatie Protocol Protonen Therapie longcarcinoom*) [8]. This protocol

advises a *normal tissue complication probability* model (NTCP model). NTCP models are mathematical models that estimate the probability of certain normal tissue complications occurring due to radiation therapy. The three models used in Holland PTC are radiation pneumonitis, acute dysphagia, and mortality due to cardiac toxicity. In these models, the probability of certain 'normal tissue complications' when receiving proton therapy is compared to the same probability in regular photon therapy. A certain decrease in NTCP needs to be achieved for proton therapy to be indicated. The absolute two years mortality risk needs to improve by at least 2% compared to photon therapy, or the absolute chance of grade 2 complications of either pneumonitis or dysphagia need to decrease by 10% [9].

A photon and proton plan of a lung cancer patient can be seen in figure 1.6. While the tumor coverage is almost equal, the dose in the critical tissue, such as the lungs and heart tissue, is lower in the proton plan.

## 1.3 Esophageal cancer

Squamous cell carcinoma is the most common type of esophageal cancer worldwide [10]. It originates in the squamous epithelium, most often in the upper two-thirds of the esophagus.

Adenocarcinoma is the most common type of esophageal cancer in the USA, The Netherlands, and other Western countries [10], [11].

Adenocarcinoma often develops as a result of gastroesophageal reflux disease (GERD). In GERD, acid from the stomach goes back into the esophagus after meals. This acid can lead to Barrett's esophagus, in which the squamous epithelium in the esophagus is replaced by columnar epithelium. The columnar epithelium is better adapted to resist acidity but is more likely to mutate into cancerous cells.

Important risk factors for both tumor types are smoking, age over 60 years, and gastric reflux. Risk factors for squamous cell carcinoma are alcohol, cigarette smoke, and hot fluids. Adenocarcinoma is primarily associated with significant risk factors such as chronic GERD and Barrett's esophagus, wherein Barrett's esophagus carries a substantial odds ratio of 12.0. Furthermore, being male and obesity increase the risk of adenocarcinoma. [10]

The first common symptom is difficulty swallowing or progressive dysphagia. This often starts with solid foods, but liquids can also become hard to swallow as the disease progresses. This is due to the narrowing of the esophagus as a result of the tumor's growth. Pain when swallowing (odynophagia) and heartburn often occur as well.

The primary diagnosis is made with an endoscopy and biopsy. A PET-CT is often used to evaluate if the cancer has spread to nearby lymph nodes [12].

Esophageal cancer is generally considered a cancer with a poor prognosis because its symptoms often appear only in later stages. 41% Patients in this stage only have a five years survival rate of 3%. Patients diagnosed with stage I esophageal cancer have a five years survival rate of 64% [12].

In the early stages of esophageal cancer, treatment can consist of surgically removing (a part of) the esophagus via gastroscopy [12]. Other options are endoscopic tumor resection or mucosal ablation.

For more advanced cases, neoadjuvant chemoradiotherapy is often used as treatment.

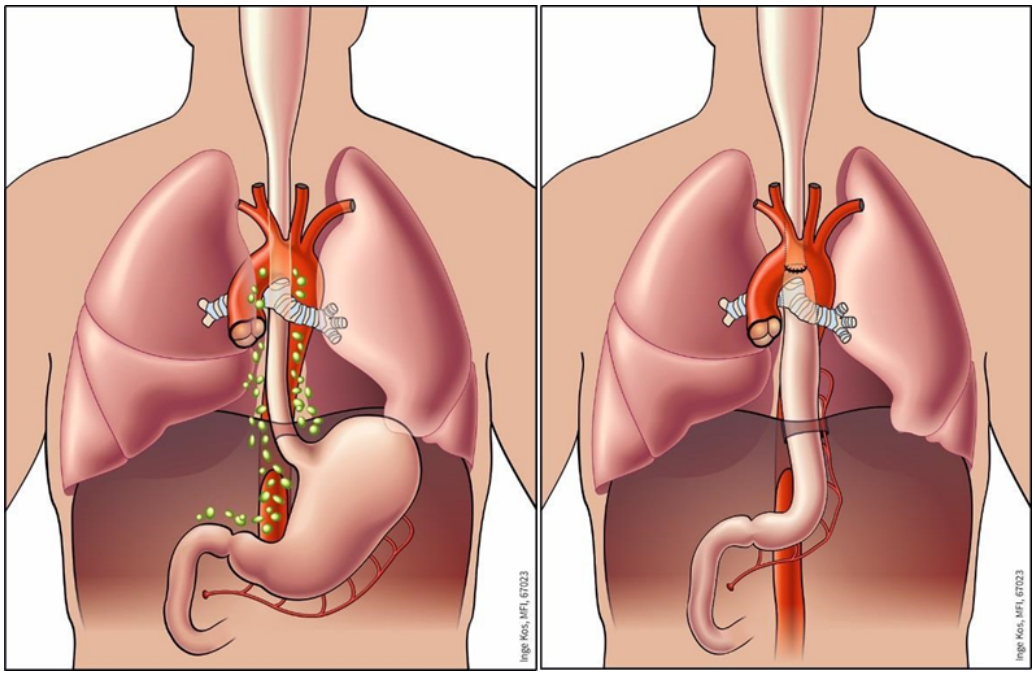

Figure 1.3: **A radical esophageal resection, followed by a cervical gastroesophageal anastomosis.**
Image Source: [16]

Dutch guidelines recommend chemoradiotherapy prior to surgery in the case of surgically resectable tumors (except in the case of T1N0 patients) [13].

This surgery consists of surgically removing (a part of) the esophagus and performing a cervical gastroesophageal anastomosis (figure 1.3). Neoadjuvant chemoradiotherapy has been shown to increase five-year survival from 40% to 49% when compared to surgery alone [13]–[15].

Since esophageal cancer, and especially adenocarcinoma, is often located close to the gastric-esophageal sphincter and, therefore, close to the heart, reducing the dose delivered to OARs surrounding the tumor can significantly decrease the mean heart dose.

In a 2020 randomized phase IIB trial, Li *et al.* showed proton beam therapy could reduce total toxicity burden when compared to intensity-modulated radiotherapy (IMRT) by a factor of 2.3 [17]. The same research group also found a significant difference in the rate of pulmonary complication (16.2% vs. 24.2%) and wound complications (4.5% vs 14.1%), comparing proton beam therapy to IMRT [18].

## 1.4 Lymphoma

Lymphomas are tumors of the lymphatic system, a key component of the body's immune system, which comprises lymph nodes, spleen, thymus, and bone marrow.
Lymphomas are divided into two types: Hodgkin's lymphoma and the more common non-Hodgkin lymphoma. Since five out of six lymphoma patients included in this study are Hodgkin's lymphoma patients, this type will be the primary focus of this section. Hodgkin's lymphoma can be subdivided into multiple subtypes, each with a different prognosis and prevalence.

Hodgkin lymphoma is a tumor derived from mainly B-cell and T-cell lymphocytes, which mostly live in the lymph nodes and the lymphatic system. Cells can start to divide uncontrollably as a result of a genetic mutation. When this happens to cells located in the lymph nodes, these types of tumors are known as nodal lymphomas.

Hodgkin's lymphoma is a rare disease: in The Netherlands, 478 patients were diagnosed with Hodgkin's lymphoma in 2021 [19].

It is more common in men than women. It has a bimodal age distribution: the first peak is in people between 15-34 years old, and the second peak is in patients older than 50 years old. Patients with Hodgkin's disease are generally younger than patients with non-Hodgkin.

The exact cause of Hodgkin's lymphoma is unclear, except that it is a result of a genetic mutation in a patient's lymphocytes. An important risk factor is (prior) infection with the Epstein-Barr virus. Also, people with weakened immune systems, such as HIV patients and patients who take immunosuppressive medication after an organ transplant, are at greater risk of Hodgkin's lymphoma [21], [22].

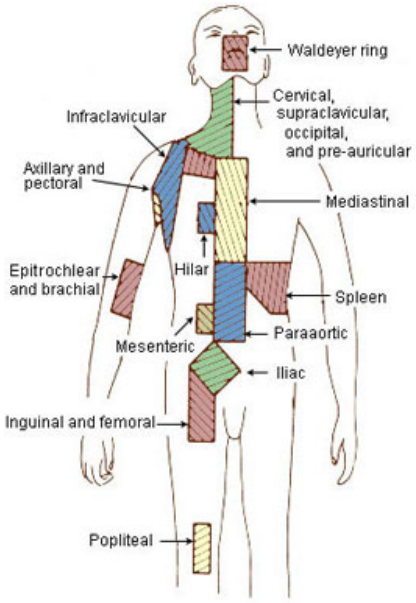


Figure 1.4: **Anatomical Regions for the Staging of Hodgkin's Lymphoma**
Image Source: [20].

An important symptom is swelling of the lymph nodes, known as lymphadenopathy. This commonly starts in the supraclavicular and anterior mediastinal regions (see figure 1.4). Other important symptoms include intermittent fever, drenching night sweats, and weight loss. Core needle biopsy of the swollen lymph nodes can be used to diagnose Hodgkin's lymphoma. A complete blood count is a broad diagnostic method that can provide extensive insights into the content of a patient's blood. Next, PET-CT is used to determine the extensiveness of the disease [19]. Contiguous properties are common in Hodgkin's lymphoma: this means the lymphoma spreads from lymph node to lymph node in the same local area. This is different from NHL, where there is distant spread [19].

The most common treatment is a combination of chemotherapy and radiotherapy

[19], [23], [24]. In localized Hodgkin's lymphoma, chemoradiotherapy is used. In some patient groups, radiotherapy can be omitted due to the long-term side effects of radiation. For example, in women below 35 with bilateral axillary- and mediastinal-affected lymph nodes, radiotherapy can be undesirable [23].

In the case of advanced (stage III-IV) Hodgkin's lymphoma, Dutch guidelines recommend radiotherapy (36 Gy in 18 fractions) only if there are still PET-positive lymph nodes visible in FDG-PET/CT four to six weeks after chemotherapy.

For Hodgkin lymphoma patients, the overall 10-year survival is 83% [19].

## 1.5 Proton therapy

In conventional photon therapy, dose delivery is highest, where the photon beam enters the body. It gradually decreases the deeper it passes through the body. By irradiating the clinical target volume (PTV) from multiple directions, dose distribution can be high in the PTV while sparing the healthy organs at risk (OAR). Despite great efforts to keep the dose in the OARs to a minimum, this method inevitably leads to the dose being delivered to the healthy cells, leading to short-term and long-term side effects that can have a great impact on the quality of life and mortality of the treated patient. Nowadays, plan optimization is used to decrease the dose in the OARs as much as possible without reducing the target volume dose.

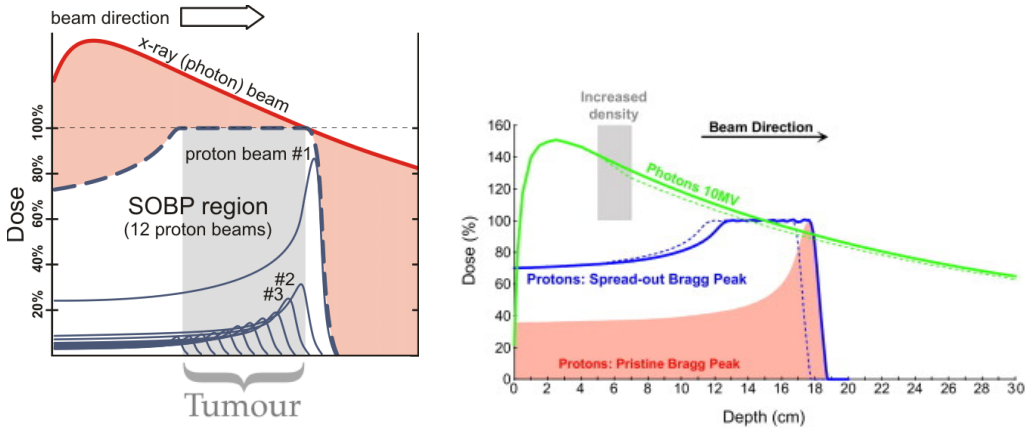


(a) **The foundation of proton beam therapy. A photon beam delivers a dose (shaded red area) before and beyond the target, while in a proton beam, the majority of the dose is delivered in one narrow peak. Combining multiple Bragg peaks (gray dashed line) results in a more uniform dose distribution in the target volume. Image Source: [25].**

(b) **One of the reasons position verification is extra important in proton therapy. In the case of an area of increased density (gray area), the photon beam is attenuated slightly more (green dashed line). In the case of a proton beam, an increased density results in a different location of the Bragg peak, which in turn can result in a completely different location of dose delivery (blue dashed line). Image source: [26].**

Figure 1.5: **Important differences between photon therapy and proton therapy.**

A beam of proton particles has a different dose delivery characteristic compared to a photon beam. The promise of the effectiveness of proton therapy relies on the existence of the Bragg peak.

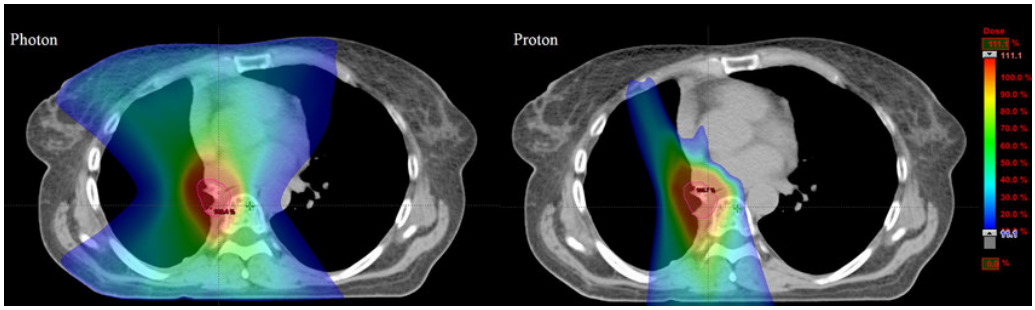


Figure 1.6: **An example of two treatment plans for lung cancer; a photon therapy plan on the left and a proton therapy plan on the right. Notice the decreased dose in organs surrounding the tumor, especially the lungs and heart.**
**Image source:** [27]

#### Bragg peak

Beams of protons with uniform energy have the characteristic of delivering their dose mainly in one large peak, as can be seen in figure 1.5a (*proton beam #1*). As protons pass through atoms, they gradually lose their kinetic energy and decelerate. This decrease in speed causes them to collide with tissue more frequently, leading to further energy loss. Eventually, the protons come to a sudden halt, causing loco-regional release of energy. Due to this finite range of the beam, virtually no dose is delivered beyond the Bragg peak.

The depth of this peak can be influenced by changing the energy of the protons. By intelligently manipulating the energy of different proton beams, which results in a spread out Bragg peak (SOBP, figure 1.5a), a uniform dose distribution can be delivered in the tumor volume with very little dose in the OARs (figure 1.6).

However, due to the large dose that is delivered in a small volume, position and density verification is even more important in proton therapy. A small change in density or position can result in too much dose being delivered in normal healthy tissue (figure 1.5b).

### 1.5.1 Pencil beam scanning

Holland Proton Therapy Centre (Holland PTC, Delft, The Netherlands) uses the technique of pencil beam scanning (PBS) using the Varian Probeam 4.0 (Varian, Palo Alto, California, USA).

In PBS, the target volume is divided into different layers. In each iso-dose layer, the dose is delivered via a series of discrete irradiation spots. The beam is moved to the desired location using magnetic fields, turned on, and when the required amount of protons are delivered in the spot, the beam and moved to the next spot location. Once the entire iso-dose layer is irradiated, the beam is turned off, and the energy is adjusted to

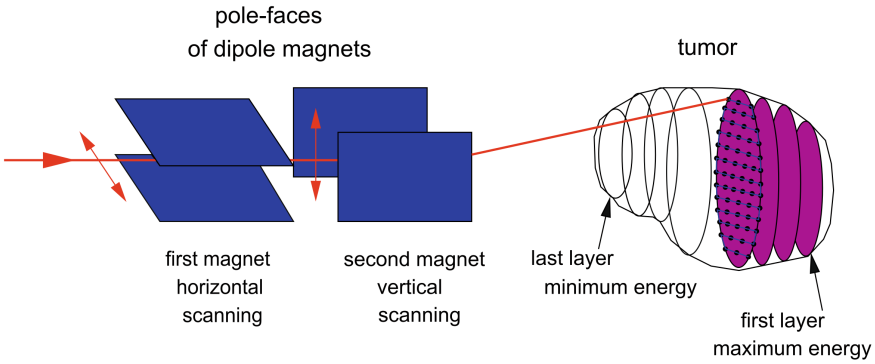


Figure 1.7: **In pencil beam scanning, a narrow beam of protons with uniform energy is shifted using sets of magnets to hit the tumor at a predetermined spot. The tumor is divided into energy iso-layers (purple fields), which are irradiated from distal to proximal. Image source: Krämer *et al.* [28].**

conform to a different depth (figure 1.7). This process is not instantaneous, giving room for position uncertainty due to tumor movement. This will be discussed more extensively in section 1.6 Organ motion.

Figure 1.8 shows an example of a treatment plan. It shows 12 frames from beam measurements of the MatriXX PT quality assurance detector array. Each orange dot shows the location of one detector chamber. The blue dots show the radiation measured by each detector chamber. The size of the dots is arbitrarily scaled to the actual dose (in mGy). The temporal resolution between frames is 40 ms. The last three frames show no measured dose. This is a result of the energy layer switching time (ELST). During this step, the beam is turned off as the energy is changed to conform to a different depth.

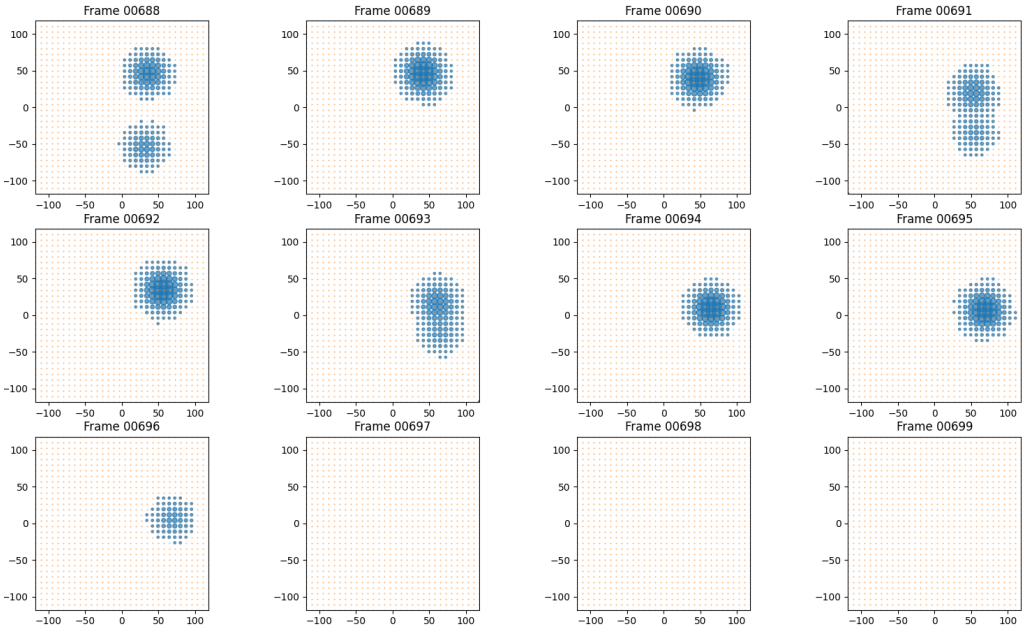


Figure 1.8: **Twelve consecutive frames from the beam measurements of P01_B1, as measured by the MatriXX PT quality assurance detector array. Values on the axis represent the distance from the center of the detector array in mm.**

#### Potential advantages of proton therapy

The potential dosimetric advantages of proton therapy compared to photon therapy have been extensively researched. Liao *et al.* performed a randomized control trial on patients with in-operable NSCLC. Patients received either passive scattering proton therapy or intensity-modulated photon radiotherapy (IMRT). The mean heart dose was significantly lower in the proton therapy group. The loco-regional tumor control was equal in both groups, which indicates the effectiveness of tumor control is equal [29].

Increased mean heart dose has been associated with a decrease in overall survival and an increase in all grade cardiac events [30]. In Holland PTC, mean heart dose is the primary decision parameter between the photon and proton treatment plan.

Another study compared the risk of secondary cancer between 3D conformal RT, IMRT, and proton therapy. This database study showed an overall lower risk of second cancer versus IMRT (adjusted OR of 0.31) [31].

### 1.5.2 Quality assurance

The process of treatment planning and dose calculation for PBS proton therapy is characterized by significant complexity, primarily due to the inherently stochastic nature of the interaction between the proton beam and tissue.

Therefore, patient-specific pre-treatment quality assurance (QA) is performed on a sample of patients before the start of treatment to verify that the dose planned by the

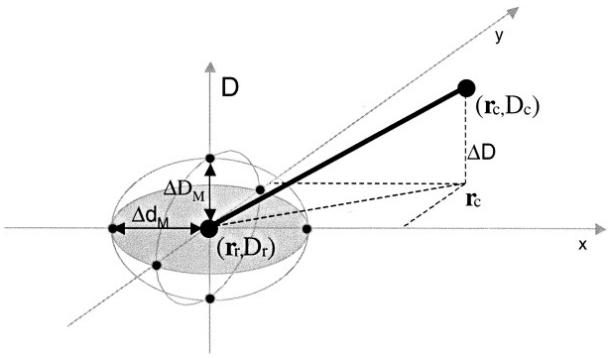


Figure 1.9: **A representation of the theoretical concept of the Gamma evaluation method, by Depuydt *et al.* [32]. The reference point dose distribution $(\mathbf{r}_r, D_r)$ and the comparison dose distribution $(\mathbf{r}_c, D_c)$ are depicted. The dose difference $\Delta D$ and the distance between the two points are divided by their acceptance criteria to normalize them. This way, two doses can be compared based on the set acceptance criteria and a combination.**

treatment planning system (TPS) aligns with the delivered dose by the machine. QA involves different processes and procedures to verify treatment planning and patient positioning, with one of the steps involving beam delivery performance verification. During this QA, the treatment plan is irradiated using the gantry and measured using a MatriXX PT detector array (*IBA Dosimetry, Schwarzenbruck, Germany*) without the patient. One method to verify the delivered dose is the Gamma Index.

### 1.5.3 Gamma Index

The Gamma Index is a measure first proposed by Low *et al.* to compare two dose distributions quantitatively [33]. It is typically used to compare a calculated (goal) distribution to the measured (actual) distribution. Certain acceptance criteria are set; for example, a dose difference ($\Delta D_M$) of 2% and a distance to agreement ($\Delta d_M$) of 2mm is maintained for lung cancer patients in Holland PTC.
An imaginary three-dimensional ellipsoid is created (figure 1.9), with two axes (x and y) being the distance from the comparison point to the reference point and one axis being the dose difference between the two. All distances and doses are divided by their corresponding acceptance criteria. The result is that the comparison point's distance to the reference point ($\Delta r = |\mathbf{r}_r - \mathbf{r}_c|$) and dose difference compared to the reference point ($\Delta D = D_c(\mathbf{r}_c) - D_r(\mathbf{r}_r)$) is relative to the acceptance criteria. Using Formula 1.1, the distance from the comparison to the reference point is checked. Note that distance in the case of the ellipsoid (figure 1.9) refers to the combination of the normalized dose difference and normalized positional difference.

$$\Gamma_r(\mathbf{r}_c, D_c) \equiv \sqrt{\left(\frac{\Delta r^2}{\Delta d_M^2}\right) + \left(\frac{\Delta D^2}{\Delta D_M^2}\right)} \leq 1 \tag{1.1}$$

If the distance ($\Gamma_r$) is greater than 1, the comparison point fails the test. This test is

performed for all comparison points. The percentage of all comparison points that pass this test (Gamma pass rate) is considered a good indication of how much the dose distributions 'match' [32], [34]. In Holland PTC, calculated and measured dose distributions need to have a Gamma pass rate of 95% for the plan to be accepted [35].

Often, a large part of the measured field receives no dose. If the Gamma index of all these points were calculated, computational time would increase drastically without adding anything to the results. One method to avoid this type of redundant calculation is by setting a certain threshold of 5%. All points where the dose is less than 5% of the prescribed treatment dose are not considered. This approach omits Gamma index calculation in low-dose regions, prioritizing analysis within the high-dose region.

**Possible alternatives to Gamma Index** The Gamma index is one of the most common metrics used for verification in radiotherapy, even though it has some downsides. It can be computationally expensive since it needs to search all points in an evaluated distribution. This can be especially disadvantageous when the algorithm works on two 3D dose distributions. Another problem is that the metric simplifies the entire dose distribution differences to a single value; It tells nothing of the location or severity of the dose difference [36].

A commonly used alternative to the Gamma index is the Homogeneity Index (HI). There is not one generally accepted method to calculate the HI. One example formula is HI $=D_5/D_{95}$, representing the dose received by 5% and 95% of the target volume, respectively. These values essentially represent the maximum and minimum dose in the target volume, leaving out the most extreme 5% on both sides. Ideally, the maximum and minimum doses in the target volume are equal. Any inhomogeneity in the dose distributions increases the HI value [37].

Rana *et al.* use seven different metrics, each with a stringent and a lenient threshold. The treatment plan must meet all seven stringent criteria to be considered acceptable. If it meets five of the stringent criteria and the other two metrics' lenient criteria, it is considered 'acceptable with a minor deviation' [38].

Since the Gamma Index is the metric used in Holland PTC's clinical workflow and decision support, it will be used as the metric in this thesis.

## 1.6 Organ motion

Radiotherapy treatment plans are made on CT and/or MRI data. The International Commission sets target volume definitions on Radiation Units and Measurements (ICRU). The first volume is the gross tumor volume (GTV). This is the tumor volume that is visible or palpable, without adding any margin. The clinical target volume (CTV) is the GTV plus direct, local sub-clinical spread plus a tumor-specific margin (figure 1.10). This can include surrounding tissue or draining lymphatic vessels [39]. This tumor-specific margin is 5 mm in NSCLC [41]. The tumor movement due to breathing must be considered to ensure adequate irradiation. This is done by fusing (union) the CTVs in all phases that are captured in the 4D-CT. The resulting structure is called the internal target volume (ITV). This is the volume on which the treatment plan is based.

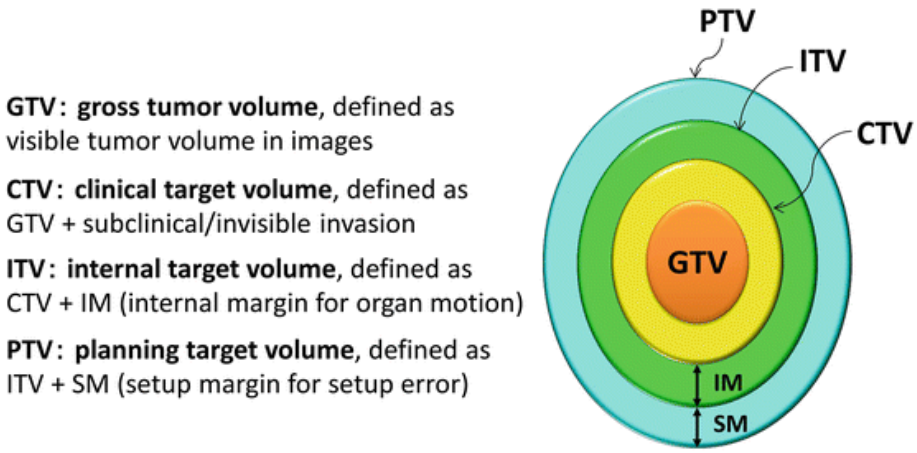


Figure 1.10: **The different types of tumor volume and target volume, as defined by the ICRU [39].** Image Source: [40].

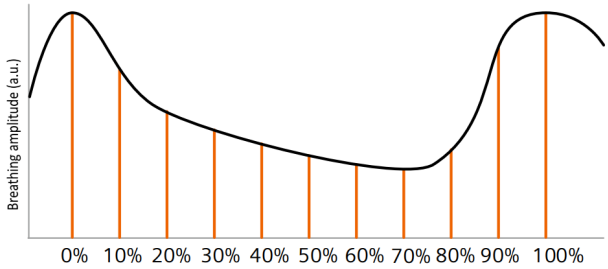


Figure 1.11: **A breathing amplitude, and the ten 'bins' in which the breathing is categorized. The ten bins each have their corresponding CT image, making it possible to see the anatomical changes in each of the ten breathing steps.**

### 4DCT

A 4DCT is a type of CT scan that takes multiple images in rapid succession. These images are reconstructed to create a 4D representation of the moving structures. This way, the treatment plan can be evaluated on different breathing phases. Of these ten images, an average, 3D CT is created. This average CT is used to create the treatment plan.

To incorporate respiration in the measurement, the Anzai belt (Anzai AZ-733 V respiratory gating system) is used. This respiratory cycle is divided into ten sections of equal time length. All CT images are sorted into one of these respiratory bins. The full expiratory phase (Fex) and full inspiratory phase (Fin) (70% and 0%/100% in figure 1.11, respectively) and the average of all ten cycles are used for target delineation.

### Interfraction motion

Interfractional movement can be described as the organ motion that occurs on a day-to-day basis. There can be alignment issues caused by daily variations in bowel- and bladder filling or changes in the breathing cycle. Other influences could be changes in patients' weight, or swelling of tissue [42]. Subtle different positioning of the patient on the table can also be of influence.

The way to compensate for this is using on-line position verification. Using a cone beam CT (CBCT), the patient's anatomy is visualized while on the gantry table. This image is registered to the planning CT, and minor adjustments are made if necessary to compensate for variations in anatomy. If the old and new anatomy varies too much, a new plan will need to be made.

Den Otter *et al.* investigated the change in GTV motion amplitude of 41 locally advanced NSCLC patients during a treatment course. They found that one-third of patients with initial amplitudes below 5mm had an increase in GTV motion beyond 5mm. Patients who had a low initial amplitude (<2mm) stayed below a GTV amplitude of 5 mm [43].

However, Bissonnette *et al.* states that they observed no statistically significant differences in tumor motion during fractionated treatment. They found an increase of over 2mm in 7.2% (n=29/405) of their observations and an increase of over 5mm in 2.2%. In eight of the nine patients with a change of over 5mm, the tumor motion amplitude decreased. [44]

### Intrafraction motion

Intrafractional movement is the movement that occurs while a patient is being irradiated. Respiratory and cardiac motion are the main contributors, and they mostly influence organs and tissue in the thorax and abdominal region. For lung tumors, motion is usually largest for those near the diaphragm and largest in the SI direction [42], [45], [46]. Much data has been published regarding this type of motion, including papers regarding the simulation of respiratory movement (section 1.8 Literature study). Tumor motion is commonly simplified to vectors in the three primary directions: cranial-caudal or superior-inferior (SI), lateral-medial or left-right (LR), and anterior-posterior (AP) (figure 1.14).

Seppenwoolde *et al.* used fiducial markers to track 3D tumor location during radiotherapy in 20 patients [45]. The greatest tumor motion was in the superior-inferior (SI) direction (12 ± 2 mm) for tumors in the lower lobes of the lung, not attached to rigid structures. Time-averaged tumor position was closest to the exhale position because the tumor spent more time in exhale phase.

Knybel *et al.* analyzed log files from online respiratory tumor tracking of 145 patients [46]. They found a mean tumor motion amplitude of 6.0 ± 2.2 mm, 2.2 ± 1.3 mm, and 2.8± 1.6 mm in SI, LR, and AP direction, respectively. In addition, they found a correlation between tumor SI position and mean motion amplitude in the SI direction. Also, they found a strong correlation (r=0.86) between intrafraction motion variability and mean motion amplitude in the SI direction, meaning a high tumor motion amplitude corresponds to higher intrafraction motion variance.

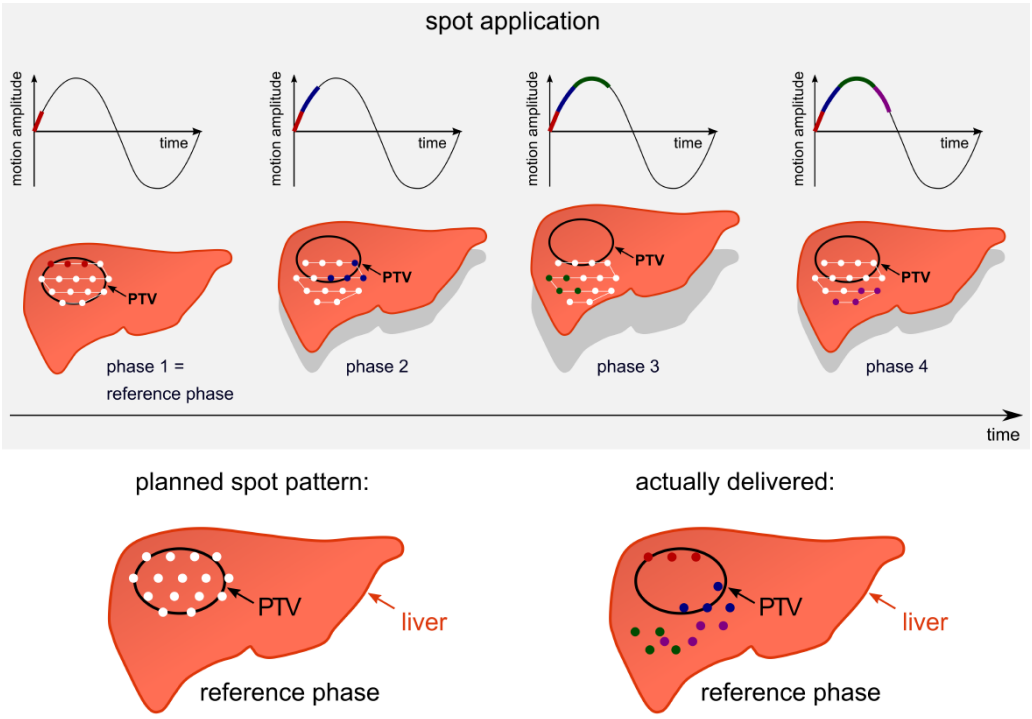


Figure 1.12: **Visualisation of the interplay effect. The planned treatment is visualized in white. The liver is moving due to breathing motion. The spot pattern is delivered as if the liver is stationary.**
**Image source:** [47]

### 1.6.1 Interplay effect

In conventional photon therapy, density variations are less concern than in proton therapy. The dose-depth distribution is more shallow, meaning a small shift in density has only a limited dosimetric effect. In proton therapy, however, this can mean the difference between the tumor receiving 0% or 100% of the prescribed dose (figure 1.5b). For a photon beam, this difference may only be a few percent. Especially if multiple treatment fractions are delivered, commonly in curative radiation therapy, the required safety margin for moving tumors can be applied by essentially blurring the dose distribution [42].

If proton therapy were an instantaneous delivery of the intended dose distribution, the problem of interplay would be less severe. However, in the case of pencil-beam scanning (PBS), delivery is not instantaneous. The interplay effect refers to the complex interaction between the tumor motion and the delivery of proton beams, in which the relative motion of the tumor and the beam is an important factor.

As described in 1.5.1 Pencil beam scanning, the dose distribution in PBS is delivered by dividing spot positions into range layers. Though delivery within one range layer is almost instantaneous (order of milliseconds), switching between consecutive energy layers (commonly referred to as Energy layer switching time, ELST) is generally between 0.5 and 1 second for the hardware used in Holland PTC (Varian Probeam 4.0) [48]. Since the

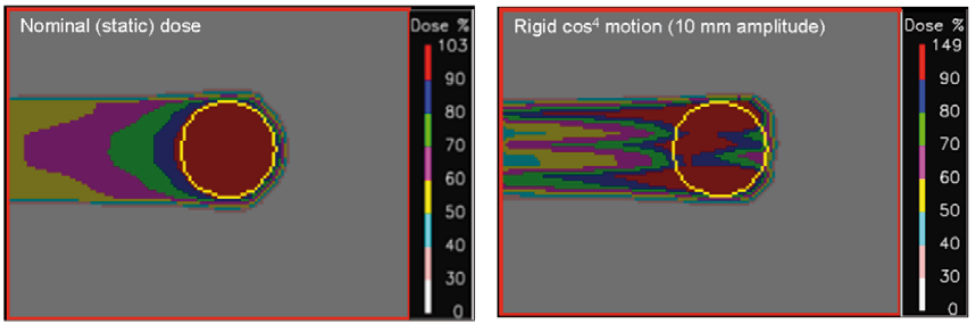


Figure 1.13: **Left: dose distribution of a static measurement. Right shows the same dose, delivered to a target that moves with a 10mm amplitude. Image source:** [49]

breathing period is in the range of a few seconds, this ELST is relatively large compared to the time it takes to irradiate one layer. If the beam momentarily stops delivering the dose, but the target volume keeps moving, the beam might skip a spot it was supposed to irradiate or scan the same position twice. This can result in dose hotspots or coldspots, leading to sub-par tumor control (figure 1.12 and 1.13). Figure 1.13 shows a decrease of up to 40% in the distal (right) side of the target and a similar increase in dose proximal to the target.

The impact of the interplay effect on dose coverage has been researched extensively, including by Bert *et al.* They found a target volume coverage with 95% of the prescribed dose of 71.0% ± 14.2%. In other words, on average, only 71% of the target volume received the minimum of the prescribed dose. This was based on 4DCT of five lung tumor patients with one fraction and one field [50].

The primary patient parameter resulting in the interplay effect is the breathing motion [42]. Big and small fluctuations in breathing amplitude and frequency can occur during a fraction and in between fractions. These fluctuations are unsystematic and unpredictable. Many models are designed trying to simulate the breathing motion of patients specifically [51]–[53].

### Interplay mitigation

There are multiple methods possible to mitigate the effect of target motion of coverage [54]. The methods used in Holland PTC will be discussed here.

**Repainting** Repainting, also known as rescanning, is a technique that involves delivering the dose in multiple cycles instead of a single pass [42]. This approach aims to smooth the dose distribution and reduce dose inhomogeneities. However, there are some drawbacks to consider. When repainting is performed multiple times, each scan's dose is reduced to 1/4th of the original dose. Consequently, the number of monitor units (MU) per spot is also reduced by the same factor. In some cases, this reduction in MU can fall below the detection threshold of the gantry head's internal quality assurance components. As a result, these low-weight spots are eliminated from the treatment plan, necessitating other spots to increase their intensity to meet the dose requirements. This adjustment to

the treatment plan can result in a more inhomogeneous dose distribution or challenges in conforming to lateral and distal target contours. Additionally, repainting increases the overall treatment time.

**Spot Size** Another option to mitigate the interplay effect is by changing the spot sizes and the distance between spots laterally [42]. Bert *et al.* showed an 'intrinsic rescanning' if the overlap between pencil beam spots was increased [55]. This overlap increase can be achieved by decreasing the distance or increasing the spot size.
Increasing the spot size is achieved by using a larger range shifter. A range shifter is a uniform slab of plastic that can be placed between the gantry and the patient. It moves the Bragg peak of a bundle closer to the surface without needing to change the energy of the beam.
A secondary effect is that it results in more lateral scatter. This decreases the quality of the lateral penumbra but simultaneously makes the spots bigger. This way, it is used to counter the interplay effect by allowing for more overlap per spot.

#### Coordinates convention

One important aspect to understand is the convention of the used coordinates system. RayStation used a convention according to *IEC 61217* [56]. [1]

In this convention, the left-right position is referred to in the x-axis, superior-inferior in the y-axis, and anterior-posterior in the z-axis. This is the case for all patients in head first supine position, which applies to all patients included in this thesis (figure 1.14). Note that the DICOM export standard is different, but that will not be used in this thesis.

## 1.7 QA method to validate robustness for interplay

Holland PTC uses the MatriXX PT detector array and a motion simulation script to assess the interplay effect in delivered beams retrospectively. Holland PTC interns have validated this simulation script [57], [58].

### 1.7.1 MatriXX PT dosimetric measurements

The MatriXX PT by IBA (Schwarzenbruck, Germany) is an ionization chamber detector array designed for patient quality assurance (QA, see section 1.5.2 Quality assurance). It consists of 1020 ion chambers arranged in a 32 x 32 grid, with 7.62 mm spacing [59]. The MatriXX PT can be used to measure the output of a beam gantry with a temporal resolution as low as 40 ms [58], [59].

During quality assurance (QA), a real treatment plan is irradiated. This beam is measured using the MatriXX PT.
The detector array is placed on the patient table. With a temporal resolution of 40ms, it

[1] From RayPhysics Manual: *The gantry coordinate system rotates with the gantry. The gantry coordinate system has the fixed coordinate system as its mother system.*
*For the IEC standard, it is defined to coincide with the fixed coordinate system when the gantry angle is zero. The gantry angle increases gradually for clockwise rotation as viewed by an observer facing the gantry.[56]*

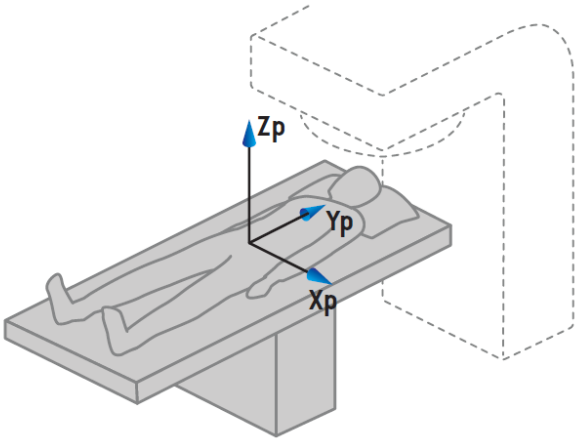


Figure 1.14: **The patient coordinates system, which is equivalent to the machine coordinates system. The patient is in head first supine position.**
**From RayPhysics Manual:** *"In general, in RayStation10B the patient coordinates are reported as Right-Left, R-L (right-left = x -/+), Inf-Sup, I-S (inferior-superior = y -/+) and Post-Ant, P-A (posterior-anterior =z -/+)"* [56].

measures the dose each of the ionization chambers receives. Since the detector array only measures a 2D plane instead of the entire three-dimensional treatment plan, the MatriXX PT is placed at a height corresponding to the maximum dose's location. Both a reference field and the actual patient plan are irradiated and measured. Gamma index analysis is performed using MyQA software to calculate the plan's Gamma pass rate (The fraction of the reference points that pass the Gamma acceptance criteria) [60].

The output can be exported as a list of .opg files. These files contain the measured dose of every detector array at every 40 ms time interval. This can subsequently be transformed into a representation of the delivered dose.

One problem is that this dosimetric measurement is performed in a static environment; the MatriXX PT does not move as the tumor does in a real, breathing patient. Ideally, it is possible to move the MatriXX PT to detect the effect of tumor movement on the dose distribution. Dr. Y. Wang has created a model that simulates the motion of a tumor as a sinusoidal movement and can determine the severity of the interplay effect. This has been validated by Holland PTC [57], [58].

### 1.7.2 Current simulation model

The current interplay simulation script, created by Dr. Y. Wang, allows the following inputs:

- Number of fractions: The number of treatment fractions that are simulated. The Gamma pass rate tends to increase the more fractions are irradiated due to the blurring effect of fractionation.

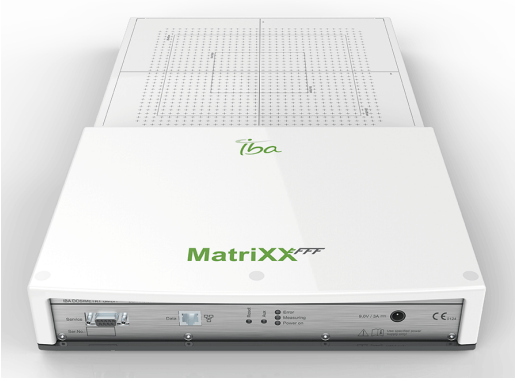


Figure 1.15: **MatriXX PT by IBA.**

- Number of simulations: The number of times an entire fractionation scheme should be simulated again. The main difference is that the initial breathing phase in which the treatment starts (always random) is randomized every time. This way, many different starting conditions are considered.
- time/frame [s]: The time interval at which MatriXX PT measurements are performed, preferably 40 ms. This is the highest temporal resolution of the MatriXX PT.
- Respiratory model [sin/Lujan]: whether a regular sinusoidal movement or irregular (Lujan, $sin^{2n}$) movement is used for simulation.
- Peak-to-peak amplitude [mm]: The peak-to-peak amplitude (full inhale to full exhale) of the tumor, retrieved from the *respiratory amplitude analysis* script.
- Asymmetry factor: The power (n) of the sin used in the Lujan model. Commonly set at 2 in literature.
- Gamma Dose [%]: The acceptance criterion for dose difference.
- Gamma distance[mm]: The acceptance criterion for distance to agreement.
- X- and Y-resampling [mm]: The option for resampling the frames to a specific size.
- Folder containing the frames (.opg files): the folder which contains the MatriXX PT measurements of the treatment beam.

This results in a sinusoidal motion that can be easily manipulated with many parameters.

The simulation of tumor motion is executed as follows:

- One 'blurred' image is created. This is considered the reference dose distribution. This is achieved by accumulating all the frames of one beam measurement and calculating the integrated dose.

- A simulation of an infinite number of fractions is performed by integrating with respect to time. It is convoluted with a sinusoidal signal, determined by the parameters set.
- This results in the reference dose distribution, discussed in section 1.5.3 Gamma Index. This theoretical dose measurement can be considered the ideal situation if no interplay would be present.
- To create the comparison dose, or the actually measured dose, the same sinusoidal motion is applied iteratively to each MatriXX PT frame (figure 1.16). Consequently, each frame undergoes a slight shift in position.
- The accumulation of all shifted frames is added to the accumulated dose of the previous fractions and compared to the blurred reference dose distribution using the Gamma Index. This results in a Gamma pass rate for every fraction that determines to what extent the comparison dose differs from the reference dose.

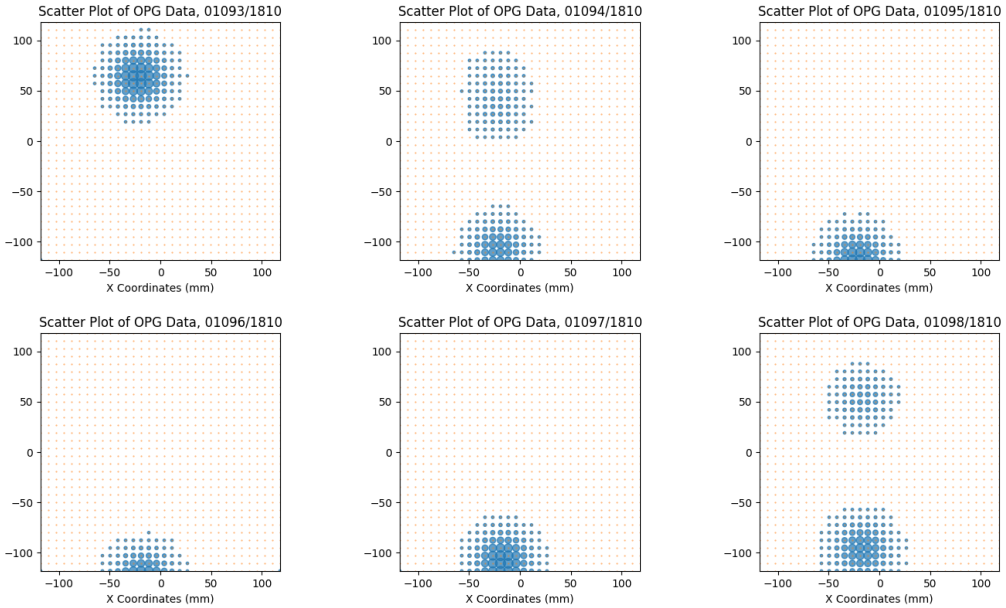


Figure 1.16: **Six consecutive frames from P01_B1 are arranged from left to right, top to bottom. The x- and y-axes display coordinates, while the small dots indicate the exact locations of the detector array elements. The size of the blue dots is arbitrary. The sinusoidal shift has not been applied to these frames yet.**

## 1.8 Literature study: Simulation of tumor motion for the estimation of the interplay effect in pencil beam scanning proton beam therapy

**Introduction:** The interplay effect refers to the complex interaction between the tumor motion and the delivery of proton beams, in which the relative motion of the tumor and the beam is an important factor. This can lead to dose inhomogeneities in the target volume and in the OARs. In order to evaluate the magnitude of the interplay effect, simulations of tumor movement and beam movement are often conducted. Optimization of these simulation models can result in treatment plans with increased resilience against the interplay effect while keeping the dose in OARs at a reasonable minimum, using patient-specific mitigation techniques.
**Goal:** The ultimate goal of this literature study is to improve proton therapy plan quality for lung tumors, by selecting the best model for interplay effect mitigation strategies, leading to robust and homogeneous target coverage, with the least effect of dose conformity and OAR dose. We first determine which parameters, data, methods of data acquisition, and assumptions are used in scientific literature to simulate the tumor movement of 4D tumors in proton therapy pencil beam scanning.
**Method:** Using a PUBMED database search, articles describing the simulation of the interplay effect of pencil beam proton therapy in 4D tumors are analyzed.
**Results:** 76 articles are screened, of which 43 are included in the analysis. Findings are divided into two groups: model parameters and patient-based parameters. Model parameters are tumor motion amplitude, breathing period, and sinusoidal/irregular breathing pattern. Patient-based parameters are tumor motion amplitude, tumor motion direction, breathing period, and method of acquisition of tumor movement information.
Model-based and patient-based breathing periods are not statistically different (p-value = 0.360) with a mean ± SD of 4.5 ± 1.36 s and 4.21 ± 1.52 s, respectively. Model-based tumor motion in SI direction is 12.58 ± 9.05 mm, while reported patient-based tumor motion in SI direction is 8.19 ± 6.90 mm ($p<0.05$). Only 2 of 35 articles that used model-based tumor motion parameters considered movement in AP or LR direction.
**Conclusion:** Commonly used model parameters are breathing period, tumor motion amplitude in SI direction, and using a $sin$ or $sin^4$ to model the movement. Patient-based parameters are breathing period and tumor motion. Tumor motion is often reported as an amplitude in SI direction, and less frequently the LR and AP direction is also reported. In few cases, the patient-based tumor motion is a 3-dimensional movement. The breathing period used in model-based simulations is similar to simulations based on real patient data. Tumor motion in model-based simulations is significantly higher than tumor motion in patient-based simulations.

# Chapter 2

# Thesis

## 2.1 Introduction

### PBS and Interplay

Holland Proton Therapy Center (Holland PTC) is an independent outpatient clinic in Delft, The Netherlands. It uses pencil beam scanning (PBS) proton therapy to treat various tumor types, including esophageal cancer, breast cancer, brain tumors, and head and neck tumors.

PBS delivers a precise, narrow beam of proton radiation to the tumor, minimizing damage to healthy tissues. In PBS, the target volume is divided into different layers, called an iso-dose layer. In each iso-dose layer, the dose is delivered via a series of discrete irradiation spots. The beam is moved to the desired location using magnetic fields, turned on, and when the required amount of protons are delivered in the spot, the beam is turned off and moved to the next spot location. Once the entire iso-dose layer is irradiated, the beam energy is adjusted to conform to a different depth.

Some of these tumor types, like esophageal cancer and lung cancer, are located in the thoracic region. This means that the tumor moves during treatment as a result of breathing. The magnitude of this motion can depend on various factors, such as the tumor type, tumor location, and patient breathing characteristics.

In PBS, scanning of one layer plus switching to the next layer happens in the order of one second. Since dose delivery is not an instantaneous process, and the tumor constantly moves, the beam spots might not always deliver dose in the position they are planned (figure 1.12 and 1.13). This can result in an inhomogeneous dose delivery with hotspots and coldspots of delivered dose in the target tissue and OARs [42]. This characteristic is even more critical in proton therapy than photon therapy due to the sharp dose fall-off at the end of the proton Bragg peak. The interplay effect refers to the complex interaction between the tumor motion and the delivery of proton beams, in which the relative motion of the tumor and the beam is an important factor.

Extensive research has investigated the impact of the interplay effect on dose coverage, including studies by Bert et al. They reported a target volume coverage of $71.0\% \pm 14.2\%$, meaning that, on average, only 71% of the target volume received the minimum prescribed dose. This was based on 4DCT of five lung tumor patients with one fraction and one field

[50].

Dolde et al. conducted simulations that demonstrated individual fractions could exhibit an underdosage of up to 70%. However, fractionation showed promise in mitigating the interplay effect, as sufficient clinical target volume (CTV) coverage was achieved after seven fractions on average [61]. Furthermore, tumor motion amplitude has been identified as a significant factor influencing the interplay effect [62].

## Mitigation of the interplay effect

There are treatment planning strategies to reduce the interplay effect, like repainting and using breath-holding techniques [42], [62]. In repainting, the dose delivery is divided into several cycles that are irradiated consecutively, essentially smoothing the delivered dose distribution.

The primary methods at Holland PTC are repainting and changing the spot size, as explained in section 1.6.1 Interplay mitigation. Repainting is applied for esophageal and lung patients when tumor motion exceeds 5 mm in the SI (superior-inferior) direction [63]. Holland PTC has not yet incorporated breath-holding into the clinical workflow.

Many metrics have been used in literature to quantify robustness against the interplay effect. These include the homogeneity index (HI), $D_5 - D_{95}$, and the Gamma pass rate. Different metrics result in different definitions and requirements for robustness.

A phantom study by Spautz *et al.* showed Gamma pass rates of $\geq 95\%$ with peak-to-peak amplitudes $\leq 15$ mm. However, the Gamma acceptance criteria used were 3%/3 mm compared to the stricter 2%/2 mm in Holland PTC [64].

Muck Af Rosenschöld *et al.* report a substantial decrease in robustness after 10 mm tumor motion amplitude in SI direction. The robustness criteria used in their article is GTV $V_{95}$, the percentage of the GTV that is covered by 95% of the prescribed dose [65].

Dolde *et al.* also found a strong correlation between CTV motion and interplay robustness. All pancreatic cancer patients in their cohort had a tumor motion amplitude below 15 mm and were robust against the interplay effect before the end of their treatment scheme[61].

All patients' plans in the article by Rana *et al.*, with amplitudes up to 13.2 mm tumor motion amplitudes, met their acceptance criteria. Only the one with the largest amplitude was considered acceptable with a minor deviation. The ten lung cancer patients received up to ten repaints [38].

While these interplay mitigation techniques might decrease the interplay effect's severity, they can negatively impact other aspects of the dose distribution in the target volume and OARs. Repainting tends to reduce large dose inhomogeneities but results in an increase of smaller dose inhomogeneities in the entire target volume. The use of larger spot sizes, another method that can reduce the interplay effect, has been shown to negatively impact the lateral penumbra of the pencil beam [42].

## Interplay effect simulation

The interplay effect can have serious repercussions for the dose homogeneity in the target volume, as discussed in section 1.6.1 Interplay effect. Determining its severity is the first step to improving mitigation tactics for the interplay effect. Accurate simulation of patient-specific tumor motion is an important step to determine this severity. This

step is known as Quality Assurance (QA, see section 1.5.2 Quality assurance) and can play a crucial role in determining if the treatment plan is robust against the interplay effect. Simulation of the interplay effect involves measuring a treatment plan's beams using a detector array. Holland PTC used the MatriXX PT detector array by IBA (*Schwarzenbruck, Germany*). The static measurement is simulated to move according to a patient-specific motion model, and this dynamic dose distribution is compared to the static measurement. The difference between these two dose distributions is an accurate approximation of the interplay effect. As explained in section 1.7.2 Current simulation model, the current interplay model used in the Holland PTC simulated tumor motion as a periodic, asymmetrical, unidirectional sinusoidal motion [51], [66]. While this is a commonly used method to model tumor motion, tumor motion is known to be more complex than regular up and down motion. Using more patient-specific tumor motion parameters, such as multidimensional motion, can increase the quality of the simulation model.

This model can be used to perform clinical validation of treatment plans that have been measured in the Holland PTC. Clinical evaluation can indicate which plans' beams are not robust against the interplay effect. This can be used both retrospectively and prospectively to review patients' treatment plans. Subsequently, this information can be used to re-evaluate the requirements for applying mitigation techniques at Holland PTC. Improving the requirements to use mitigation tactics allows the treatment team to consider better the benefits and drawbacks of measures in the pencil beam scanning plan. This allows for more patient-specific planning and improves the overall treatment planning quality of patients with moving tumors.

## 2.2 Goals

The ultimate goal of this thesis and internship is to improve treatment plan robustness against the interplay effect. This can be achieved by refining current interplay mitigation strategies. This goal will be divided into steps in the following sections.

**Clinical Evaluation** The first goal is to perform clinical evaluation of the beams of 18 patients' treatment plans. The extent to which the interplay effect affects each beam of the patients (and, by extension, the treatment plans) will be analyzed.

**Factors influencing the interplay effect** The second goal is to assess which patient-specific factors affect the interplay effect. Data was gathered on factors influencing the interplay effect in pencil beam scanning. Determining to which extent they can be regulated can gain a better understanding of how to mitigate the interplay effect in the best possible way while minimally affecting plan quality.

# Chapter 3

# Clinical Evaluation

## 3.1 Methods

Figure 3.1 shows all the steps required to perform the interplay simulations.

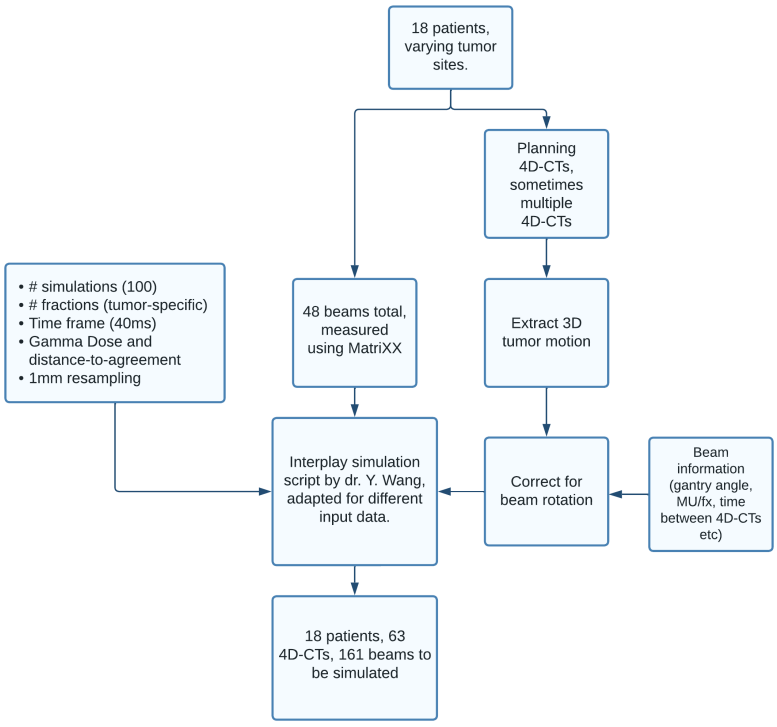


Figure 3.1: **General overview of data preparation methods used.**

### 3.1.1 Data

Two types of data have been used in this thesis: patient data, primarily gathered from RayStation, and QA Data.

#### Patient data

The data from 18 patients with varying tumor sites have been used to model tumor motion. All patients have signed informed consent forms to enable access to their patient data for developmental goals within Holland PTC. A total of 65 4D-CTs are available. Figure 3.2 shows examples of the CTV delineations of the three tumor types.

One or more 4D-CTs are available for all of these patients. The patient's treatment plan has been made on the first of their 4D-CTs. This scan will be called CT0 throughout this thesis. Contouring, deformable image registration, and treatment planning have been performed according to internal protocol[41].

From this planning 4D-CT, tumor motion information will be extracted. See section 3.1.1 Tumor motion data preparation for a comprehensive explanation.

All 4D-CTs' and plan beams' information was available in RayStation. This includes a beam's angle of incidence, CTV volume, MU/fraction, use of range shifter, date of 4D-CTs, and tumor motion amplitude between full inhale and full exhale phase. The voxel size of the 4D-CTs is [LR, SI, AP] = [x, y, z] = [1, 3, 1] mm.

See Appendix A Patient and Beam data for an overview of tumor motion information.

#### QA Data

From the 18 patients, all treatment beams were previously measured using the MatriXX PT Detector array by IBA (Schwarzenbruck, Germany). This data was anonymously stored and will be used in this internship assignment. See figure 3.4 bottom right for an example of one random measurement frame of a patient.

The IBA MatriXX PT detector array consists of 1020 ion chambers arranged in a 32 x 32 grid, with 7.62 mm spacing [59]. The MatriXX PT can be used to measure the output of a beam gantry with a temporal resolution as low as 40 ms [58], [59]. For more information regarding this detector array, read section 1.7.1 MatriXX PT dosimetric measurements.

Figure 3.3 shows an overview of how the patient data and QA data have been combined. For this specific patient, two 4D-CTs are available, meaning two different patient-specific motion situations can be simulated. For the treatment, two beams are used at certain angles. These angles are generally predefined per tumor type but can be adjusted to improve treatment planning. The gantry rotation ([SI, LR, AP]) corresponding to each beam is applied to each tumor motion amplitude situation(section 3.1.3 Beam rotation). This results in a total of four treatment beams that are simulated. Since the MatriXX PT detector array only measures in two dimensions, the anterior-posterior (AP) motion is omitted. For each patient, the number of simulated treatment beams is therefore equal to their number of 4D-CTs multiplied by their number of treatment beams.

Whenever beams or treatment beams are mentioned in this report, it refers to the combination of the beam's angle and a patient's specific tumor motion scenario unless otherwise specified.

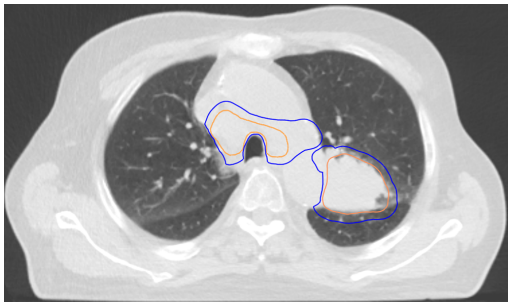

(a) **P04: a lung patient with a left-sided tumor. Lateral orange delineation is the primary tumor. Central delineation is affected lymph nodes.**

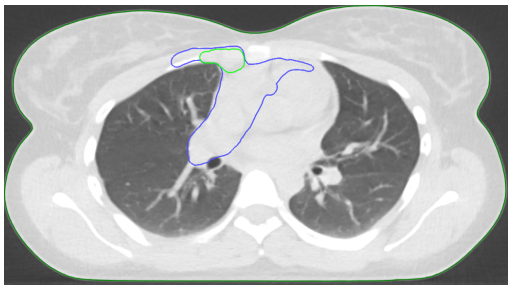

(b) **P01: a Hodkin lymphoma patient. Green indicates high dose CTV, which received a dose of 3570 Gy instead of 3060 like the regular CTV.**

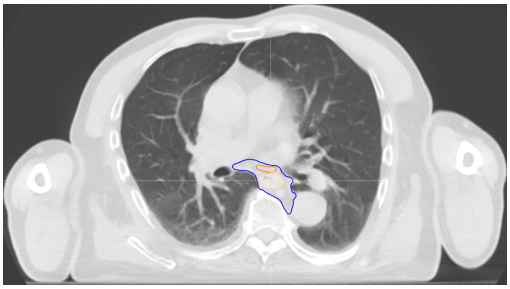

(c) **P07: an esophagus cancer patient. The larger orange structure depicts the primary tumor, while the smaller structure depicts an affected lymph node.**

Figure 3.2: **CT images of the three tumor types. Blue indicates CTV.**

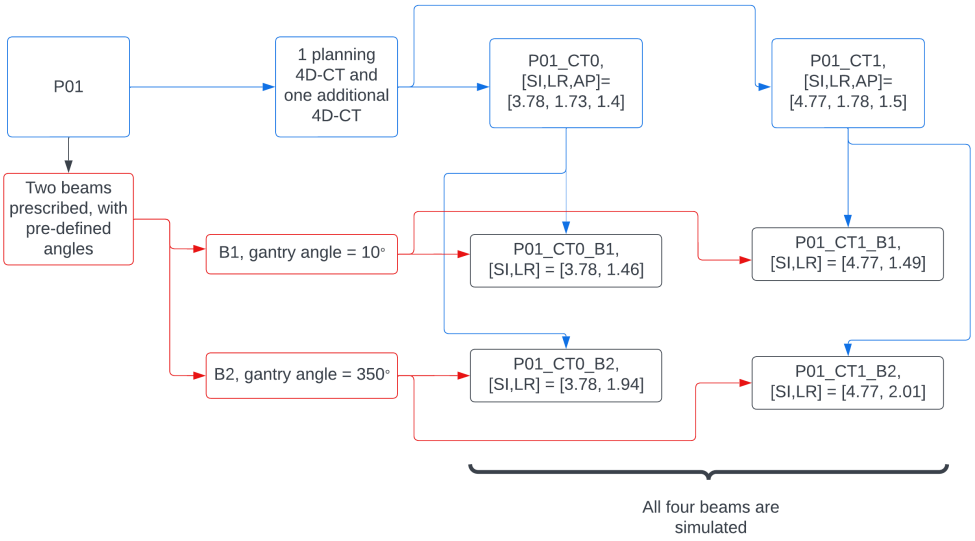


Figure 3.3: **Schematic overview of how the patient data and QA data are combined. The four resulting tumor motion scenarios are applied to the QA beam measurements by the MatriXX PT detector array.**

#### Tumor motion data preparation

In all planning 4D-CTs, the CTV was delineated prior in all ten phases. However, the CTV was not always delineated in the scans taken after the planning 4D-CT. If the CTV was delineated in at least one of the ten scans, the contour was propagated to all phases using Raystation's *contour propagation* functionality. If the CTV was delineated in none of the phases, the 4D-CT was discarded.

Since real patient breathing data was not retrospectively available, the breathing period is assumed to be 4 seconds for all patients. The average breathing period found in the literature study was 4.21 seconds, based on 87 patients. 4 seconds is a similar value but slightly more conservative since the tumors move slightly more rapidly.

The CTV corresponding to chest lymph nodes was used for lymphoma patients, and the CTV corresponding to the neck was ignored.

### 3.1.2 Interplay simulation script

The interplay simulation script works by creating an 'ideal dose' by performing a convolution of the input sinus signal and the integrated dose of all the MatriXX frames. Next, this same sinus signal is iteratively applied to all the individual dose measurement frames. The accumulation of these shifted doses is compared to the ideal dose, which results in a single Gamma pass rate per fraction. The Gamma pass rate is a score representing the number of comparison dose points that match the ideal dose distribution within predefined criteria.

In section 1.7.2 Current simulation model, an elaborate explanation is provided of the working of the interplay simulation script.

A derivative script of the clinically validated was created. It used the same functions as the original, validated script. The major difference was that it allowed for left-right motion to be used as input, besides the superior-inferior input. This derivative script will be discussed extensively in Chapter 5 Unvalidated script.

### 3.1.3 Expanding interplay simulation parameters

**Extracting 2D tumor motion** The respiratory amplitude script, created by Dr. Wang, uses the deformation vector field between the full-in and full-ex breathing phases. The tumor is assumed to reach its lowest and highest point in motion in those phases, respectively. The deformation vector field records each voxel in the first phase and maps it to its corresponding location in the second phase, allowing us to track the tumor's motion from its lowest to highest point throughout the respiratory cycle.

The Euclidean distance between the CTV voxel's coordinates in the breath-in phase and the breath-out phase is recorded in all three primary directions: superior-inferior (SI), Left-right (LR), and Anterior-posterior(AP). These amplitudes are stored for each patient's 4D-CT. After applying beam rotation, explained in the next section, the SI and rotated LR tumor motion amplitudes are used as input for the interplay simulation script. This method is applied to all 161 beams. See figure 3.4 for an example.

The MatriXX PT measurements are resampled in the simulation script to 1 mm in X and Y direction, from 7.6 mm in both directions.

#### Beam rotation

The current interplay simulation script assumes the tumor moves in a direction perpendicular to the proton beam (in SI direction, or $y_p$ in figure 1.14). However, the gantry head irradiates the patient from different angles. This rotation is only around the $Y$ axis in the plane of the X and Z axis. When the tumor motion is simulated in three dimensions rather than solely SI direction like the current simulation script, the angle of incidence becomes a factor of relevance. The gantry angle was extracted from RayStation's planning software for each simulated beam. The tumor motion in all three directions can be adjusted for this rotation (Equation 3.1).

This way, the tumor motion change can be considered when the patient is irradiated from an angle different than 180°.

$$\begin{aligned} x &= \cos(\phi_{\text{rad}}) \cdot x - \sin(\phi_{\text{rad}}) \cdot z \\ z &= \sin(\phi_{\text{rad}}) \cdot x + \cos(\phi_{\text{rad}}) \cdot z \\ y &= y \end{aligned} \tag{3.1}$$

After correction for rotation, the tumor movement parallel to the beam (Z-direction) was negated. During QA, the MatriXX PT detector array is placed flat on the table (the plane of $X_p$ and $Y_p$ in figure 1.14). Since it only measures irradiation in two dimensions, it is not meaningful to simulate tumor motion in the $Z_p$ direction.

Notice that when the gantry revolves around a patient, the SI component of the tumor motion amplitude ($y$ in equation 3.1) does not change.

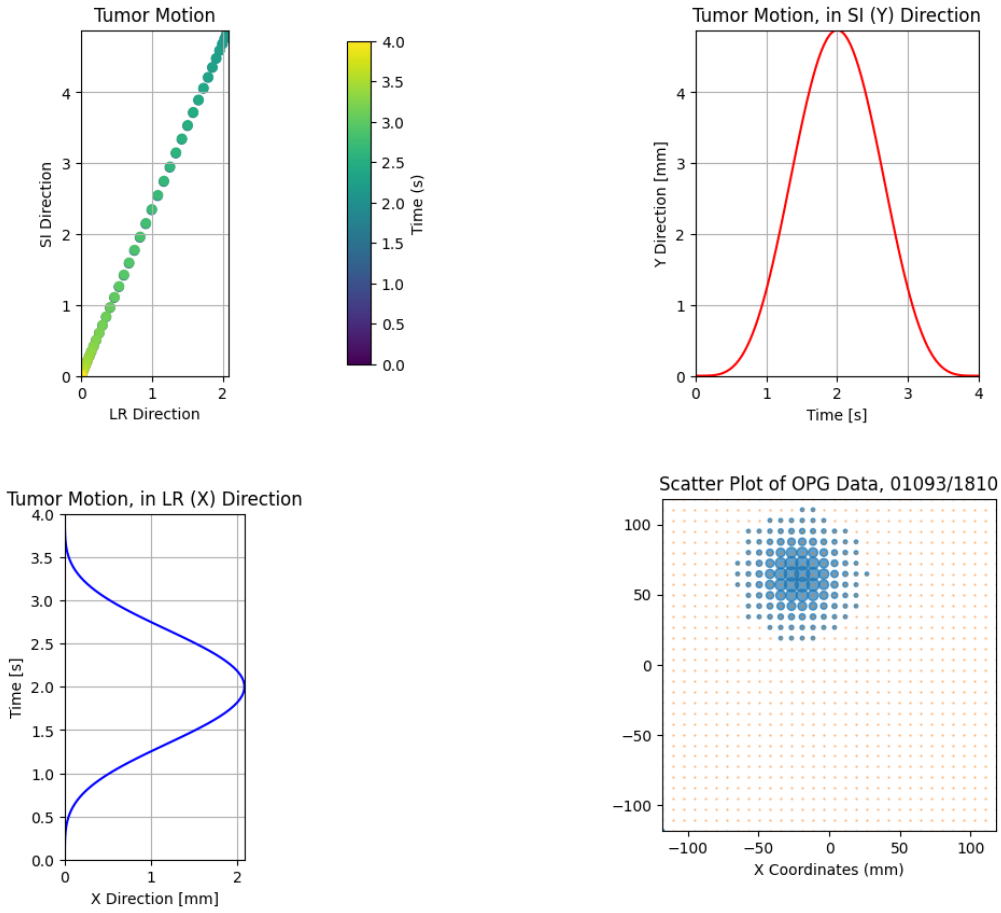


Figure 3.4: **A visualization of the tumor motion simulation of P17_CT0_B1. The blue and red lines visualize the simulated tumor motion (in the form of x=$sin^4(t)$) in their respective direction, resulting in the top left motion. The bottom right figure shows the entire MatriXX PT measurement of one frame of this patient. The values of X and Y are in mm everywhere. The MatriXX PT measurement has not been resampled to 1 mm yet in this image but still has a 7.6 mm resolution.**

### 3.1.4 Clinical evaluation

The first goal is to perform clinical evaluation of the beams of 18 patients' treatment plans. For each patient beam (and, in extension, the treatment plans), we will determine to what extent the beam is subject to the interplay effect.

### QA tool to assess interplay effect

In the field of Quality Assurance, the Gamma index and the corresponding Gamma pass rate are employed as a metric to evaluate the presence of interplay in clinical plans (see Background section 1.5.3 Gamma Index). A cutoff value of 95% is commonly used in practice. This value serves as a threshold to determine whether a patient's measured plan during Quality Assurance is sufficiently close to the reference (planned) dose distribution [60].

The Gamma pass rate assesses the extent to which predefined criteria are met by the reference and measured dose distributions. In this thesis, the criteria consist of a maximum dose difference of 2% of the prescribed dose and a distance to agreement of 2 mm at most [60]. Analyzing the Gamma pass rate makes it possible to determine the number of reference points that satisfy these criteria.

The parameters that are used for simulation can be viewed in Table 3.1.

The treatment plan that is irradiated and measured using the MatriXX PT is based on one 4DCT. However, for some patients, multiple 4DCTs are available. Usually, these are taken a few weeks after the first 4DCT, when the proton therapy treatment process has already started. This allows the use of motion data of the same patients at different time points. The tumor motion at different time points will be used as input for the interplay simulation model. This will show if the treatment plan was robust not only for the treatment-planning 4D-CT but also for the different motion scenarios that might be encountered during proton therapy.

| **Parameter** | **Value** |
|---|---|
| Frame Time [s] | 0.04 |
| Number of Simulated Fractions | 30 |
| Number of Repetitions | 100 |
| Resampling Resolution X and Y [mm] | 1 |
| Gamma dose difference [%] | 2 |
| Gamma distance to agreement [mm] | 2 |

Table 3.1: **The most important simulation parameters in the interplay simulation script. For a more elaborate overview of the parameters, see Table A.1 in the Appendix.**

In each treatment fraction for every simulated treatment beam, the Gamma index is calculated for all reference points, and the Gamma pass rate is recorded. To illustrate this, consider an example involving patient 1, who is undergoing proton therapy for lymphoma. Patient 1 receives a total of 17 treatment fractions, with each fraction involving the delivery of two beams.

During the first fraction, the motion data of the Clinical Target Volume (CTV) obtained from the initial 4D-CT scan is applied to the MatriXX PT measurements corresponding to the first beam of the treatment plan. The motion starts from a random position within the breathing cycle, simulating the absence of breath-hold techniques or precise breath-timing methods.

Only the initial breathing phase is changed for subsequent fractions, while other factors remain the same. **The reference dose distributions and comparison dose**

**distributions are once again compared, and the agreement is quantified using the Gamma pass rate.**

This is repeated for the next fraction, and the dose distributions are accumulated. This is repeated for 17 fractions until all 17 fractions have been simulated. This way, an entire treatment is simulated. This entire treatment simulation is repeated 100 times to capture variation in the initial breathing phase of every fraction and its cumulative effect.

Intrafraction respiratory amplitude variation or baseline shift was not considered in this thesis. The interfraction (day-to-day variation) respiratory amplitude shift is considered by using tumor motion data of 4D-CTs (that are taken after the original planning 4D-CT.)

### 3.1.5 Gamma index metrics

Each treatment is simulated 100 times, and each of these simulations yields a unique Gamma pass rate graph. To make comparisons regarding the combination of these 100 simulations, several Gamma index metrics have been created. These are selected to quantify both the average and worst-case simulation results.

**Last fraction below threshold** An important value that's at the basis of each of these custom metrics is the ***last fraction below threshold*** (LFBT).
The Gamma pass rate (a score between 0 and 100%) is a score that indicates how much two dose distributions 'match'. In the context of this thesis, it is used to compare the static dose measurement to the simulated moving dose measurement. The dose distribution of the second fraction is equal to the first fraction's simulation plus the second fraction's simulation, etc. The Gamma pass rate of each of the simulations is calculated.

Generally, the more fractions are simulated, the more the Gamma pass rate tends to increase toward 100%. In each simulation, if the Gamma pass rate starts below the threshold (95%) at fraction one and is above this value after the last fraction, the last fraction where the Gamma pass rate was below this value is recorded. This value is defined as the last fraction below threshold, the LFBT.
If the Gamma pass rate is above the threshold in every fraction, the LFBT is 0. If the Gamma pass rate is below the threshold of 95% after the last fraction, the LFBT is equal to the number of delivered fractions (between 10 and 30, patient- and tumor-specific).

Since each simulation results in a single LFBT value and 100 simulations are performed of each treatment beam and the corresponding tumor motion, statistical analysis can be applied to all the sets of LFBT values.

From the Gamma pass rate of each treatment beam, three important parameters are extracted:

- Mean last fraction below threshold
- Median last fraction below threshold
- $90^{th}$ percentile last fraction below threshold.

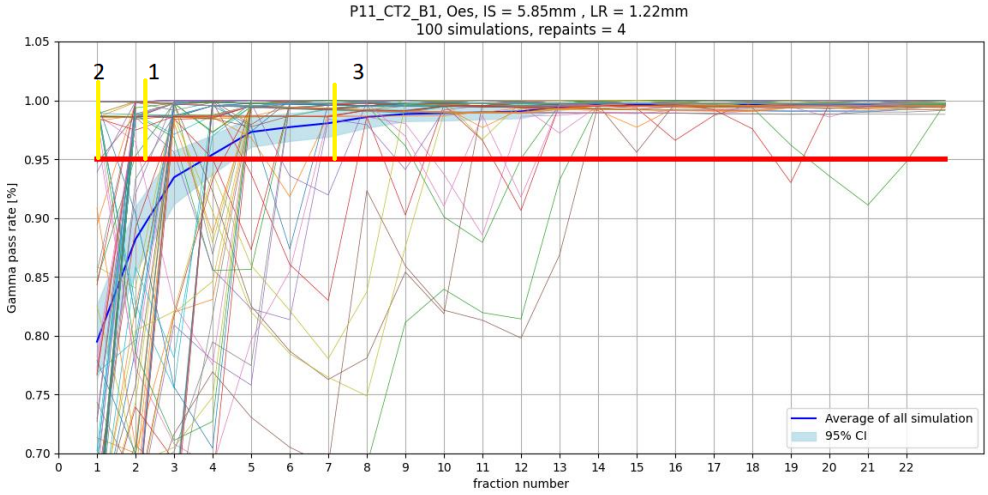


Figure 3.5: **Example of the Gamma index metrics, explained in section 3.1.5 Gamma index metrics.**
**For each beam, a simulation with several fractions was performed (thin lines). For each treatment simulation, the last fraction with a Gamma pass rate below the threshold of 95% was recorded. The following metrics are extracted and indicated in the figure:**
**1: Mean LFBT: 2.17**
**2: Median LFBT: 1**
**3: 90th percentile of LFBT: 7.1**

### Mean last fraction below threshold

The mean LFBT indicates the average last fraction that is below the threshold of all simulations.

### Median last fraction below threshold

The median of the LFBT, which corresponds to the 50th percentile, represents the value where an equal number of simulations have a higher or lower LFBT.

### 90th percentile of last fraction below threshold

This is the last fraction number where 90% of all simulations are below the threshold. This means that after this fraction, 90% of all simulations meet the requirement.

Figure 3.5 gives an example of the values. The thick blue lines indicate the mean Gamma pass rate of all simulations.

### Clinical evaluation criteria [1]

[1] During the final week of writing this thesis, I discovered the criteria for interplay robustness I use is slightly different from the one that is used by the clinical physicists in Holland PTC. After comparing both methods, the decision was made to continue with the 90th percentile LFBT methods as described here since the differences were small. See chapter E Different robustness criteria for the comparison

The Gamma pass rate of a patient's treatment plan is required to meet the criteria of 95% at the end of the patient's treatment scheme. For this reason, a treatment beam is considered robust against the interplay effect if the 90th percentile LFBT is equal to or smaller than the number of prescribed fractions. This means that in 90 out of 100 simulations, the fractionation scheme reached the threshold before the end of the patient's treatment.

### Repainting

Repainting has been applied in 7 of the 18 patients (Table 3.2). These patients' data have been separated to investigate the influence repainting has on interplay robustness. Correlation plots have been created using a sigmoid fit.

## Obsolete Approaches

During my internship, three methods to model tumor motion amplitude more elaborately were attempted that were later discarded. The first was using the center of mass of the CTV to model tumor motion. The second was by tracking the voxel motion during ten phases and taking a certain percentile of voxel motion between the consecutive phases. This one is called the percentile motion method. The third method consisted of tracking each voxel's coordinates in all then phases using the deformation vector information, called the voxel tracking method. After validating the methods, the results of all three methods were deemed insufficient. The methods were discarded. For the explanation of the method, the validation, and the reason for discarding, see Appendix C Obsolete Approaches.

results.

## 3.2 Results clinical evaluation

**Disclaimer**:
As discussed in the outline of this report and in chapter 5 Unvalidated script, the discovery was made that the results from the script used throughout this thesis differ greatly from the clinically validated script.
The outcomes presented in section 3.2.1 Tumor motion extraction remain unaffected by the unverified script's output. All outcomes within section 3.2.1 paragraph Examples and subsequent sections within this chapter are outdated.
. While the clinical implications of these results are obsolete, the results are left in to show the thought process.
For a comparison between both scripts, see chapter 5 Unvalidated script.

### 3.2.1 Tumor motion extraction

For an overview of the patient information and tumor motion amplitudes, see Table 3.2 and Table A.2 in the appendix.

**Scans excluded** One of the 4D-CTs of P06 (P06_CT2) had an amplitude that was a factor 10 to 20 smaller in all three directions as compared to the other four 4D-CTs of the same patient. This 4D-CT scan was excluded for that reason.

The fifth 4D-CT of P05 was also excluded because deformable registration yielded errors that could not be resolved, even after multiple attempts.

In two of P15's 4D-CTs, no CTV had been delineated. These were also excluded. All the scans and information in Table A.2 are included in the results of this thesis.

| Pt ID | Tumor type | Nr of beams | Nr of fractions prescribed | Nr of repaints | CTV Volume [$mm^3$] † | Nr 4D-CTs ‡ | Tumor location | Prescribed dose [cGy] |
|---|---|---|---|---|---|---|---|---|
| 1 | Lymp | 2 | 17 | 1 | 328,71 | 2 | ant med | 3060 |
| 2 | Lymp | 4 | 10 | 1 | 140,83 | 2 | hilar L R, med | 2000 |
| 3 | Lymp | 2 | 15 | 1 | 204,93 | 2 | supraclav R, med | 3000 |
| 4 | Lung | 3 | 24 | 1 | 295,08 | 6 | LUL | 6600 |
| 5 | Oes | 2 | 28 | 1 | 313,25 | 6 | mid | 5040 |
| 6 | Oes | 2 | 23 | 4 | 328,79 | 5 | dist | 4140 |
| 7 | Oes | 2 | 23 | 4 | 106,95 | 2 | dist | 4140 |
| 8 | Lung | 3 | 24 | 1 | 82,48 | 5 | RUL | 6600 |
| 9 | Oes | 2 | 23 | 4 | 231,52 | 5 | dist | 4140 |
| 10 | Lung | 3 | 24 | 5 | 66,34 | 5 | RUL | 6600 |
| 11 | Oes | 2 | 23 | 4 | 355,73 | 5 | dist | 4140 |
| 12 | Oes | 3 | 28 | 1 | 140,65 | 6 | mid | 5040 |
| 13 | Oes | 3 | 23 | 4 | 124,06 | 1 | mid | 4140 |
| 14 | Oes | 3 | 23 | 4 | 424,04 | 2 | dist | 4140 |
| 15 | Lung | 3 | 30 | 1 | 416,26 | 4 | RUL | 6000 |
| 16 | Lymp | 2 | 18 | 1 | 112,81 | 3 | med | 3600 |
| 17 | Lymp | 3 | 15 | 1 | 147,75 | 2 | L R supra- and infra-clav, med | 3000 |
| 18 | Lymp | 2 | 15 | 1 | 95,85 | 2 | med | 3000 |

Table 3.2: **Overview of the patients used in this study. oes = oesophageal cancer patient, lung = lung cancer patient, lymph = lymphoma cancer patient.**
**†: on planning CT, Fin phase**
**‡: 4D-CTs available with CTV delineated in at least one phase**
**When Nr of repaints is 1, it means that all layers have been irradiated once, so essentially no repainting was applied.**
**Tumor location abbreviations: ant = anterior, med = mediastinum, LUL = left upper lobe, RUL = right upper lobe, dist = distal, clav = clavicular.**

**Tumor motion amplitude** Table A.2 in the appendix shows the tumor motion amplitude in the three primary directions after correction for beam rotation. The SI amplitude of one 4D-CT does not change as the beam rotates.

However, in some patients, there is quite some variation in tumor motion amplitude. Consider P06, for example: The CTV motion in SI direction in each consecutive 4D-CT is 6.61 mm, 12.57 mm, 7.93 mm, and 12.53 mm, respectively.
In P08, the SI motion is between 3.18 mm and 4.12 mm in the first four 4D-CTs but drops to 0.75 mm in the last 4D-CT. While research [43], [44] discussed in section 1.6 Interfraction motion suggest some interfraction change in tumor motion amplitude is possible, the severe fluctuations seen in P06 seem unrealistic. More likely, this results from a discrepancy in delineation between different 4D-CTs.

The delineations were checked by the author, but no unexplained abnormalities could be detected. The decision was made to include the 4D-CT data and it's corresponding tumor motion in the thesis.

### Examples

Some examples of Gamma index metrics graphs can be seen in figures B.1, B.2, and B.3 in the appendix. For each beam, a separate graph is created. Each thin line in these figures shows the Gamma pass rate as the simulation progresses through the number of fractions. Due to the tendency of fractionation in radiotherapy to yield a more homogeneous dose distribution, an upward shift in the Gamma pass rate can be anticipated within a single treatment simulation. This is generally the case, especially looking at the mean line (dark blue). In some beams (B.2), almost all the simulations reach a Gamma pass rate of over 95% during the first fraction. In others, the cumulative Gamma pass rate rapidly fluctuates with every fraction number (B.3).

## 3.2.2 Clinical evaluation

Figure 3.6 shows the correlation between 2D tumor motion and the three Gamma index metrics. The data confirm that there is a strong correlation between the tumor motion amplitude and the plan's robustness against the interplay effect.

Figure B.4 and B.5 in the appendix show the correlation between the Gamma index metrics and the LR and SI motion, respectively. There is a strong correlation between most Gamma index metrics and the SI motion. However, the correlation between the LR motion and the Gamma index metrics is weak in all cases.

### Clinical evaluation per tumor type

Tables B.3, B.2 and B.1 show the Gamma index metrics and the tumor motion amplitude in the three primary directions and the 2D direction.

Figure 3.6 visualizes the same Gamma index metrics data. It shows the correlation between a patient beam's tumor motion and the three Gamma index metrics, separated by tumor type. The red X's show the beams where the metric on the y-axis is equal to the number of fractions prescribed in that patient's treatment plan. The N in these subplots' titles represents the number of beams that are simulated for that specific tumor type. Keep in mind that the total number of beams for a single patient is calculated by multiplying the number of beams specified in the treatment plan by the count of available 4D-CT scans for that particular patient (section 3.1.1). [2]

As explained in section 3.1.4 Clinical evaluation, a beam is considered robust for the interplay effect if the 90th percentile of the last fraction below threshold (LFBT) is smaller than the number of prescribed fractions. In other words, the beam should reach the Gamma pass rate threshold of 95% before the last fraction's end in 90 out of 100 simulations.

[2] Figure 3.6 shows the same data as figure B.6 in the appendix, but also split into the three tumor groups and only taking the 2D motion into account. Figure B.7 in Appendix B shows the same data as figure 3.6 but with a sigmoid correlation line instead of a linear one.

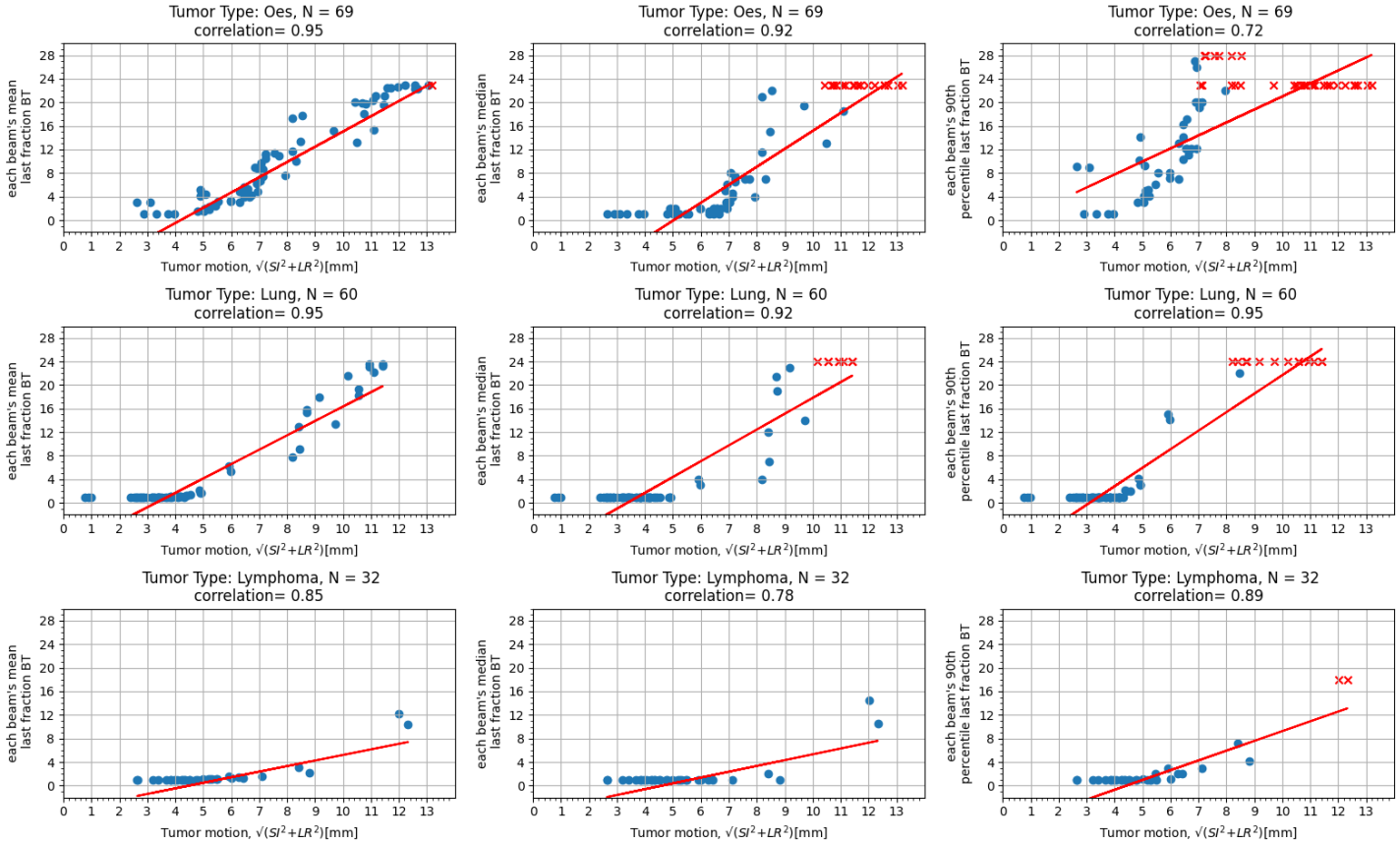


Figure 3.6: **Correlation between 2D tumor motion of all three tumor types and the three primary Gamma index metrics. Each data point depicts one of the 161 beams. The red X's show the beams where the corresponding metric is equal to the number of fractions prescribed in that patient's treatment plan.**

**Esophagus patients** For esophagus patients (Table B.1 and figure 3.6 top row), results are diversified.
Beams with tumor motion amplitudes between 7 and 13.5 mm do not always reach the threshold for clinical acceptance. Between 6 and 8 mm 2D tumor motion amplitude, the value for each beam's 90th percentile LFBT increases rapidly. The data suggests that when the 2D Tumor motion amplitude is below 6 mm, the influence of the interplay effect on plan quality is of little impact. However, when it increases beyond 6 mm, interplay robustness rapidly decreases.

**Lung patients** Table B.2 and figure 3.6, middle row, shows all lung patients' beams are sufficiently robust against the interplay effect, except for patient 10. This patient has a significantly higher tumor motion amplitude in all 4D-CTs.

Figure 3.6 shows that for lung patients, the interplay effect is of little influence on plan robustness for amplitudes $< 5$ mm. However, in all beams with a CTV amplitude greater than 8 mm, the 90th percentile of the LFBT did not reach 95% after the number of prescribed fractions was delivered, with one exception. Since there are only two beams with a CTV amplitude between 5 and 8 mm (P04_CT4_B2 and P04_CT4_B3), generalizations regarding tumor motion amplitude between 5 and 8 mm should be cautiously approached.

**Lymphoma patients** For all lymphoma patients (Table B.3 and figure 3.6 bottom row), the 90th percentile metric shows the plan is robust against the interplay effect. The only exceptions are both beams of patient 16's second repeat-CT (P16_CT2_B1 and P16_CT2_B2). The tumor motion in this 4D-CT is significantly higher than that of patient 16's other 4D-CTs and all other lymphoma patients. These beams are the two data points on the far right in figure 3.6.

Figure 3.6 suggests that for lymphoma patients with a 2D amplitude below 9 mm, the influence the interplay effect has on the interplay robustness is small.

### 3.2.3 Patient-specific clinical evaluation

Besides tumor group-based clinical evaluation, patient-specific clinical evaluation is also essential.

Remember the criterion set for interplay robustness: A treatment beam is considered robust against the interplay effect if the 90th percentile LFBT is equal to or smaller than the number of prescribed fractions.

Table 3.3 shows for each patient's 4D-CT's tumor motion whether the beams meet the requirement set in section 3.1.4 Clinical evaluation: is the 90th percentile last fraction below threshold (LFBT) equal to or smaller than the number of prescribed fractions? The beam is robust against the interplay effect if the answer is yes.

The different 4D-CTs of each patient (e.g., P05_CT0 up to P05_CT4) yield different tumor motion amplitudes that are applied to the measured beam data. As explained in section 3.2.2, there is a strong correlation between the Gamma index metrics and the 1D (SI) and 2D tumor motion.

In some patients, it is clear that each beam and the entire treatment plan is robust against interplay:
In P01, P02, P03 (Figure B.1 in Appendix B), P04(Figure B.2 in Appendix B), P05, P08, P15, P17 and P18, all treatment beams have a 90th percentile LFBT that occurs before the end of the treatment. This is 50% of the patient group.

For P06, P07, P09, P11, P12, P14, and P16, the beams were robust in some tumor motion scenarios and not others. This is 38.8% of the patient group.

In P13 (Figure B.3 in Appendix B), none of the beams are robust. It is important to note that no repeat 4D-CTs are taken in the case of P13, so only one motion scenario has been simulated.
Only one of the total 15 beams of P10 is robust against the interplay effect.

Out of the eighteen patients, only in three cases, all beams are not robust when the tumor motion is derived from CT0, the planning 4D-CT.

| PT ID | beam nmb | 90th perc LFBT reached | all beams reach criterium |
|---|---|---|---|
| P01_CT0 | B1 | Yes | Yes |
| | B2 | Yes | |
| P01_CT1 | B1 | Yes | Yes |
| | B2 | Yes | |
| P02_CT0 | B1 | Yes | Yes |
| | B2 | Yes | |
| | B3 | Yes | |
| | B4 | Yes | |
| P02_CT1 | B1 | Yes | Yes |
| | B2 | Yes | |
| | B3 | Yes | |
| | B4 | Yes | |
| P03_CT0 | B1 | Yes | Yes |
| | B2 | Yes | |
| P03_CT1 | B1 | Yes | Yes |
| | B2 | Yes | |
| P04_CT0 | B1 | Yes | Yes |
| | B2 | Yes | |
| | B3 | Yes | |
| P04_CT1 | B1 | Yes | Yes |
| | B2 | Yes | |
| | B3 | Yes | |
| P04_CT2 | B1 | Yes | Yes |
| | B2 | Yes | |
| | B3 | Yes | |
| P04_CT3 | B1 | Yes | Yes |
| | B2 | Yes | |
| | B3 | Yes | |
| P04_CT4 | B1 | Yes | Yes |
| | B2 | Yes | |
| | B3 | Yes | |
| P04_CT5 | B1 | Yes | Yes |
| | B2 | Yes | |
| | B3 | Yes | |
| P05_CT0 | B1 | Yes | Yes |
| | B2 | Yes | |
| P05_CT1 | B1 | Yes | Yes |
| | B2 | Yes | |
| P05_CT2 | B1 | Yes | Yes |
| | B2 | Yes | |
| P05_CT3 | B1 | Yes | Yes |
| | B2 | Yes | |
| P05_CT4 | B1 | Yes | Yes |
| | B2 | Yes | |
| P06_CT0 | B1 | Yes | Yes |
| | B2 | Yes | |
| P06_CT1 | B1 | No | No |
| | B2 | No | |
| P06_CT3 | B1 | Yes | No |
| | B2 | No | |
| P06_CT4 | B1 | No | No |
| | B2 | No | |

| PT ID | beam nmb | 90th perc LFBT reached | all beams reach criterium |
|---|---|---|---|
| P07_CT0 | B1 | Yes | Yes |
| | B2 | Yes | |
| P07_CT1 | B1 | No | No |
| | B2 | No | |
| P08_CT0 | B1 | Yes | Yes |
| | B2 | Yes | |
| | B3 | Yes | |
| P08_CT1 | B1 | Yes | Yes |
| | B2 | Yes | |
| | B3 | Yes | |
| P08_CT2 | B1 | Yes | Yes |
| | B2 | Yes | |
| | B3 | Yes | |
| P08_CT3 | B1 | Yes | Yes |
| | B2 | Yes | |
| | B3 | Yes | |
| P08_CT4 | B1 | Yes | Yes |
| | B2 | Yes | |
| | B3 | Yes | |
| P09_CT0 | B1 | Yes | Yes |
| | B2 | Yes | |
| P09_CT1 | B1 | No | No |
| | B2 | No | |
| P09_CT2 | B1 | Yes | Yes |
| | B2 | Yes | |
| P09_CT3 | B1 | No | No |
| | B2 | No | |
| P09_CT4 | B1 | No | No |
| | B2 | No | |
| P10_CT0 | B1 | No | No |
| | B2 | No | |
| | B3 | No | |
| P10_CT1 | B1 | No | No |
| | B2 | No | |
| | B3 | No | |
| P10_CT2 | B1 | No | No |
| | B2 | No | |
| | B3 | No | |
| P10_CT3 | B1 | No | No |
| | B2 | No | |
| | B3 | No | |
| P10_CT4 | B1 | No | No |
| | B2 | No | |
| | B3 | Yes | |
| P11_CT0 | B1 | Yes | No |
| | B2 | No | |
| P11_CT1 | B1 | No | No |
| | B2 | No | |
| P11_CT2 | B1 | Yes | Yes |
| | B2 | Yes | |
| P11_CT3 | B1 | No | No |
| | B2 | No | |
| P11_CT4 | B1 | Yes | No |
| | B2 | No | |

| PT ID | beam nmb | 90th perc LFBT reached | all beams reach criterium |
|---|---|---|---|
| P12_CT0 | B1 | Yes | Yes |
| | B2 | Yes | |
| | B3 | Yes | |
| P12_CT1 | B1 | Yes | Yes |
| | B2 | Yes | |
| | B3 | Yes | |
| P12_CT2 | B1 | No | No |
| | B2 | No | |
| | B3 | Yes | |
| P12_CT3 | B1 | Yes | No |
| | B2 | No | |
| | B3 | Yes | |
| P12_CT4 | B1 | No | No |
| | B2 | No | |
| | B3 | No | |
| P12_CT5 | B1 | Yes | No |
| | B2 | No | |
| | B3 | Yes | |
| P13_CT0 | B1 | No | No |
| | B2 | No | |
| | B3 | No | |
| P14_CT0 | B1 | Yes | Yes |
| | B2 | Yes | |
| | B3 | Yes | |
| P14_CT1 | B1 | No | No |
| | B2 | No | |
| | B3 | No | |
| P15_CT0 | B1 | Yes | Yes |
| | B2 | Yes | |
| | B3 | Yes | |
| P15_CT1 | B1 | Yes | Yes |
| | B2 | Yes | |
| | B3 | Yes | |
| P15_CT2 | B1 | Yes | Yes |
| | B2 | Yes | |
| | B3 | Yes | |
| P15_CT3 | B1 | Yes | Yes |
| | B2 | Yes | |
| | B3 | Yes | |
| P16_CT0 | B1 | Yes | Yes |
| | B2 | Yes | |
| P16_CT1 | B1 | Yes | Yes |
| | B2 | Yes | |
| P16_CT2 | B1 | No | No |
| | B2 | No | |
| P17_CT0 | B1 | Yes | Yes |
| | B2 | Yes | |
| | B3 | Yes | |
| P17_CT1 | B1 | Yes | Yes |
| | B2 | Yes | |
| | B3 | Yes | |
| P18_CT0 | B1 | Yes | Yes |
| | B2 | Yes | |
| P18_CT1 | B1 | Yes | Yes |
| | B2 | Yes | |

Table 3.3: **Shows for each of the patients' treatment beam whether the beam meets the requirement of having a 90th percentile LFBT that is less than the number of prescribed fractions. In other words,**
**Perc= percentile. LFBT = last fraction below threshold.**
**See Table B.3, B.2 and B.1 in Appendix B for the underlying data.**

### 3.2.4 Repainting

In a number of esophagus and lung cancer patients, repainting has been used as a measure to make the treatment plan more robust against interplay (Table 3.2). For an explanation of repainting, see section 1.6.1 paragraph Repainting.

Figure 3.7 shows the correlation between IS tumor motion and the three Gamma index metrics, separated for patients who are not repainted.

Even though repainting is applied to patients with a CTV motion in SI direction of 5 mm or more, some beams in figure 3.7 have a higher amplitude yet have not been repainted. This is because the decision to use repainting is based on tumor motion data from the planning 4D-CT, CT0. If the patient's SI CTV motion increases beyond 5 mm during treatment, the protocol does not require repainting to be applied [63].

Lymphoma patients have been excluded from figure 3.7 because according to Holland PTC repainting protocol, repainting is only applied in the case of lung patients and esophagus patients with a CTV motion $> 5$ mm in SI direction, and only in the planning 4D-CT [63].

The red lines show the correlation regression line of the blue data points with a sigmoid function. A line that is less steep and has a lower maximum value to which it converges indicates greater robustness against the interplay effect.
Most data points of the repainting group in figure 1.13 are below the sigmoid correlation line of the no-repainting group. This suggests that plans in which repainting has been applied are more robust against the interplay effect than when repainting has not been applied.

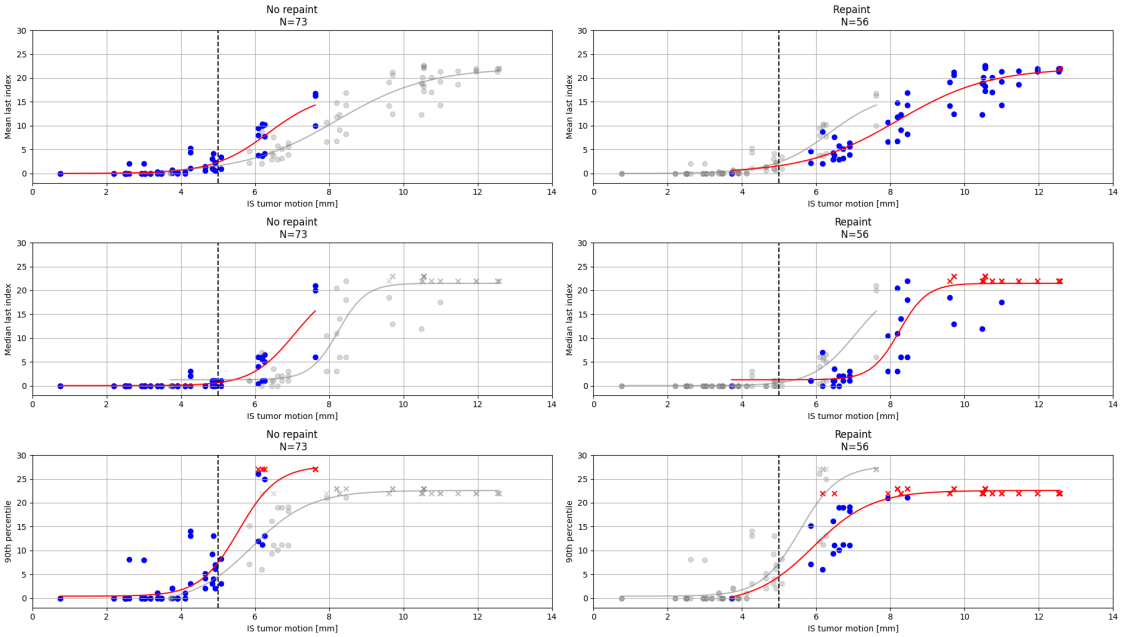


Figure 3.7: **All lung and esophagus patients' SI motions were plotted against the three primary Gamma index metrics. The black dashed line (5mm) is the cut-off value clinically used to decide whether or not to use repainting. The grey data points and line in the left plot correspond to the blue data points and line in the right plot, and vice versa. Red X's show the beams with a corresponding Gamma index metric equal to or higher than the prescribed number of fractions. The gray dots represent the data of the adjacent graph.**

# Chapter 4

# Factors influencing the interplay effect

## 4.1 Methods

Besides the tumor motion amplitude, there could be other factors that influence the robustness against the interplay effect. To answer the second goal of this thesis, many beam- and patient parameters have been collected to assess the impact of these parameters on the quality of the plans. Tumor motion amplitudes have been adjusted to investigate the effect of different tumor motion amplitudes on interplay robustness.

#### Artificial amplitude

A different round of simulations was performed to assess if the variation of the Gamma pass rate was entirely based on the tumor motion or if this also depends on plan characteristics. All parameters in Table 3.1 were maintained in these simulations. All the tumors' motion amplitudes were changed: [SI, LR] = [4, 2], [6, 3], [8, 4], [10, 5], [12, 6], and [16, 8], all in mm. These values were picked because they represent the range of tumor motion found in patients.

This way, all treatment plans were simulated with the exact same motion. This eliminated the influence of differences in the tumor motion on the Gamma pass rate. The only factors that could influence the Gamma pass rate are the characteristics of a treatment plan.

The resulting Gamma index metrics, as discussed in section 3.1.4 Clinical evaluation, were compared to their real tumor motion counterpart

#### Unidirectional amplitude

Results of the artificial amplitude showed a discrepancy: when tumor motion amplitudes were manually set, the Gamma index metrics were lower (indicating greater robustness) than when real patients' tumor motion amplitude was used as input, even when the artificial amplitude was similar to the real patients' amplitude.

To investigate if either the SI or LR motion had a stronger effect on interplay robustness, additional simulations were performed. In these simulations, SI tumor motion amplitude was set at 5, 7.5, 10, 12.5, and 15 mm, while LR motion was set to 0. Likewise, simulations were performed with the LR motion ranging from 5 to 15 while the SI motion was set to 0.

This could indicate if either the SI or LR tumor motion had a stronger effect on the interplay robustness.

Since simulations of all patient beams require great computational power, simulations are only performed on P01, P03, P04, P06, P07, P11, and P14. These patients' data were picked because they included both patients with high and low robustness against the interplay effect (Table 3.3).

### Influence of later CTs on Gamma index metrics

The time between the initial planning 4D-CT (CT0) and subsequent repeat 4D-CTs has been compared to the change of the Gamma index metrics of these later 4D-CTs to see if there is a correlation (Pearson product-moment correlation).

### Influence of later CTs on tumor motion

The time between the initial planning 4D-CT (CT0) and subsequent repeat 4D-CTs has been compared to the change in tumor motion amplitude of these later 4D-CTs. This might show the degree of change in tumor motion amplitude.
Factors influencing this might be changes in body composition, shrinking or enlargement of the tumor, changes in the breathing cycle, or subtle changes in patient positioning on the table.

### Simulations with 100 fractions

In about half the patients, interplay robustness was not reached after the prescribed number of fractions. If a patient received 28 fractions, no more than 28 simulations were performed and analyzed.

For all patients, simulations have been performed in which patients were simulated to receive 100 fractions instead of their clinically prescribed number

The goal of this was to determine if the Gamma pass rate converges towards 100% or if, which a high enough tumor motion amplitude, the Gamma pass rate converges to a smaller value. Each beam's simulation is still repeated 100 times, but the simulations now continue up to 100 fractions.

Results are discussed in section 100 fractions in Appendix B.

## 4.2 Results factors influencing interplay effect

**Disclaimer**:
As discussed in the outline of this report and in chapter 5 Unvalidated script, the discovery was made that the results from the script used throughout this thesis differ greatly from the clinically validated script.
The sections Artificial amplitude, Unidirectional amplitude and the part in section Influence of later CTs on Gamma index metrics and tumor motion discussing change in Gamma index metrics all use data based on the unvalidated script's output. While the clinical implications of these results are obsolete, the results are left in to show the thought process.

Results from section SI:LR ratio and the part in section Influence of later CTs on Gamma index metrics and tumor motion focussing on change in tumor motion amplitude are independent of the unvalidated script's output.

For a comparison between both scripts, see chapter 5 Unvalidated script.

**Artificial amplitude** Figure 4.1 shows the three primary Gamma index metrics (mean last fraction below 95% threshold (LFBT), median LFBT, and 90th percentile LFBT) against the artificial tumor motion amplitude ([SI, LR] = [4, 2], [6, 3], [8, 4], [10, 5], [12, 6] and [16, 8]), all in mm. Note that the amplitude values in figure 4.1 are the 2D amplitude, so $\sqrt{(SI^2 + LR^2)}$.

The red number above each boxplot shows the fraction of beams with that specific tumor motion amplitude with a corresponding Gamma index metric equal to the number of fractions prescribed to that patient. For example, looking at the 90th percentile LFBT for lymphoma patients (bottom right), in 14 out of 32 patients (44%), the 90th percentile of LFBT has not been reached at the end of the patient's treatment.

Up to and including 11.18 mm (10 by 5 mm) tumor motion amplitude, the mean LFBT and median LFBT results were very similar for all three tumor types. At a tumor motion amplitude of 13.42 mm (similar to the maximum 2D amplitude observed in real patients' CTV motion), all three tumor types have a mean and median LFBT below the prescribed number of fractions.

The 90th percentile LFBT was chosen as the primary metric to determine if a treatment beam is considered robust against the interplay effect (See section 3.1.4 Clinical evaluation). If the 90th percentile LFBT was below the number of prescribed fractions, that means that in 90 out of 100 simulations, the treatment was robust against the interplay effect before the end of the treatment.

In beams that move with an artificial amplitude of 8.94 mm or less, all beams (except one lymphoma patient's beam) reach an adequate level of interplay robustness before the end of their treatment plan in 90 out of 100 simulations.

Comparing figure 3.6 and figure 4.1 yields useful information regarding the influence of tumor motion amplitude on interplay robustness.
Figure 3.6 shows the relationship between the real patients' tumor motion amplitude and the Gamma index metrics. Figure 4.1 shows the same information but with artificial, hand-picked tumor motion amplitudes.

In the real patient amplitude data (figure 3.6), no beams for lung and lymphoma patients' beams (except one) have an adequate 90th percentile LFBT beyond 8 mm tumor motion amplitude. However, when the amplitude is artificially set, all lung and lymphoma patients' beams have an acceptable 90th percentile LFBT at 8.94 mm tumor motion amplitude.

With an artificial amplitude, 85.5% of lymphoma patients' beams and 95% of lung patients' beams still have an adequate 90th percentile LFBT at 11.18 mm.
No esophagus patients with a real amplitude beyond 8 mm reach the Gamma pass rate threshold in 90 of 100 simulations before the end of their treatment. However, when the amplitude of the same treatment plan is artificially set to 8.94 mm, all patients meet this criterion.

This is an important discrepancy that should not be overlooked. When tumor motion amplitude values are manually picked, their Gamma index metrics are different from when

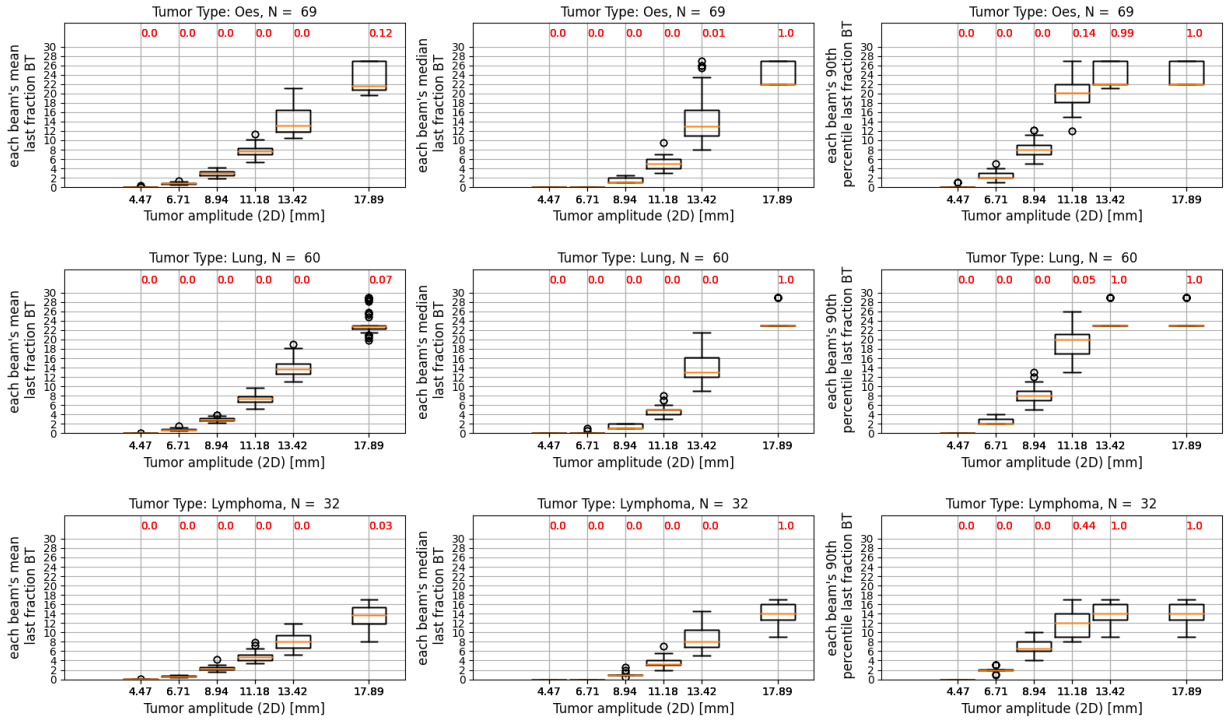


Figure 4.1: **Boxplots showing the three primary Gamma metrics versus the artificial tumor motion amplitude: [SI, LR] = [4, 2], [6, 3], [8, 4], [10, 5], [12, 6] and [16, 8], all in mm.**
**The red number above each boxplot shows the fraction of beams with that specific tumor motion amplitude with a corresponding Gamma index metric that is equal to the number of fractions prescribed to that patient, meaning beams in which the Gamma pass rate threshold was not reached at the end of the treatment (similar to the red X's in figure 3.6).**
**BT = Below Threshold (95% Gamma pass rate)**

they are based on patients' 4D-CTs.

Figure 4.2 shows the 3D render of P02_CT0's CTV in three different viewing directions. This lymphoma patient's clinical target volume consists of many different anatomical regions, starting 3.5 mm above the clavicula and ending at the anterior part of the heart, spanning approximately 155 mm. The tumor motion amplitude, extracted using the *respiratory_amplitude* script, is 3.31 mm in SI direction.
As explained in section 1.6 Organ motion, the treatment plan is based on the internal target volume (ITV), which is the accumulation of the CTV in all ten breathing phases of a 4D-CT. This means that for this specific patient and 4D-CT, 90 percent of the CTV moved 3.31 mm or less during the entire breathing period.

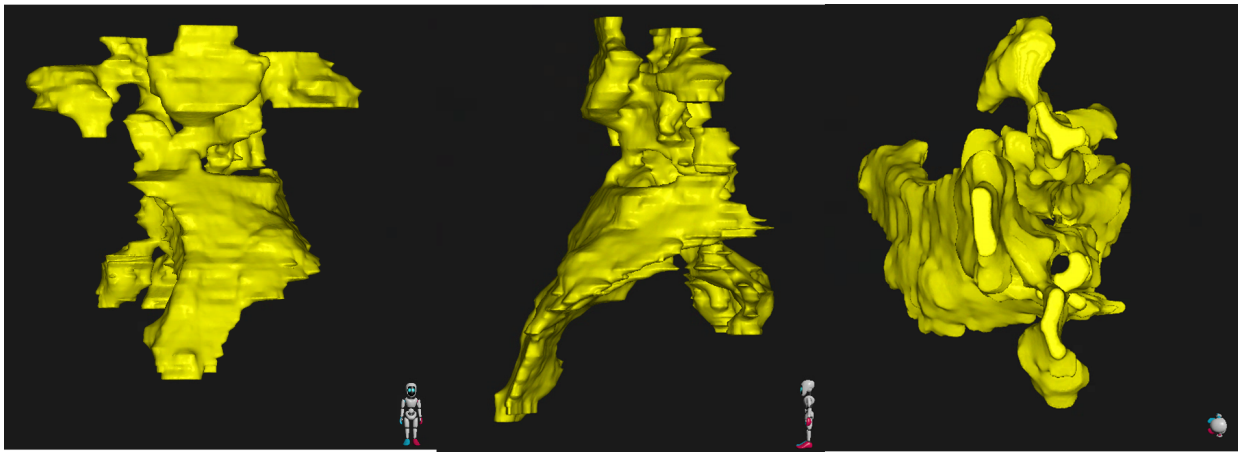

Figure 4.2: **Anterior, lateral and superior view of a 3D render of the CTV of P02_CT0, a lymphoma patient.**

If the tumor normally has an amplitude of 3.31 mm, artificially setting the amplitude to much higher values, up to 17.89 mm, would intuitively decrease interplay robustness; the treatment beam undergoes an amplitude much higher than what it was designed for. This does not explain the discrepancy of the increased interplay robustness when the amplitude is artificially increased.

**Unidirectional amplitude** Figure 4.3 displays the Gamma index metrics for 53 beams. The blue bars on the right represent the Gamma index metrics when the SI motion is varied from 5 to 15 mm while keeping the LR motion fixed at 0. Conversely, the green bars on the left represent the Gamma index metrics when the LR motion is varied from 5 to 15 mm, with the SI motion set at 0 mm.

Regardless of the direction of motion—whether it is in the superior-inferior (SI) or left-right (LR) direction—there appears to be no significant difference in its influence on interplay robustness. This observation holds true even at higher motion amplitudes, suggesting that the direction of motion does not play a substantial role in affecting interplay robustness.

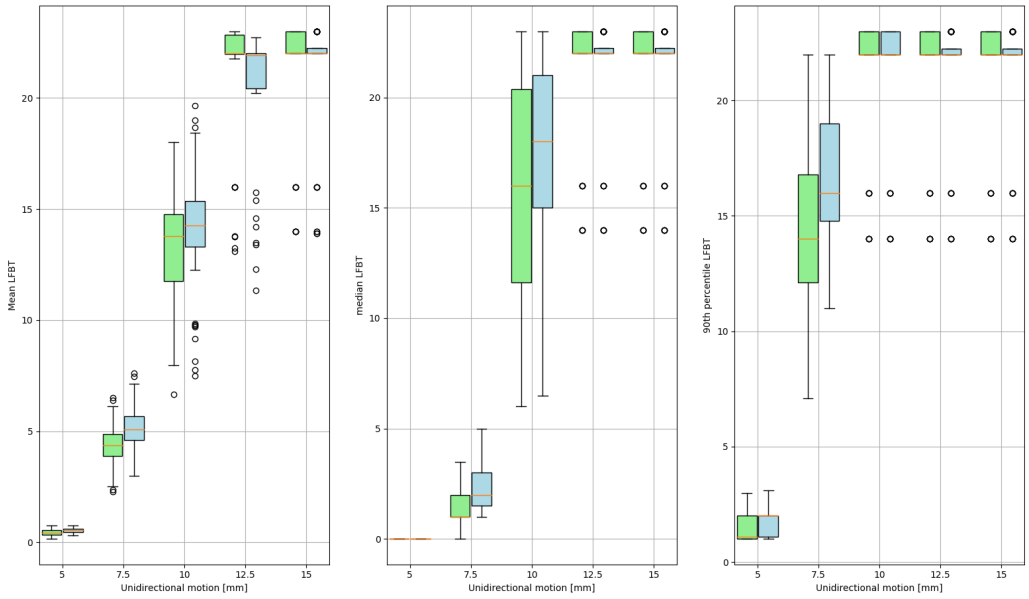


Figure 4.3: **Comparing the Gamma index metrics of the tumor motion amplitude is artificially set in one direction while keeping the other direction amplitude 0 mm. Blue: Tumor motion is only in SI direction. Green: Tumor motion is only in LR direction.**

### Influence of later CTs on Gamma index metrics and tumor motion

The influence of later CTs on Gamma index metrics and tumor motion is discussed in appendix B Other results, in paragraph Time since planning CT vs change in Gamma index metrics and Time since planning CT vs change in tumor motion amplitude respectively.

The average change in tumor motion amplitude between CT0 and all of the later 4D-CTs is 1.16 mm, 0.64 mm, 0.64 mm, and 1.53 mm in SI, LR, AP, and 3D direction, respectively (Figure 4.4).

Note that if from one patient multiple 4D0-CTs are taken, the change in tumor motion is relative to CT0, not to the previous 4D-CT.

These results regarding the change in Gamma index metrics as a result of time were not used in answering the research questions of this thesis.

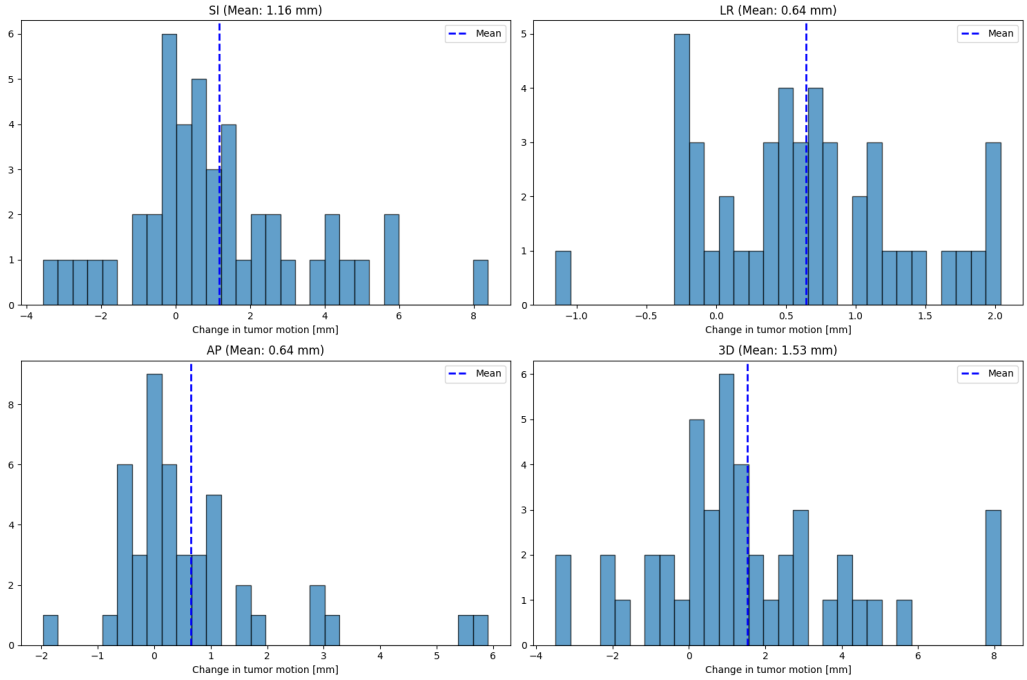


Figure 4.4: **Change in tumor motion between a patient's CT0 and later 4D-CTs. 45 values total per histogram, one for each 4D-CT after CT0. Note that if from one patient multiple 4D0-CTs are taken, the change in tumor motion is relative to CT0, not to the previous 4D-CT.**

**SI:LR ratio** Figure 4.5 shows the ratio between the SI tumor motion and its corresponding (absolute) LR tumor motion. Note that in these ratios, the LR amplitude has been corrected for beam rotation. Depending on the combination of the LR amplitude, AP amplitude and the gantry angle, the LR amplitude could become very small. In P09_CT3_B1 in table B.1 in appendix B for example, the tumor motion has an SI amplitude of of 11.46 mm and and LR amplitude of 0.16 mm, resulting in a ratio of 71.6 (capped at 25 in figure 4.5).

Figure B.10 in appendix B shows the same data as figure 4.5, not separated per tumor type.

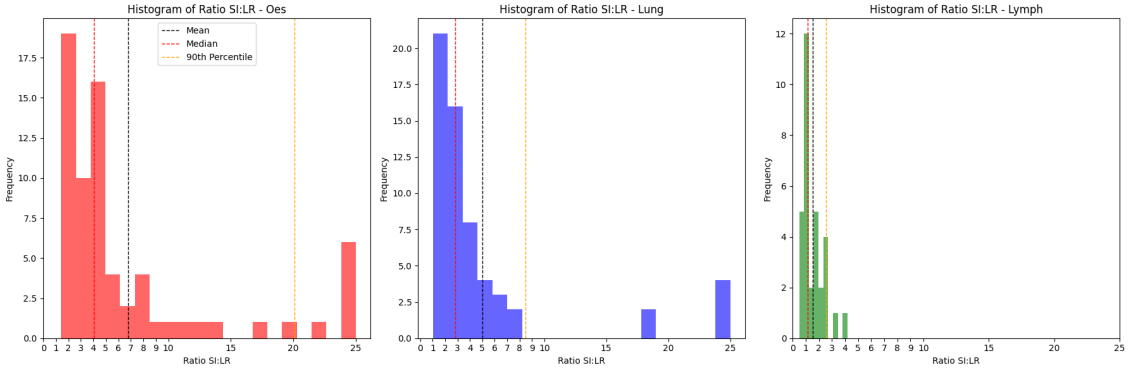


Figure 4.5: **The Ratio between the real patients' SI and LR motion. The LR motion has already been corrected for beam rotation. To handle values above 25 have been capped and grouped into the bin corresponding to the value of 25.**

# Chapter 5

# Unvalidated script

Near the end of thesis completion, clinical physicists noted that the interplay simulation results in my thesis were distinctly different from the results that came from similar interplay simulations performed in the past. For this reason, simulations were repeated using the script that was clinically validated for a few patients with very poor interplay robustness results to roughly compare simulation outcomes. We made sure all simulation- and Gamma parameters were equal. The script that was used throughout this thesis indicated that the patient's treatment beams had a low Gamma pass rate of approximately 20% after 25 fractions. However, when the clinically validated script was used for simulations, the same patient consistently achieved a high Gamma pass rate of over 95% in every treatment fraction.

This has severe implications regarding the conclusions that are drawn in this thesis. From my results, I concluded that in 50% of the patients, the treatment plan was not robust against the interplay effect. This conclusion might be completely wrong in light of the difference in the outcome of the two scripts.

In the clinically validated script, the input variables were given using an interface, as can be seen in figure 5.1.

In the interplay script that was used in this thesis (from here on referred to as derivative script), the interface was omitted. The different Python functions used to construct the sinusoidal signal, perform the simulations, extract Gamma values, etc, are run through a regular Python interface. This allows different treatment beams to be entered and analyzed consecutively. It allowed both SI and LR tumor motion amplitude as input, whereas the clinically validated script only allowed SI amplitude. Also, this resulted in greatly increased computational efficiency because the 161 simulations did not need to be manually started one by one, which is the case with the clinically validated script.

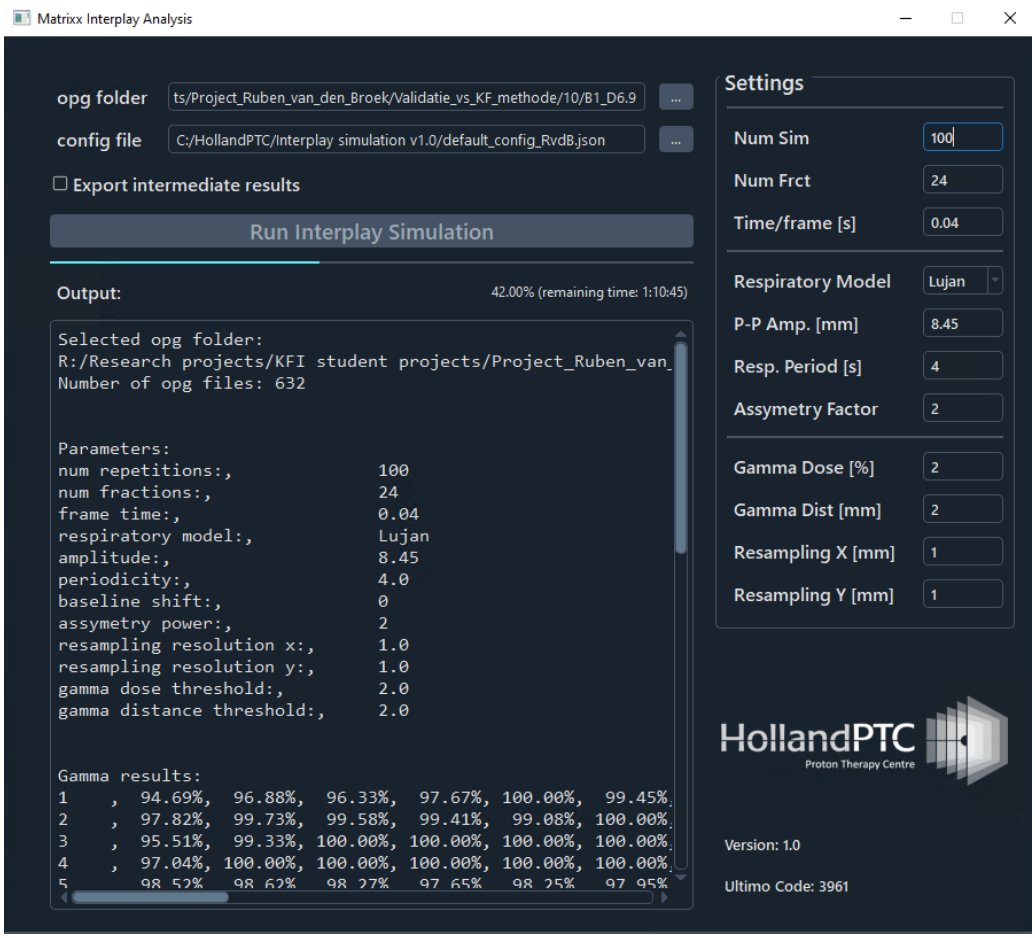


Figure 5.1: **The interface of the clinically validated interplay script. The folder containing the MatriXX PT measurement frames (opg files) can be specified at the top. All relevant parameters can be set on the right. The *config file* input allows for a predefined set of parameters to be chosen. The output is stored as a .csv file, which contains the data visualized in the *Output* frame.**

Mistakingly assuming that the results from the derivative script would mirror those of the clinically validated script, it was decided, due to time limitations, not to replicate all simulations using the clinically validated script.

A thorough manual comparison of the various functions employed in both scripts was undertaken to identify the underlying cause of the substantial discrepancy. This resulted in no obvious differences. Since both scripts are complex scripts with many different functions and dependencies, it would be best to go over the script with the creator to see if the cause of the discrepancies can be found.

**Comparing both scripts** For a few patients, interplay simulations were run using the clinically validated script (table 5.1).

For each of the three tumor groups, a beam was selected that had a SI tumor motion of approximately 4, 7, and 12 mm. These values were chosen because they roughly represent the entire range of tumor motion amplitudes. From these patients, the SI tumor motion was used as input for the clinically validated script. The same data was also run using the derivative script, with the SI amplitude set to the same input value as in the clinically validated script and the LR amplitude set to 0. All other parameters were also equal throughout both sets of simulations. [1]

Table 5.1 shows the input and results of these simulations. Remember the 90th percentile LFBT is the chosen metric to determine interplay robustness; if the 90rth percentile LFBT is smaller than the number of fractions prescribed (#fx), the treatment beam is considered robust. It is clear that the results are vastly different. According to the clinical script, all treatment beams are robust against the interplay script after very few fractions in 90 of 100 treatment simulations.

The responsibility for this error lies solely with the author of this thesis. Since the derivative script was largely based on a clinically validated script, the assumption was made that this validation would also extend to the derivative script. The creator of the derivative script even recommended, in the corresponding email, to double-check the results because he might have made a mistake. I overlooked doing this.

Once these mistakes have been found, corrected, and validated, it would be possible to repeat most of the simulations from this thesis and receive viable results. Almost all figures and tables are automatically generated using Python scripts that only require the output data of the Interplay simulation script as input. The results and discussion would most likely be vastly different.

[1] Lujan asymetry power was set at 2 (resulting in a $sin^4$ motion) and the breathing period was set at 4 s. X and Y resampling was set at 1 mm and Gamma dose thresehold and distance to agreement were kept at 2%/2 mm.

| | SI motion | #fx | 90th perc LFBT, derivative script | 90th perc LFBT, clinical script. |
|---|---|---|---|---|
| Oes | | | | |
| P09_CT2_B2 | 3,72 | 23 | 1 | 1 |
| P14_CT0_B1 | 6,9 | 23 | 12,2 | 1 |
| P13_CT0_B1 | 10,99 | 23 | 23 | 1 |
| Lung | | | | |
| P08_CT2_B3 | 3,9 | 24 | 1 | 1 |
| P10_CT4_B1 | 8,45 | 24 | 24 | 1 |
| P10_CT1_B1 | 10,55 | 24 | 24 | 2 |
| Lymp | | | | |
| P01_CT1_B1 | 4,77 | 17 | 2 | 1 |
| P03_CT0_B1 | 7,46 | 15 | 13 | 6 |
| P16_CT2_B1 | 11,22 | 18 | 18 | 4 |

Table 5.1: **The 90th percentile last fraction below threshold (LFBT) values for the script used throughout this thesis, and the clinically validated one. # fx = number of prescribed fractions. Amplitude in mm.**

# Chapter 6

# Discussion

## Discrepancy between scripts

The majority of this discussion was written before discovering that the derivative script produced different results from the clinically validated script. This essentially makes all the results that are based on this script obsolete. The clinical evaluation is entirely based on the results from this script. Table 5.1 in chapter 5 shows that for these specific treatment beams, the derivative script severely underestimates the interplay robustness.
P10, for example, has a treatment plan that, according to the derivative script, does not reach interplay robustness before the end of treatment in half of the treatment simulations (table B.2 'med' column). Meanwhile, the script that has been clinically validated demonstrates strong interplay robustness in 90% of the treatment simulations in the initial fraction. The significant contrast observed in a patient with one of the most unfavorable outcomes, according to the derivative script, raises the potential concern that the estimation of interplay robustness in all treatment beams could be notably underestimated.

The crucial lesson from this entire scenario is to always validate scripts, even if they are built upon a script that has already undergone clinical validation. There is always a possibility that a small error could emerge unexpectedly, potentially coming to light only when it's already too late.

Unfortunately, the difference between the clinically validated script and its derivative script was only discovered a week before the thesis deadline. If it had been discovered earlier, there is a chance it could have been corrected, and the simulations would have been repeated with a correct and validated script. Most likely, some of the additional simulations and comparisons, like the artificial amplitude, would not have been performed due to time constraints.

## 6.1 Background information

In order to determine a treatment plan's robustness against the interplay effect and to make the correct considerations regarding the use of interplay mitigation techniques, we performed clinical evaluation of 18 Holland PTC patients' (esophagus cancer, lung

cancer, and lymphoma patients) treatment plan QA measurements. The secondary goal is to determine which other factors influence the plan's interplay robustness.

By modeling a patient's tumor motion and applying this motion on a static measurement of a real treatment beam, we determined the robustness of the treatment plan against the interplay effect using the Gamma evaluation [33].
The main metric used to determine if a beam is robust against the interplay effect is the 90th percentile *last fraction below threshold* (LFBT). For each simulated treatment scheme, the last fraction that is below the Holland PTC criterion of 95% Gamma pass rate is recorded. The 90th percentile LFBT indicates that 90 out of 100 simulations are robust after that fraction number.

## 6.2 Key results

Results show a strong correlation between tumor motion amplitude (both SI and 2D motion) and the robustness against the interplay effect (Figure 3.6).

### 6.2.1 Clinical evaluation per tumor type

Interplay robustness results varied between tumor groups.

Lymphoma patients showed great robustness against the interplay effect up to 7 mm. Unfortunately, there is little data available on tumor motion amplitude greater than 7mm. Since the current Holland PTC protocol dictates the use of a larger range shifter when the amplitude is between 5 and 10 mm, and it does not recommend proton therapy if the lymphoma tumor motion is greater than 10mm, more information is needed regarding the interplay robustness of tumor with an amplitude between 5 and 10 mm.

Lung patients showed interplay robustness up to 6 mm. Little data is available for lung cancer patients with tumor motion amplitudes between 6 and 8 mm.

In esophagus patients, the treatment beams are robust up to 6 mm. Between 6 and 8 mm, results were variable. 90th percentile LFBT varied between 7 to 28 in this tumor motion range. Above 8 mm, no esophagus beams showed interplay robustness.

### 6.2.2 patient-specific clinical evaluation

In nine out of eighteen patients, all beams showed robustness against the interplay effect in all the different motion scenarios.
38.8% of patients' plans were robust in some tumor motion scenarios and not in others.
In two patients, none of the treatment plans were robust. Both of these patients had tumor motion amplitudes greater than 8 mm.

### 6.2.3 Second goal: Factors influencing the interplay effect

Results show that interplay robustness is primarily influenced by the tumor motion in the SI direction. No other factors are found that have a significant impact on a treatment plan's robustness to the interplay effect.

**Artificial amplitude** The patient-specific 2D tumor motion amplitude is changed to artificial values, ranging from 4.47 to 17.85 mm. Results show a strong increase, relative to patient-specific tumor motion, in interplay robustness up to 11.18 mm in artificial amplitude. This was the case for all tumor types across the entire range of tumor motion amplitudes. No clear explanation could be determined for this occurrence.

**Unidirectional amplitude** The study found that manually set tumor motion amplitudes led to better robustness than using real patient amplitudes. Investigating the impact of different motion directions, simulations were executed for selected patients (P01, P03, P04, P06, P07, P11, and P14) with amplitude artificially adjusted to only be in one direction: either in LR direction or SI direction. amplitudes ranged from 5 to 15 mm with 2.5mm incremental steps.

Regardless of the direction of motion — whether it is in the superior-inferior (SI) or left-right (LR) direction — there appears to be no significant difference in its influence on interplay robustness. This observation holds true even at higher motion amplitudes, suggesting that the direction of motion does not play a substantial role in affecting interplay robustness.
The reason behind the stronger correlation between interplay robustness and SI tumor motion compared to LR tumor motion could be attributed to the observation that the amplitude of SI tumor motion is greater than that of LR tumor motion in nearly all cases (section 4.2 and figure B.10). The LR tumor motion amplitude is often dwarfed by the SI tumor motion amplitude, which is, on average, six times greater (figure B.10).

**Change in tumor motion amplitude through time** An average increase of SI direction tumor motion amplitude of 1.16 mm has been found in 4D-CTs taken after the initial planning 4D-CT. This increases to 1.53 mm in the 3D direction ($\sqrt{SI^2 + LR^2 + AP^2}$). In one lymphoma patient, tumor motion increased from an SI amplitude of 2.84 mm in the initial 4D-CT to 11.22 mm in the last 4D-CT. Lymphoma patients generally do not receive proton therapy if their tumor motion amplitude is greater than 10 mm. This shows that it is important to check the respiratory amplitude in every 4D-CT, and create protocol of what should be done in cases of extreme increase in tumor motion amplitude.

## 6.3 Comments on key results

## Differences with literature

The tumor motion amplitude thresholds for interplay robustness found in this thesis are lower than those found in literature [38], [61], [64], [65].
One explanation might be that different articles used different criteria for robustness. The article by Spautz *et al.* uses the Gamma index as well but has slightly more lenient acceptance criteria of 3%/3mm [64]. The other articles use different metrics altogether.

The criteria for interplay robustness in this report state that in 90 out of 100 simulations, the Gamma pass rate threshold of 95% needs to be reached before the end of treatment in order to call a beam robust. This ensures that it is very likely that, assuming other parameters don't change, the plan that is irradiated is actually robust.

## 6.4 Clinical implications

In current Holland PTC clinical practice, repainting is applied in lung- and esophagus cancer patients with a tumor amplitude greater than 5 mm. If a patient's tumor motion is over 20 mm, proton therapy is not indicated [24], [41], [67].
Lymphoma patients with a tumor motion amplitude in the planning 4D-CT $>$ 10 mm are not indicated for proton therapy. If their tumor motion amplitude exceeds 5 mm, larger spot sizes are created using a larger range shifter (5cm).

It is important to note that in some of the treatment plans that are used in this thesis, interplay mitigation tactics have been used. If these tactics had not been applied, the interplay robustness might be different. Using the methods and data in this thesis, it is not possible to determine to what extent a beam's interplay robustness was affected by mitigation tactics.
Investigating to what extent mitigation tactics play a role in interplay robustness is beyond the scope of this thesis but would provide valuable information regarding these tactics and could help update clinical guidelines.

Some treatment plans have shown to be very robust even after few fractions. While this is in itself a positive outcome, it can mean that the interplay mitigation tactics have been very conservative. Since mitigation tactics like repainting come at a dosimetric cost, clinical physicists and radiation oncologists could decide to omit some mitigation tactics in individual cases if interplay robustness can still be demonstrated beyond doubt.

## 6.5 Limitations

### Single beam vs multi beam analysis

It is important to note that each treatment beam is considered individually, while treatment plans range from two to four beams per treatment. If one or more of the beams is not robust against tumor motion, it is possible that the other beams compensate for the dosimetric errors of one beam. This is essentially similar to dose averaging. For example, looking at P12_CT5 in Table 3.3, two of the three beams are robust against the interplay effect. It might be possible that the dose in the target volume areas that are not sufficiently covered by B3 are 'smeared out' by B1 and B2, resulting in a uniform dose after all.
Based on the methods and data presented in this thesis, it remains inconclusive to ascertain whether this was the situation in these patients. One piece of information that could provide that knowledge is the region-specific Gamma score rather than the Gamma pass rate.

Remember that the Gamma index is a score that is given to every reference point. It shows how much the reference point's dose differs from the planned dose in that area. The Gamma pass rate tells which percentage of the reference points meet the acceptance criteria (2%/2mm in Holland PTC).

When a measurement point receives a 'perfect' dose from one beam, with no disparity between planned and measured doses, and the dose from another beam slightly exceeds the acceptance criteria (e.g., a 2.1% dose difference compared to the maximum acceptable 2%), it is conceivable that the combined dose from both beams falls within the acceptance criteria. Determining this requires the Gamma score of all spots that are measured by the

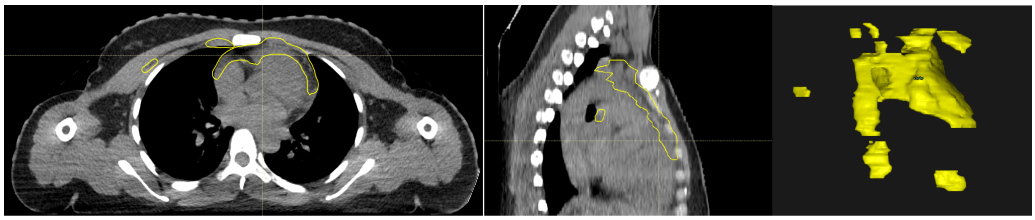

Figure 6.1: **left: Axial CT view op patient 17, with the CTV delineated. Middle: Sagittal view of the same patient. Right: 3D render of the CTV, anterior view. This patient's CTV spans lymph nodes from the height of the clavicula down to the caudal part of the sternum, including some interpectoral lymph nodes. It consists of 9 separate volumes, the largest of which covers the anterior part of the heart.**

MatriXX PT dosimeter. Using the displacement of the MatriXX PT dosimeter to align it to the gantry beam, it is possible to determine to what degree multiple beams compensate for each other's dose distribution discrepancies. Appendix D Beam compensation calculation example discusses how this might be calculated and provides an example.
Due to time constraints, it was not realistic to perform these calculations during this thesis. The data that is required for these calculations is available, as it is created by the interplay simulations software.

One important note is that this method does not work if different dose measurements are in a different plane. The angle of incidence of different beams can be as large as 60° (Table A.2). 2D dose measurements, like the ones created using the MatriXX PT, can only be combined if the dose distributions they measure are in the same plane.
There is a 3D ionization chamber detector array available, but the interplay simulation script is currently only validated on 2D MatriXX PT input data. Also, 3D dosimetry is often performed using radiochromic films. These can be very labor-intensive.

A 2021 study by Loginova *et al.* resulted in *"correction coefficients as functions of the accelerator gantry angle"*, allowing MatriXX PT dosimetry at an angle while still yielding meaningful results [68]. This way, it could be possible to combine the dosimetry measurements of beams at different angles and determine the compensation effect of different beams.

**Uniform motion** The simulation of the entire Clinical Target Volume (CTV) movement as a single uniform motion raises questions about its realism in clinical applications. Figure 6.1, for example, shows the CTV of P17 in two directions, plus the 3D render. It consists of lymph nodes at many different anatomical sites. It is unrealistic that the interpectoral lymph node far left in the axial 4D-CT scans has the same motion during breathing as a mediastinal node. Uniform motion of all parts of the CTV is assumed in this thesis.

Using different motions for different parts of the CTV would be more realistic. The deformable image registration provides single-voxel information regarding the tumor motion. However, this would require significant changes in the current interplay simulation script since that script assumes uniform 1D or 2D sinusoidal tumor motion.

One of the discarded methods, Voxel tracking (Appendix C), was supposed to track

the path of individual voxels in the ten phases of the CTV. If, in the future, this method can be used, it would be possible to use different voxel paths as input for the interplay simulation script. This way, different anatomical parts of the CTV could be selected to provide the tumor motion information.

While 2D tumor motion takes into account an extra patient parameter as compared to 1D tumor motion, it's still far from capturing the intricate tumor motion that happens during one breathing cycle.

Since this thesis exclusively simulates sinusoidal tumor motion, it remains unclear whether the tracking of individual voxels yields clinically meaningful improvements in interplay robustness, compared to the relatively straightforward and simplistic simulation using amplitudes of 1D or 2D tumor motion.

**Challenges Associated with the Gamma Index** While the Gamma Index is a widely used index, it has some downsides. One limitation inherent to the Gamma index arises in scenarios where a substantial portion of the target volume, for instance, 96%, satisfies the acceptance criteria for dose distribution. However, in the remaining 4% of the target volume, the dose can either be absent or excessively high, yet the Gamma pass rate would still indicate a seemingly adequate 96% agreement. Furthermore, even in situations where the entire dose distribution experiences a displacement of 2 mm, the Gamma pass rate remains unaffected at 100%. This is due to the ability of all pixels within the shifted curve to still find corresponding pixels within a 2 mm radius[69].

Another issue with how dose distribution comparisons is summarized using the Gamma pass rate is as follows: When the dose in an Organ-at-Risk (OAR) near the target volume is lower than the expected dose, it is considered as not meeting the Gamma acceptance criteria threshold, even though it could be clinically beneficial [36].

This type of information is not incorporated in the Gamma pass rate. The Gamma pass rate in its current form indicates nothing regarding the severity of the interplay effect. One way to improve the reporting of the Gamma index is to provide a histogram showing the distribution of the Gamma index values for all points, rather that just the condensed Gamma pass rate.

Another option would be to add different robustness criteria and metrics, like the ones discussed in section 1.5.3 paragraph Possible alternatives to Gamma Index. Rana *et al.* use a combination of seven different metrics, all with different pros and cons [38].

This problem could partially be resolved by incorporating the methods explained in section 6.5 paragraph Single beam vs multi beam analysis and Appendix D Beam compensation calculation example.

Another problem of the Gamma index is the selection of the thresholds and acceptance criteria. Currently, 95% of the high dose volume needs to meet the 2mm distance to agreement and 2% dose difference acceptance criteria for the planned treatment to 'match' the measurement treatment. If any of these values are changed, some plans would no longer be robust or would 'lose' their robustness. At what values you set these thresholds is always up for debate. While stricter thresholds might lead to even more robust treatment plans, this might not be a clinically significant difference.

**Strong changes tumor motion amplitude** The results suggest interplay robustness is strongly and primarily dependent on tumor motion amplitude. In some patients, tumor motion appears to change drastically during the course of treatment: looking at P06 and

P16 in Table A.2, the patients' amplitude increase greatly. Amplitudes between P06's planning 4D-CT and later 4D-CTs almost double, decrease again, and increase to 12.53 mm in SI direction in the final 4D-CT. In P16, tumor motion amplitudes increase almost four times. [1] While some change in tumor motion amplitude is to be expected [43], [44], a doubling seems excessive. Another reason for change in tumor motion amplitude is simply a change in inter-fractional breathing patterns. Patients are known to not always breathe the same way, which can result in different motion of all tissue in the thoracic region.

Since the tumor motion amplitude is based on CTV delineation in RayStation, the most likely cause of this sudden change in motion amplitude is different inclusion of tumor volume and OARs in the patient's CTV. Studying P16's 4D-CT scans, the author could find no differences in delineation or anatomical structures that could explain a strong increase in tumor motion amplitude.

In clinical practice, occasionally, plans are discarded, and replanning is applied. This is generally the case if the patient's anatomy deviates too much from the original planning 4D-CT. In all patients in this thesis, only the original plan has been taken into consideration.

**Omitting AP motion**
Since the MatriXX PT measures beams in a 2D plane, it does not register the delivered dose in the depth direction. For this reason, tumor motion in the direction parallel to the beam can not be taken into account in the interplay simulation script. This is an inherent problem when working with a 2D dosimetric device. Though 3D dosimetry (see section 6.5 Single beam vs multi beam analysis, the last paragraph) is possible, I'm not aware of the possibilities and devices within Holland PTC.

**Consistency of breathing** In this thesis, patients' breathing is expected to be regular and constant. However, it is known that patients' breathing can be irregular, both inter-fractionally and intra-fractionally. An attempt was made to extract the real patients' breathing information in order to incorporate this variability into the model. This data was created during the 4D-CT, but it was not easily accessible and cleared every three months, so this information was not incorporated into the simulation. In the future, saving the breathing signal during a 4D-CT and incorporating it in the interplay simulation script might improve QA quality by making the interplay simulations more patient-specific.

**Effect of change in motion on robustness** Since new 4D-CTs are taken during a patient's treatment, the new tumor motion amplitudes could be used to continue the simulation. This is not currently possible in the interplay simulation script. If this were implemented in clinical practice, clinical physicists could determine if a change in interfraction tumor motion would result in loss of interplay robustness, taking the previous fractions into account.

[1] Remember that the LR motion is influenced by the gantry rotation angle, while the SI motion stays constant. For an explanation of this, see section 3.1.3 paragraph Beam rotation.

**Treatment beam output larger than MatriXX** During this internship, a script was created that turns the MatriXX PT output frames into a video. This video shows the measurements of each of the detector arrays with the correct temporal resolution of 0.04 s.

Figure 6.2 shows see six consecutive frames of beam 1 of P01. In some frames, part of the irradiation is not captured by the detector arrays. This means the measurements show an incomplete picture of the entire dose that is used in clinical practice, possibly missing large parts of the delivered dose. This is an inherent and unavoidable problem when working with detector arrays of a limited size. The unit of these measurements (in mGy) is known, so it's possible to calculate how much of the planned dose is not measured by the MatriXX PT.

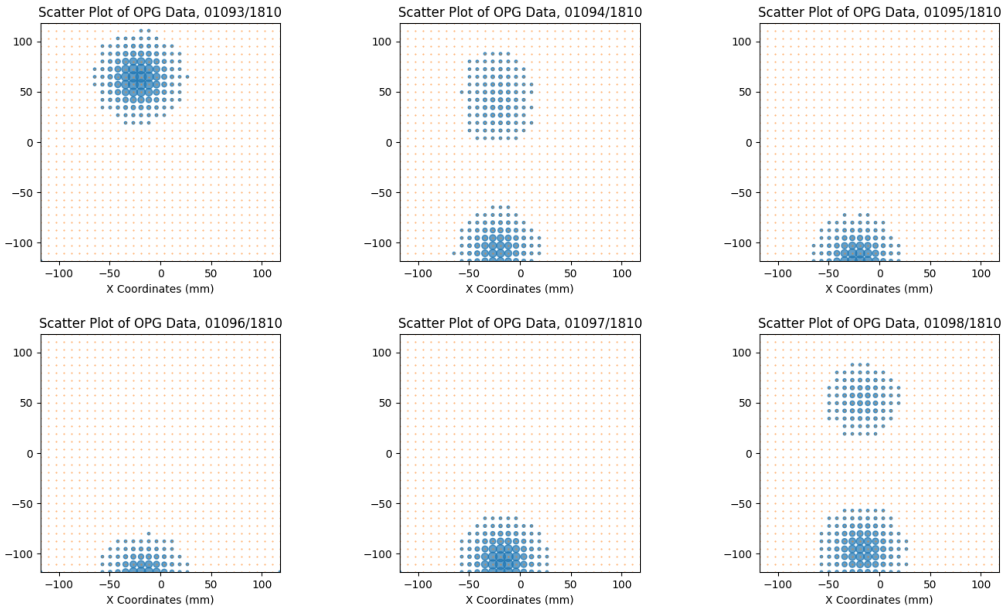


Figure 6.2: **Six consecutive frames from P01_B1 are arranged from left to right, top to bottom. The x- and y-axes display coordinates, while the small dots indicate the exact locations of the detector array elements. The size of the blue dots is arbitrary.**

## 6.6 Recommendations for future implementations

**Intergrate interplay simulations in clinical practice** The updated interplay simulation script's input data consist primarily of data that is available in RayStation. This means that it could be possible to integrate the interplay simulation into a RayStation script that could perform interplay robustness evaluation, both retrospectively and prospectively.

**Measurements of plans with large amplitudes** Little data is available for lymphoma patients beyond 9 mm motion and for lung cancer patients between 5 and 8 mm motion. This is the case because there were few patients with a tumor motion amplitude in those ranges. Nonetheless, the presence of patients with both larger and smaller motion amplitudes suggests the possibility of such tumor motion amplitudes. Since the transitional amplitude between beams being robust and not robust appears to be in these amplitude ranges, it is important to gather knowledge regarding these critical tumor motion amplitudes and their corresponding interplay robustness.

**Incorporating beam parameters into the simulation** Jasica Paramasamy, a former intern at Holland PTC [48], conducted a comprehensive study on beam parameters within the realm of interplay simulation. Notably, the investigation delved into the Energy Layer Switching Time (ELST), a parameter indicating the time required for gantry transition between two energy layers. The time it takes to irradiate one energy layer is in the order of milliseconds, while the ELST is around 0.8-1 second. A 1-second delay between every energy layer can greatly increase the duration of the treatment, increasing the interplay effect. While the ELST is inherent to the beam delivery system and can not be influenced by its users, it is important to have knowledge of the variation in this parameter. For this reason, it can be worthwhile to incorporate this gantry-specific parameter into the interplay effect. I've shortly worked on this before abandoning it and focusing on tumor motion parameters. See Appendix F ELST for a summary of my results and findings.

**Incorporating Tumor Motion Amplitudes** The analysis reveals a strong correlation between interplay robustness and a patient's SI and two-dimensional (2D) tumor motion. Conversely, the lateral (left-right, LR) motion exhibits a weak correlation with interplay robustness. While the ratio between SI and LR tumor motion can be relatively small, particularly in cases such as lymphoma patients, it is beneficial to consider both SI and LR tumor motion amplitudes in future interplay scripts. It's noteworthy that the LR amplitude in the *respiratory amplitude* script lacks beam orientation correction, unlike the LR component in the 2D tumor motion considered in this thesis. All SI and LR tumor motion amplitude data, along with gantry rotation angles, are readily available within RayStation. This availability enables the output of both unrotated tumor motion amplitudes and beam-specific, rotated tumor motion amplitudes, facilitating a more patient-specific approach to interplay simulations.

## 6.7 Conclusion

The primary goal of this thesis was to perform clinical evaluation of the beams of 18 patients' treatment plans. The extent to which the interplay effect affects each beam of the patients (and, by extension, the treatment plans) was analyzed.

The results of the clinically validated script suggest all nine beams up to 11.22 mm tumor motion amplitude are robust against the interplay effect. Since only nine out of 161 beams have been simulated using this script, no general conclusions can be drawn from this data. Simulations will need to be repeated with the clinically validated script before general conclusions can be drawn.

# Chapter 7

# Persoonlijke reflectie

**Aanpak literatuurstudie** Het was voor mij niet direct duidelijk dat de literatuurstudie een echt losstaand, zelfstandig project/verslag moest worden. Ik was in eerste instantie van plan om het meer in mijn thesisverslag te verwerken. Hierdoor heb ik wat werk dubbel gedaan. Op zich was dit uiteindelijk geen probleem, want ik heb hierdoor veel gelezen over protonentherapie, het interplay-effect, enz.
Ik vond het lastiger dan ik had verwacht dat er zo veel tijd zat tussen de eerste versie van mijn literature study en het late verwerken. In januari was mijn eerste versie af, maar vanwege zwangerschapsverlof is het een paar maanden blijven liggen. Hierdoor moest ik later me opnieuw volledig storten in dit onderdeel. Dit had ik eerder kunnen en moeten. Wel heb ik lang gewacht op feedback op het verslag, waardoor het ook lang duurde voordat ik een afsluitende presentatie kon geven etc.

**Werkstijl** Ik weet van mezelf dat ik soms erg chaotisch kan zijn. Dat heb ik de afgelopen jaren (tijdens mijn studie en stages) ook gemerkt. Tijdens deze scriptie heb ik echter hard geprobeerd om daaraan te werken, en met succes. Veel van de documenten, scripts, gegevens, enzovoort die ik heb verzameld, heb ik redelijk goed gecategoriseerd. Ik ben er zelden tegenaangelopen dat ik bijvoobeeld informatie kwijt was. Hierdoor kon ik relatief makkelijk onderdelen die ik maanden geleden heb verzameld weer naar boven halen.
Ik vind het erg prettig om eens in de week met begeleiders te zitten om de voortgang te bespreken. Hierdoor dwing je jezelf om even goed te verzamelen wat je de afgelopen tijd hebt gedaan, en kan je goed de vragen die je tegenkomt bespreken.

Ook vond ik het fijn om me een relatief langere periode (in tegenstelling tot een tienweekse stage) echt te verdiepen in een probleem. Hierdoor had je de ruimte om echt nieuwe dingen te proberen en kon je deze zonder problemen naast je laten liggen. Hierdoor was het goed mogelijk om verschillende invalshoeken te bekijken.

**Verkeerde script** Dit was wel een erg grote domper. Ik had al pech dat veel van de methodes die ik had geprobeerdom tumor beweging te modeleren uiteindelijk op niets uitliepen, maar ik was blij dat ik aan het einde in ieder geval resultaten had die ik kon laten zien en die enige klinische betekenis hadden. Er is vaak benadrukt dat validatie van script die ik maak (of gebruik) cruciaal is. Als ik dat in dit geval eerder had gedaan

was het nog mogelijk geweest om de simulaties te runnen met het gevalideerde de scripts. hopelijk waren er dan nuttige resultaten uit gekomen.

Toen ik voor het eerst de resultaten deelde waren oa Kees en jeremy al verbaasd dat de resultaten zo negatief waren: de helft van de patienten zouden niet robuust bestraal worden. Omdat een deel van de mitiagtion tactics gebaseerd waren op eerder uitgevoerde simulaties had ik kunnen vermoeden dat als die resultaten ook zo negatief waren als deze, er misschien meer maatregelen genomen zouden worden.

**Andere methodes** Ik heb een erg groot gedeelte van mijn tijd, ik denk wel zes maanden, gewerkt aan drie verschillende methodes om ook de tumorbeweging te simuleren (C Obsolete Approaches). De hoop was dat dit meer patiëntspecifieke en realistischere tumorbeweging zou simuleren. Echter waren de resultaten bij alle drie de methodes erg wisselvallig. Bij veel patiënten bewoog de tumor erg schokkerig en onregelmatig. Hierdoor heb ik deze methode op een gegeven moment links moeten laten liggen. De complexiteit van deze methodes nam toe naarmate ik er meer mee werkte.

**Planning** In mijn originele planning zou ik in mei klaar zijn geweest met het verzamelen van gegevens en vanaf dat moment alleen nog maar bezig zijn met schrijven en het interpreteren van resultaten. Omdat de oude methodes echter steeds niet werkten, ben ik te lang doorgegaan met het proberen te perfectioneren hiervan. Hierdoor kwam ik 'plotseling' in grote tijdsdruk. Ook gaf Jeremy vaak suggesties over hoe ik iets nog net iets beter kon uitwerken, of dat ik tóch nog even dit en dat moest proberen om mijn resultaten sterker te maken. Vaak waren dit inhoudelijk goede suggesties. Hierdoor ben ik echter wel een stuk meer in tijdsnood gekomen. Ik had veel eerder willen beginnen met veel schrijven, om te voorkomen dat ik op het einde nog veel moest schrijven en er weinig ruimte was voor evaluatie vanuit mijn begeleiders. Het is mijn eigen verantwoordelijkheid om deze deadlines aan te houden en dus ook om op tijd het verslag (of delen ervan) te laten controleren.

**Veel geprogrammeerd** Tijdens deze stage heb ik zeer veel geprogrammeerd, veel meer dan ik van tevoren had verwacht en gehoopt. Ik ben blij dat ik dit heb gedaan, ik ben er een stuk beter in geworden. Ook werkt ChatGPT erg goed met programmeren. Je moet nog steeds zelf met alle ideeën komen over wat je met welke data wil doen, maar als je dat eenmaal hebt, kun je iteratief erg ver komen met ChatGPT. Ik werd steeds handiger in programmeren in Python en kon steeds beter overweg met RayStation. Ook heeft Yibing me erg veel geholpen met het wegwijs maken in het scripten binnen RayStation.

**Schrijven** Wetenschappelijk schrijven blijf ik moeilijk vinden.
Ik had eerder moeten beginnen met sommige kopjes die al veel eerder klaar hadden kunnen zijn. Dan had ik ze naar andere kunnen sturen om te laten beoordelen. Hier worden teksten altijd vele malen beter van. Echter had ik vaak een heleboel kopjes die min of meer af waren, maar met wel nog wat open einde. Als ik stukjes eerder af had gemaakt en desnoods nog niet af had, maar wel al naar mensen gestuurd om door te nemen kan ik veel eerder nuttige feedback verwerken.

**Kliniek** In de kliniek heb ik veel leuke dingen gedaan. Ik vond het meekijken en meedraaien op de ooglijn erg leuk, zeker omdat je hier zo veel samenwerkt met de laboranten. Intakegesprekken met nieuwe patiënten vond ik erg leerzaam en leuk om te voeren. Hier kreeg ik veel energie van.
Ik vind het erg jammer dat ik niet heb kunnen meekijken en meedraaien bij de dosisplanning. Dit is uiteindelijk een van de belangrijkste stappen binnen het hele proces, en wat mij betreft ook eentje waar een klinisch technoloog juist erg goed een rol in kan spelen. Ook was het erg nuttig geweest voor mijn scriptie zelf: als ik meer van de dosisplanning had begrepen had ik zeer waarschijnlijk meer nuttige suggesties kunnen doen voor de aanpak van het interplay effect die tijdens de dosisplanning juist zo relevant kan zijn.

# Appendix A

# Patient and Beam data

Table A.1 contains all the parameters set in the interplay simulation script.

| **Parameter** | **Value** |
|---|---|
| Frame Time [s] | 0.04 |
| Number of Simulated Fractions | 30 |
| Number of Repetitions | 100 |
| Resampling Resolution X and Y [mm] | 1 |
| Dose Percent Threshold | 2 |
| Distance Threshold [mm] | 2 |
| Lower Percent Dose Cutoff | 10 |
| Interpolation Fraction | 24 |
| Maximum Gamma | 2 |
| Random Subset | null |
| Local Gamma | false |
| Available RAM | $2 \times 10^{30}$ |
| Quiet | True |

Table A.1: **All simulation parameters in the files *gamma_config.json* and *simulation_config.json.***

Table A.2 contains more information regarding the tumor motion amplitude, as extracted by the *respiratory_amplitude* script by Dr. Y. Wang.

| PT ID | beam angle | beam num | Amplitudes SI; LR; AP [mm] |
|---|---|---|---|
| P01_CT0 | 10 | B1 | 3.78; 1.464; 1.613 |
| | 350 | B2 | 3.78; 1.943; 1.022 |
| P01_CT1 | 10 | B1 | 4.77; 1.494; 1.727 |
| | 350 | B2 | 4.77; 2.012; 1.118 |
| P02_CT0 | 50 | B1 | 3.31; 0.79; 1.447 |
| | 25 | B2 | 3.31; 1.975; 2.022 |
| | 335 | B3 | 3.31; 3.082; 0.115 |
| | 310 | B4 | 3.31; 2.797; 1.3 |
| P02_CT1 | 50 | B1 | 2.44; 2.083; 2.431 |
| | 25 | B2 | 2.44; 3.792; 2.781 |
| | 335 | B3 | 2.44; 4.891; 0.889 |
| | 310 | B4 | 2.44; 4.075; 2.286 |
| P03_CT0 | 10 | B1 | 7.46; 3.876; 2.987 |
| | 350 | B2 | 7.46; 4.692; 1.5 |
| P03_CT1 | 10 | B1 | 3.9; 2.785; 2.562 |
| | 350 | B2 | 3.9; 3.518; 1.467 |
| P04_CT0 | 170 | B1 | 3.48; 1.136; 1.615 |
| | 140 | B2 | 3.48; 1.615; 2.141 |
| | 80 | B3 | 3.48; 1.262; 0.993 |
| P04_CT1 | 170 | B1 | 3.37; 3.056; 1.496 |
| | 140 | B2 | 3.37; 2.874; 2.598 |
| | 80 | B3 | 3.37; 0.456; 0.279 |
| P04_CT2 | 170 | B1 | 3.46; 1.61; 1.087 |
| | 140 | B2 | 3.46; 1.669; 1.701 |
| | 80 | B3 | 3.46; 0.549; 0.398 |
| P04_CT3 | 170 | B1 | 3.76; 3.145; 1.964 |
| | 140 | B2 | 3.76; 3.178; 3.146 |
| | 80 | B3 | 3.76; 0.908; 0.644 |
| P04_CT4 | 170 | B1 | 4.26; 2.315; 4.873 |
| | 140 | B2 | 4.26; 4.106; 6.117 |
| | 80 | B3 | 4.26; 4.202; 3.35 |
| P04_CT5 | 170 | B1 | 2.94; 1.769; 1.125 |
| | 140 | B2 | 2.94; 1.798; 1.791 |
| | 80 | B3 | 2.94; 0.531; 0.379 |
| P05_CT0 | 210 | B1 | 4.85; 0.597; 0.766 |
| | 181 | B2 | 4.85; 1.378; 1.206 |
| P05_CT1 | 210 | B1 | 2.61; 0.365; 1.091 |
| | 181 | B2 | 2.61; 1.244; 1.448 |
| P05_CT2 | 210 | B1 | 4.87; 0.609; 1.055 |
| | 181 | B2 | 4.87; 1.582; 1.542 |
| P05_CT3 | 210 | B1 | 5.08; 0.194; 1.427 |
| | 181 | B2 | 5.08; 1.209; 1.739 |
| P05_CT4 | 210 | B1 | 3.0; 0.74; 0.582 |
| | 181 | B2 | 3.0; 1.471; 1.074 |
| P06_CT0 | 210 | B1 | 6.61; 0.679; 2.025 |
| | 181 | B2 | 6.61; 2.312; 2.689 |
| P06_CT1 | 210 | B1 | 12.57; 0.516; 7.377 |
| | 181 | B2 | 12.57; 4.006; 8.149 |
| P06_CT3 | 210 | B1 | 7.93; 0.401; 4.046 |
| | 181 | B2 | 7.93; 2.022; 4.404 |
| P06_CT4 | 210 | B1 | 12.53; 1.012; 7.988 |
| | 181 | B2 | 12.53; 3.669; 8.575 |
| P07_CT0 | 210 | B1 | 6.45; 0.299; 1.357 |
| | 181 | B2 | 6.45; 1.319; 1.717 |
| P07_CT1 | 210 | B1 | 8.28; 0.622; 1.447 |
| | 181 | B2 | 8.28; 1.854; 1.997 |
| P08_CT0 | 180 | B1 | 3.18; 0.68; 1.11 |
| | 10 | B2 | 3.18; 0.477; 1.176 |
| | 210 | B3 | 3.18; 0.034; 0.944 |
| P08_CT1 | 180 | B1 | 3.9; 1.39; 0.98 |
| | 10 | B2 | 3.9; 1.199; 1.173 |
| | 210 | B3 | 3.9; 0.714; 0.492 |
| P08_CT2 | 180 | B1 | 3.9; 1.51; 0.71 |
| | 10 | B2 | 3.9; 1.364; 0.936 |
| | 210 | B3 | 3.9; 0.953; 0.139 |
| P08_CT3 | 180 | B1 | 4.12; 1.48; 1.1 |
| | 10 | B2 | 4.12; 1.266; 1.303 |
| | 210 | B3 | 4.12; 0.732; 0.587 |
| P08_CT4 | 180 | B1 | 0.75; 0.65; 0.9 |
| | 10 | B2 | 0.75; 0.484; 0.97 |
| | 210 | B3 | 0.75; 0.113; 0.723 |
| P09_CT0 | 210 | B1 | 6.72; 0.254; 3.071 |
| | 181 | B2 | 6.72; 1.61; 3.371 |
| P09_CT1 | 210 | B1 | 10.48; 0.616; 4.526 |
| | 181 | B2 | 10.48; 2.015; 4.834 |
| P09_CT2 | 210 | B1 | 3.72; 0.506; 0.985 |
| | 181 | B2 | 3.72; 1.385; 1.406 |
| P09_CT3 | 210 | B1 | 11.46; 0.157; 3.949 |
| | 181 | B2 | 11.46; 2.322; 4.429 |
| P09_CT4 | 210 | B1 | 10.75; 0.375; 3.753 |
| | 181 | B2 | 10.75; 2.98; 4.497 |
| P10_CT0 | 180 | B1 | 8.19; 1.86; 2.63 |
| | 150 | B2 | 8.19; 2.926; 3.741 |
| | 210 | B3 | 8.19; 0.296; 2.13 |
| P10_CT1 | 180 | B1 | 10.55; 2.85; 3.77 |
| | 150 | B2 | 10.55; 4.353; 5.441 |
| | 210 | B3 | 10.55; 0.583; 2.973 |
| P10_CT2 | 180 | B1 | 9.71; 3.05; 5.5 |
| | 150 | B2 | 9.71; 5.391; 7.459 |
| | 210 | B3 | 9.71; 0.109; 4.817 |
| P10_CT3 | 180 | B1 | 10.55; 2.85; 3.77 |
| | 150 | B2 | 10.55; 4.353; 5.441 |
| | 210 | B3 | 10.55; 0.583; 2.973 |
| P10_CT4 | 180 | B1 | 8.45; 2.12; 3.41 |
| | 150 | B2 | 8.45; 3.541; 4.724 |
| | 210 | B3 | 8.45; 0.131; 2.888 |
| P11_CT0 | 210 | B1 | 6.49; 1.105; 2.063 |
| | 181 | B2 | 6.49; 2.967; 2.968 |
| P11_CT1 | 210 | B1 | 10.51; 2.591; 1.208 |
| | 181 | B2 | 10.51; 4.609; 2.809 |
| P11_CT2 | 210 | B1 | 5.85; 1.221; 1.459 |
| | 181 | B2 | 5.85; 2.748; 2.342 |
| P11_CT3 | 210 | B1 | 9.6; 1.213; 3.473 |
| | 181 | B2 | 9.6; 4.037; 4.639 |
| P11_CT4 | 210 | B1 | 6.17; 1.302; 2.328 |
| | 181 | B2 | 6.17; 3.429; 3.38 |
| P12_CT0 | 180 | B1 | 4.92; 2.56; 2.32 |
| | 150 | B2 | 4.92; 3.377; 3.698 |
| | 210 | B3 | 4.92; 1.057; 1.481 |
| P12_CT1 | 180 | B1 | 4.65; 2.35; 1.62 |
| | 150 | B2 | 4.65; 2.845; 2.825 |
| | 210 | B3 | 4.65; 1.225; 0.79 |
| P12_CT2 | 180 | B1 | 6.19; 3.72; 2.24 |
| | 150 | B2 | 6.19; 4.342; 4.111 |
| | 210 | B3 | 6.19; 2.102; 0.889 |
| P12_CT3 | 180 | B1 | 6.09; 3.15; 2.32 |
| | 150 | B2 | 6.09; 3.888; 3.953 |
| | 210 | B3 | 6.09; 1.568; 1.225 |
| P12_CT4 | 180 | B1 | 7.62; 2.96; 2.59 |
| | 150 | B2 | 7.62; 3.858; 4.172 |
| | 210 | B3 | 7.62; 1.268; 1.609 |
| P12_CT5 | 180 | B1 | 6.26; 3.01; 2.05 |
| | 150 | B2 | 6.26; 3.632; 3.591 |
| | 210 | B3 | 6.26; 1.582; 0.985 |
| P13_CT0 | 180 | B1 | 10.99; 1.25; 5.23 |
| | 150 | B2 | 10.99; 3.697; 6.378 |
| | 210 | B3 | 10.99; 1.532; 5.295 |
| P14_CT0 | 180 | B1 | 6.9; 1.38; 1.13 |
| | 150 | B2 | 6.9; 1.76; 1.859 |
| | 210 | B3 | 6.9; 0.63; 0.664 |
| P14_CT1 | 180 | B1 | 11.96; 2.53; 4.05 |
| | 150 | B2 | 11.96; 4.216; 5.615 |
| | 210 | B3 | 11.96; 0.166; 3.424 |
| P15_CT0 | 160 | B1 | 2.49; 0.827; 1.213 |
| | 325 | B2 | 2.49; 0.994; 0.241 |
| | 190 | B3 | 2.49; 0.34; 0.916 |
| P15_CT1 | 160 | B1 | 3.04; 1.399; 1.559 |
| | 325 | B2 | 3.04; 1.536; 0.061 |
| | 190 | B3 | 3.04; 0.854; 0.984 |
| P15_CT2 | 160 | B1 | 2.52; 1.198; 1.481 |
| | 325 | B2 | 2.52; 1.358; 0.155 |
| | 190 | B3 | 2.52; 0.649; 1.01 |
| P15_CT3 | 160 | B1 | 2.2; 1.652; 1.927 |
| | 325 | B2 | 2.2; 1.839; 0.133 |
| | 190 | B3 | 2.2; 0.96; 1.261 |
| P16_CT0 | 10 | B1 | 2.84; 2.595; 1.987 |
| | 350 | B2 | 2.84; 3.137; 0.992 |
| P16_CT1 | 10 | B1 | 5.47; 2.239; 2.713 |
| | 350 | B2 | 5.47; 3.059; 1.793 |
| P16_CT2 | 10 | B1 | 11.22; 4.288; 3.069 |
| | 350 | B2 | 11.22; 5.107; 1.437 |
| P17_CT0 | 30 | B1 | 4.88; 2.084; 3.718 |
| | 0 | B2 | 4.88; 4.19; 3.09 |
| | 330 | B3 | 4.88; 5.174; 0.089 |
| P17_CT1 | 30 | B1 | 3.71; 2.287; 3.257 |
| | 0 | B2 | 3.71; 4.05; 2.44 |
| | 330 | B3 | 3.71; 4.727; 0.251 |
| P18_CT0 | 0 | B1 | 1.76; 1.96; 0.41 |
| | 340 | B2 | 1.76; 1.982; 0.293 |
| P18_CT1 | 0 | B1 | 2.45; 2.74; 1.59 |
| | 340 | B2 | 2.45; 3.119; 0.427 |

Table A.2: The CTV amplitude in the three primary directions, after correction for beam rotation.

# Appendix B

# Results Gamma metrics

This section depicts some results that have been discussed in section 3.2 Results clinical evaluation, like tables with data instead of graphs. It also shows the Gamma pass rate graphs of three different patients to give an example of the data one might expect.

## Example of three Gamma graphs

Figure B.1, B.2 and B.3 show examples of the Gamma graphs of three 4D-CTs. The examples are selected to represent 'average', 'good', and 'bad results', respectively.

Each thin line is a simulation of one treatment scheme. The X-axis indicates the treatment fraction, and the Y-axis shows the cumulative Gamma pass rate. This entire fractionation scheme simulation is repeated 100 times for each patient's treatment beam. The thick blue line represents the average Gamma pass rate at that fraction.
Figure B.1 shows the Gamma pass rates of a patient in which the Gamma criterion is only reached after a few fractions.
In contrast, P04's simulations (B.2) are almost always above the 95% pass rate after the first treatment fraction.

For patient 13 (B.3), the average Gamma pass rate seems to converge and stop increasing.

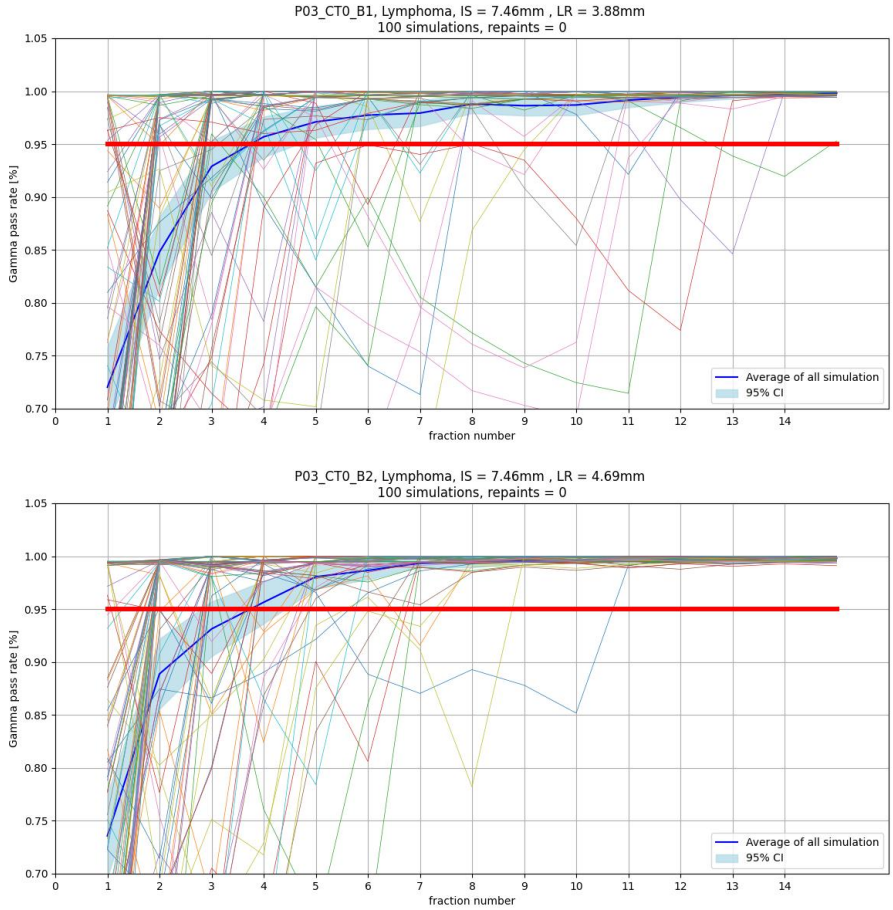


Figure B.1: **The Gamma pass rate graphs for both beams of P03, a lymphoma patient. Tumor motion was based on CT0, the planning CT. Each thin line is one simulation of an entire treatment. On average, the Gamma threshold is reached after 3 fractions, while in 90% of the simulations, the threshold is reached after 4 or 5 fractions.**
**Gamma index metrics for P03_CT0_B1: mean last fraction = 2.15, median last fraction = 1, 90th percentile = 1.**

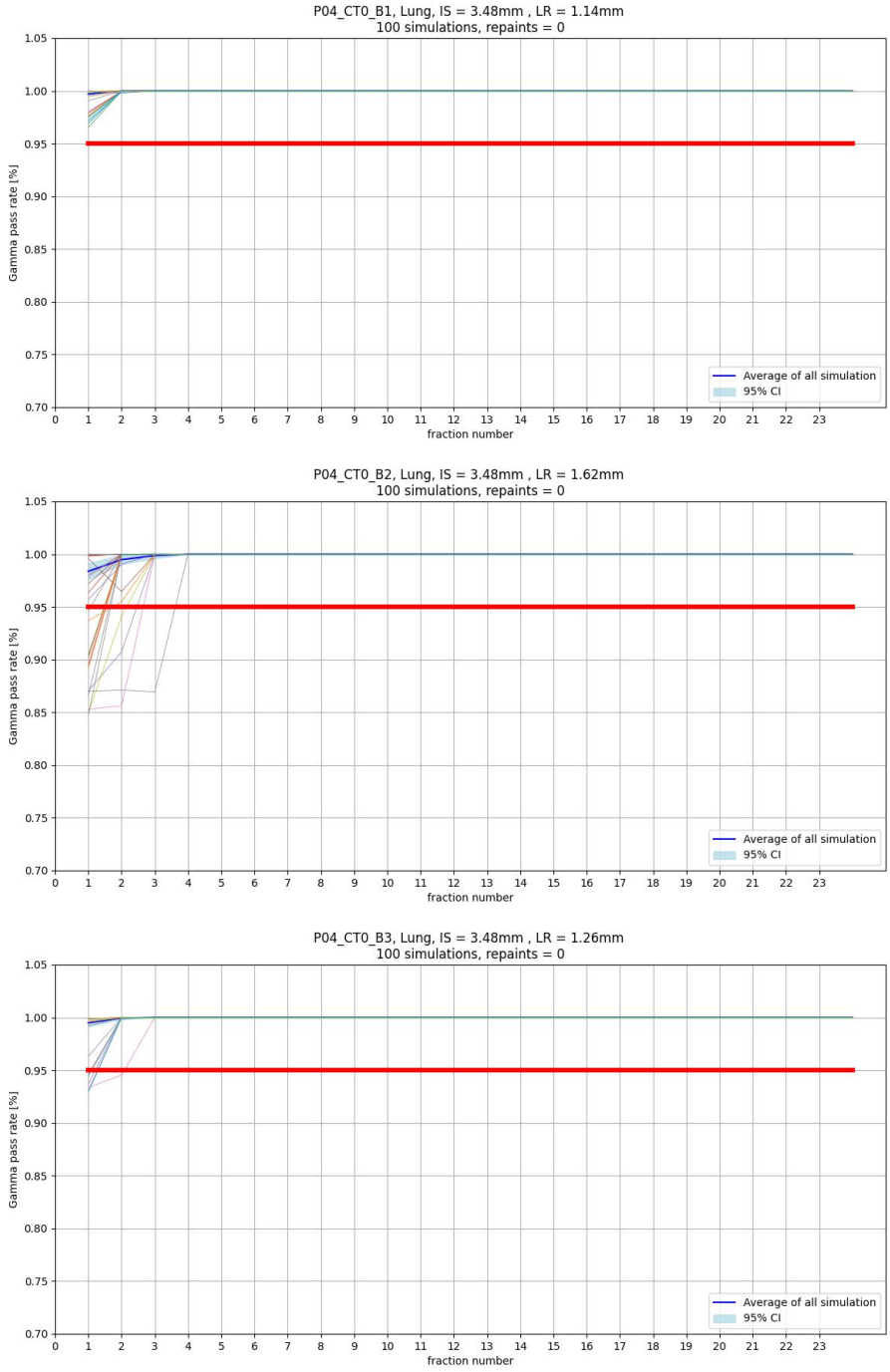


Figure B.2: **The Gamma pass rate graphs for all three beams of P04, a lung cancer patient. Notice how in only a few treatment simulations the Gamma index is ever under the 95% threshold. Gamma index metrics for P04_CT0_B2: mean last fraction = 0.05, median last fraction = 0, 90th percentile = 0.**

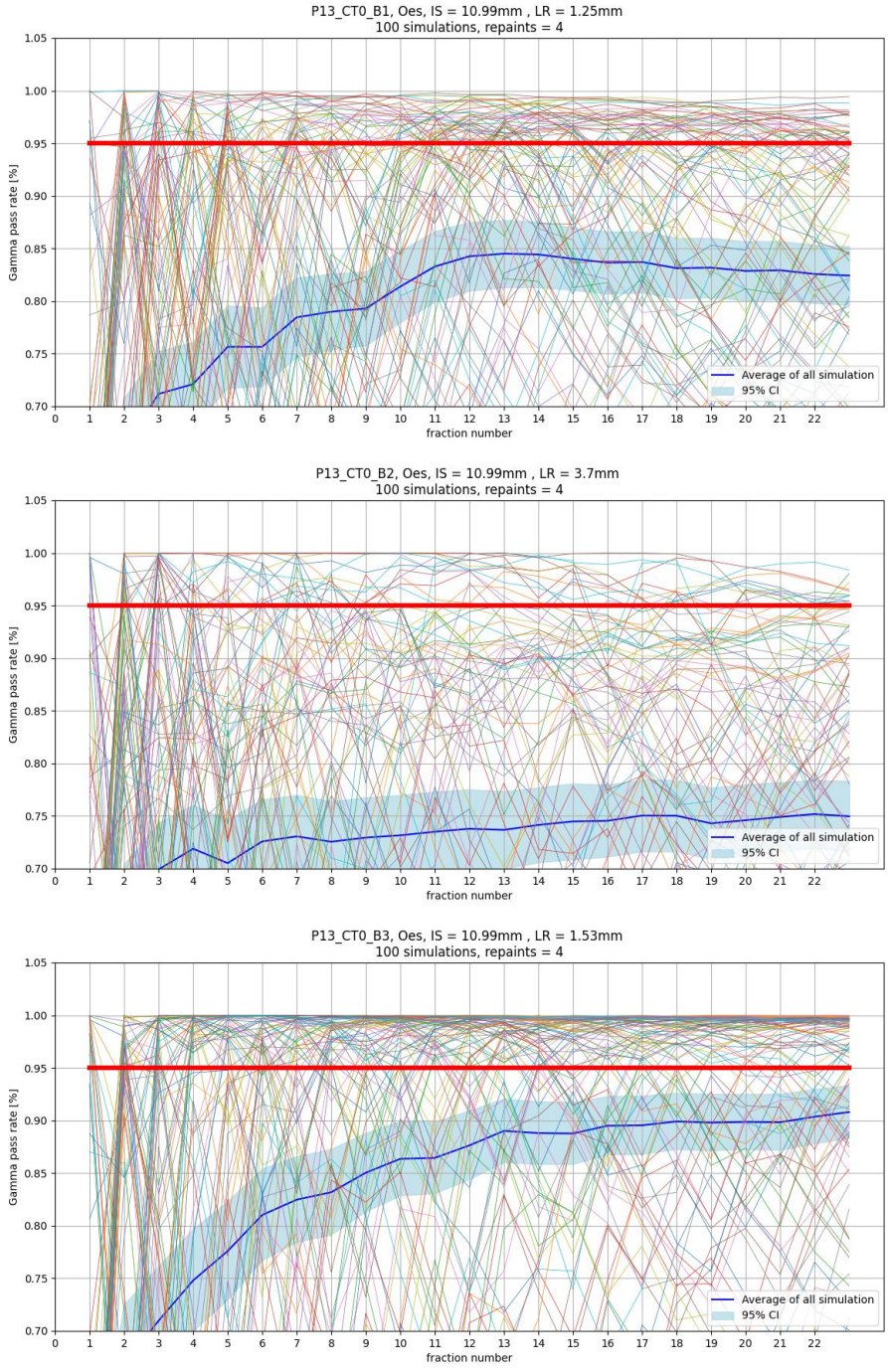


Figure B.3: **The Gamma pass rate graphs for all three beams of P13, a lung cancer patient.**
**Gamma index metrics for P13_CT0_B1: mean last fraction = 14.34, median last fraction = 17.4, 90th percentile = 23. Number of simulations that never reach the threshold = 13**
**These results are poor. In every beam, the mean of all the simulations never reaches the threshold.**

## Gamma index metrics for every beam

Table B.3, B.2 and B.1 show all Gamma index metrics for all beams, and their corresponding tumor motion in multiple direction. The beams are colored according to the decision cut-off described in section 3.1.4: A beam is considered inadequate (red) with respect to interplay mitigation if the 90th percentile of LFBT is equal to the number of prescribed fraction (presc. fx).

| pt_id | mean | med | 90th | presc. fx | #fx BT | SI [mm] | LR [mm] | AP [mm] | 2D motion |
|---|---|---|---|---|---|---|---|---|---|
| P05_CT0_B1 | 4,03 | 2 | 10,2 | 28 | 0 | 4,85 | -0,60 | -0,77 | 4,89 |
| P05_CT0_B2 | 2,02 | 1 | 4,1 | 28 | 0 | 4,85 | -1,38 | -1,21 | 5,04 |
| P05_CT1_B1 | 3 | 1 | 9,1 | 28 | 0 | 2,61 | -0,36 | -1,09 | 2,64 |
| P05_CT1_B2 | 1 | 1 | 1 | 28 | 0 | 2,61 | -1,24 | -1,45 | 2,89 |
| P05_CT2_B1 | 5,13 | 2 | 14,1 | 28 | 1 | 4,87 | -0,61 | -1,06 | 4,91 |
| P05_CT2_B2 | 1,82 | 1 | 5 | 28 | 0 | 4,87 | -1,58 | -1,54 | 5,12 |
| P05_CT3_B1 | 4,4 | 2 | 9,2 | 28 | 0 | 5,08 | -0,19 | -1,43 | 5,08 |
| P05_CT3_B2 | 1,88 | 1 | 4,1 | 28 | 0 | 5,08 | -1,21 | -1,74 | 5,22 |
| P05_CT4_B1 | 3,1 | 1 | 9 | 28 | 0 | 3,00 | -0,74 | -0,58 | 3,09 |
| P05_CT4_B2 | 1 | 1 | 1 | 28 | 0 | 3,00 | -1,47 | -1,07 | 3,34 |
| P06_CT0_B1 | 3,93 | 1 | 11,1 | 23 | 0 | 6,61 | -0,68 | -2,02 | 6,64 |
| P06_CT0_B2 | 6,8 | 3 | 20 | 23 | 1 | 6,61 | -2,31 | -2,69 | 7,00 |
| P06_CT1_B1 | 22,96 | 23 | 23 | 23 | 63 | 12,57 | 0,52 | -7,38 | 12,58 |
| P06_CT1_B2 | 23 | 23 | 23 | 23 | 75 | 12,57 | -4,01 | -8,15 | 13,19 |
| P06_CT3_B1 | 7,58 | 4 | 22 | 23 | 1 | 7,93 | 0,40 | -4,05 | 7,94 |
| P06_CT3_B2 | 11,72 | 11,5 | 23 | 23 | 4 | 7,93 | -2,02 | -4,40 | 8,18 |
| P06_CT4_B1 | 22,3 | 23 | 23 | 23 | 51 | 12,53 | 1,01 | -7,99 | 12,57 |
| P06_CT4_B2 | 22,98 | 23 | 23 | 23 | 80 | 12,53 | -3,67 | -8,57 | 13,06 |
| P07_CT0_B1 | 3,92 | 1 | 10,3 | 23 | 1 | 6,45 | -0,30 | -1,36 | 6,46 |
| P07_CT0_B2 | 5,3 | 2 | 17,1 | 23 | 1 | 6,45 | -1,32 | -1,72 | 6,58 |
| P07_CT1_B1 | 10,08 | 7 | 23 | 23 | 1 | 8,28 | -0,62 | -1,45 | 8,30 |
| P07_CT1_B2 | 13,36 | 15 | 23 | 23 | 12 | 8,28 | -1,85 | -2,00 | 8,49 |
| P09_CT0_B1 | 4,2 | 2 | 12,2 | 23 | 0 | 6,72 | 0,25 | -3,07 | 6,72 |
| P09_CT0_B2 | 6,2 | 3 | 20 | 23 | 2 | 6,72 | -1,61 | -3,37 | 6,91 |
| P09_CT1_B1 | 13,28 | 13 | 23 | 23 | 10 | 10,48 | 0,62 | -4,53 | 10,50 |
| P09_CT1_B2 | 19,92 | 23 | 23 | 23 | 23 | 10,48 | -2,01 | -4,83 | 10,67 |
| P09_CT2_B1 | 1 | 1 | 1 | 23 | 0 | 3,72 | -0,51 | -0,99 | 3,75 |
| P09_CT2_B2 | 1,04 | 1 | 1 | 23 | 0 | 3,72 | -1,38 | -1,41 | 3,97 |
| P09_CT3_B1 | 19,59 | 23 | 23 | 23 | 20 | 11,46 | 0,16 | -3,95 | 11,46 |
| P09_CT3_B2 | 22,47 | 23 | 23 | 23 | 45 | 11,46 | -2,32 | -4,43 | 11,69 |
| P09_CT4_B1 | 18,07 | 23 | 23 | 23 | 17 | 10,75 | -0,38 | -3,75 | 10,76 |
| P09_CT4_B2 | 21,16 | 23 | 23 | 23 | 36 | 10,75 | -2,98 | -4,50 | 11,16 |
| P11_CT0_B1 | 4,78 | 2 | 12,1 | 23 | 0 | 6,49 | -1,11 | -2,06 | 6,58 |
| P11_CT0_B2 | 8,66 | 4,5 | 23 | 23 | 3 | 6,49 | -2,97 | -2,97 | 7,14 |
| P11_CT1_B1 | 19,8 | 23 | 23 | 23 | 33 | 10,51 | -2,59 | -1,21 | 10,82 |
| P11_CT1_B2 | 21,09 | 23 | 23 | 23 | 41 | 10,51 | -4,61 | -2,81 | 11,48 |
| P11_CT2_B1 | 3,17 | 2 | 8,1 | 23 | 0 | 5,85 | -1,22 | -1,46 | 5,98 |
| P11_CT2_B2 | 5,61 | 2 | 16,2 | 23 | 0 | 5,85 | -2,75 | -2,34 | 6,46 |
| P11_CT3_B1 | 15,22 | 19,5 | 23 | 23 | 10 | 9,60 | -1,21 | -3,47 | 9,68 |
| P11_CT3_B2 | 20,1 | 23 | 23 | 23 | 29 | 9,60 | -4,04 | -4,64 | 10,41 |
| P11_CT4_B1 | 3,09 | 1 | 7 | 23 | 0 | 6,17 | -1,30 | -2,33 | 6,31 |
| P11_CT4_B2 | 9,78 | 8 | 23 | 23 | 4 | 6,17 | -3,43 | -3,38 | 7,06 |
| P12_CT0_B1 | 3,17 | 1 | 8 | 28 | 0 | 4,92 | -2,56 | -2,32 | 5,55 |
| P12_CT0_B2 | 3,3 | 2 | 7,1 | 28 | 0 | 4,92 | -3,38 | -3,70 | 5,97 |
| P12_CT0_B3 | 1,59 | 1 | 3 | 28 | 0 | 4,92 | -1,06 | -1,48 | 5,03 |
| P12_CT1_B1 | 2,33 | 1 | 5,1 | 28 | 0 | 4,65 | -2,35 | -1,62 | 5,21 |
| P12_CT1_B2 | 2,4 | 1 | 6,1 | 28 | 0 | 4,65 | -2,85 | -2,83 | 5,45 |
| P12_CT1_B3 | 1,58 | 1 | 3,1 | 28 | 0 | 4,65 | -1,23 | -0,79 | 4,81 |
| P12_CT2_B1 | 11,01 | 6,5 | 28 | 28 | 2 | 6,19 | -3,72 | -2,24 | 7,22 |
| P12_CT2_B2 | 11,37 | 7 | 28 | 28 | 2 | 6,19 | -4,34 | -4,11 | 7,56 |
| P12_CT2_B3 | 4,64 | 2 | 12,2 | 28 | 0 | 6,19 | -2,10 | -0,89 | 6,54 |
| P12_CT3_B1 | 8,93 | 5 | 27,1 | 28 | 1 | 6,09 | -3,15 | -2,32 | 6,86 |
| P12_CT3_B2 | 10,44 | 7 | 28 | 28 | 1 | 6,09 | -3,89 | -3,95 | 7,23 |
| P12_CT3_B3 | 4,84 | 1,5 | 13 | 28 | 0 | 6,09 | -1,57 | -1,23 | 6,29 |
| P12_CT4_B1 | 17,25 | 21 | 28 | 28 | 8 | 7,62 | -2,96 | -2,59 | 8,17 |
| P12_CT4_B2 | 17,72 | 22 | 28 | 28 | 11 | 7,62 | -3,86 | -4,17 | 8,54 |
| P12_CT4_B3 | 10,99 | 7 | 28 | 28 | 1 | 7,62 | -1,27 | -1,61 | 7,72 |
| P12_CT5_B1 | 8,8 | 6 | 26 | 28 | 1 | 6,26 | -3,01 | -2,05 | 6,95 |
| P12_CT5_B2 | 11,21 | 7,5 | 28 | 28 | 4 | 6,26 | -3,63 | -3,59 | 7,24 |
| P12_CT5_B3 | 5,21 | 2 | 14,1 | 28 | 0 | 6,26 | -1,58 | -0,98 | 6,46 |
| P13_CT0_B1 | 20,28 | 23 | 23 | 23 | 26 | 10,99 | -1,25 | -5,23 | 11,06 |
| P13_CT0_B2 | 22,4 | 23 | 23 | 23 | 45 | 10,99 | -3,70 | -6,38 | 11,60 |
| P13_CT0_B3 | 15,34 | 18,5 | 23 | 23 | 13 | 10,99 | 1,53 | -5,30 | 11,10 |
| P14_CT0_B1 | 6,66 | 3 | 19,2 | 23 | 2 | 6,90 | -1,38 | -1,13 | 7,04 |
| P14_CT0_B2 | 7,42 | 4 | 20,1 | 23 | 1 | 6,90 | -1,76 | -1,86 | 7,12 |
| P14_CT0_B3 | 4,85 | 2 | 12,1 | 23 | 1 | 6,90 | -0,63 | -0,66 | 6,93 |
| P14_CT1_B1 | 22,92 | 23 | 23 | 23 | 66 | 11,96 | -2,53 | -4,05 | 12,22 |
| P14_CT1_B2 | 22,36 | 23 | 23 | 23 | 48 | 11,96 | -4,22 | -5,62 | 12,68 |
| P14_CT1_B3 | 22,6 | 23 | 23 | 23 | 61 | 11,96 | -0,17 | -3,42 | 11,96 |

Table B.1: **LFBT = last fraction below threshold. Gamma index metrics results for all esophagus patients. Mean = mean LFBT. Max = maximum LFBT. Med = median last fraction between threshold. 90th = 90th percentile of LFBT. #fx BT = number of simulations in which no single fraction reaches the threshold (100 simulations total). LR and AP motion have been corrected for gantry rotation. SI is not affected by gantry rotation. 2D_motion =$\sqrt{SI^2 + LR^2}$. presc. # fx = number of prescribed fractions**

| pt_id | mean | med | 90th | presc. fx | #frac BT | SI [mm] | LR [mm] | AP [mm] | 2D motion |
|---|---|---|---|---|---|---|---|---|---|
| P04_CT0_B1 | 1 | 1 | 1 | 24 | 0 | 3,48 | -1,14 | -1,62 | 3,66 |
| P04_CT0_B2 | 1,05 | 1 | 1 | 24 | 0 | 3,48 | -1,62 | -2,14 | 3,84 |
| P04_CT0_B3 | 1,01 | 1 | 1 | 24 | 0 | 3,48 | -1,26 | -0,99 | 3,70 |
| P04_CT1_B1 | 1,37 | 1 | 2 | 24 | 0 | 3,37 | -3,06 | -1,50 | 4,55 |
| P04_CT1_B2 | 1,23 | 1 | 2 | 24 | 0 | 3,37 | -2,87 | -2,60 | 4,43 |
| P04_CT1_B3 | 1 | 1 | 1 | 24 | 0 | 3,37 | -0,46 | -0,28 | 3,40 |
| P04_CT2_B1 | 1 | 1 | 1 | 24 | 0 | 3,46 | -1,61 | -1,09 | 3,82 |
| P04_CT2_B2 | 1,05 | 1 | 1 | 24 | 0 | 3,46 | -1,67 | -1,70 | 3,84 |
| P04_CT2_B3 | 1 | 1 | 1 | 24 | 0 | 3,46 | -0,55 | -0,40 | 3,50 |
| P04_CT3_B1 | 1,66 | 1 | 3 | 24 | 0 | 3,76 | -3,15 | -1,96 | 4,90 |
| P04_CT3_B2 | 1,64 | 1 | 3 | 24 | 0 | 3,76 | -3,18 | -3,15 | 4,92 |
| P04_CT3_B3 | 1,01 | 1 | 1 | 24 | 0 | 3,76 | -0,91 | -0,64 | 3,87 |
| P04_CT4_B1 | 2,1 | 1 | 4,1 | 24 | 0 | 4,26 | -2,31 | -4,87 | 4,85 |
| P04_CT4_B2 | 6,22 | 4 | 15,1 | 24 | 2 | 4,26 | -4,11 | -6,12 | 5,92 |
| P04_CT4_B3 | 5,37 | 3 | 14,1 | 24 | 0 | 4,26 | -4,20 | -3,35 | 5,98 |
| P04_CT5_B1 | 1 | 1 | 1 | 24 | 0 | 2,94 | -1,77 | -1,12 | 3,43 |
| P04_CT5_B2 | 1 | 1 | 1 | 24 | 0 | 2,94 | -1,80 | -1,79 | 3,45 |
| P04_CT5_B3 | 1 | 1 | 1 | 24 | 0 | 2,94 | -0,53 | -0,38 | 2,99 |
| P08_CT0_B1 | 1 | 1 | 1 | 24 | 0 | 3,18 | -0,68 | -1,11 | 3,25 |
| P08_CT0_B2 | 1 | 1 | 1 | 24 | 0 | 3,18 | 0,48 | 1,18 | 3,22 |
| P08_CT0_B3 | 1 | 1 | 1 | 24 | 0 | 3,18 | -0,03 | -0,94 | 3,18 |
| P08_CT1_B1 | 1,16 | 1 | 1 | 24 | 0 | 3,9 | -1,39 | -0,98 | 4,14 |
| P08_CT1_B2 | 1 | 1 | 1 | 24 | 0 | 3,9 | 1,20 | 1,17 | 4,08 |
| P08_CT1_B3 | 1,06 | 1 | 1 | 24 | 0 | 3,9 | -0,71 | -0,49 | 3,96 |
| P08_CT2_B1 | 1,12 | 1 | 1 | 24 | 0 | 3,9 | -1,51 | -0,71 | 4,18 |
| P08_CT2_B2 | 1,02 | 1 | 1 | 24 | 0 | 3,9 | 1,36 | 0,94 | 4,13 |
| P08_CT2_B3 | 1,06 | 1 | 1 | 24 | 0 | 3,9 | -0,95 | -0,14 | 4,01 |
| P08_CT3_B1 | 1,27 | 1 | 2,1 | 24 | 0 | 4,12 | -1,48 | -1,10 | 4,38 |
| P08_CT3_B2 | 1 | 1 | 1 | 24 | 0 | 4,12 | 1,27 | 1,30 | 4,31 |
| P08_CT3_B3 | 1,13 | 1 | 1 | 24 | 0 | 4,12 | -0,73 | -0,59 | 4,18 |
| P08_CT4_B1 | 1 | 1 | 1 | 24 | 0 | 0,75 | -0,65 | -0,90 | 0,99 |
| P08_CT4_B2 | 1 | 1 | 1 | 24 | 0 | 0,75 | 0,48 | 0,97 | 0,89 |
| P08_CT4_B3 | 1 | 1 | 1 | 24 | 0 | 0,75 | -0,11 | -0,72 | 0,76 |
| P10_CT0_B1 | 12,86 | 12 | 24 | 24 | 4 | 8,19 | -1,86 | -2,63 | 8,40 |
| P10_CT0_B2 | 15,84 | 21,5 | 24 | 24 | 17 | 8,19 | -2,93 | -3,74 | 8,70 |
| P10_CT0_B3 | 7,74 | 4 | 24 | 24 | 2 | 8,19 | -0,30 | -2,13 | 8,20 |
| P10_CT1_B1 | 23,54 | 24 | 24 | 24 | 50 | 10,55 | -2,85 | -3,77 | 10,93 |
| P10_CT1_B2 | 23,57 | 24 | 24 | 24 | 55 | 10,55 | -4,35 | -5,44 | 11,41 |
| P10_CT1_B3 | 19,26 | 24 | 24 | 24 | 14 | 10,55 | -0,58 | -2,97 | 10,57 |
| P10_CT2_B1 | 21,57 | 24 | 24 | 24 | 37 | 9,71 | -3,05 | -5,50 | 10,18 |
| P10_CT2_B2 | 22,18 | 24 | 24 | 24 | 44 | 9,71 | -5,39 | -7,46 | 11,11 |
| P10_CT2_B3 | 13,45 | 14 | 24 | 24 | 8 | 9,71 | 0,11 | -4,82 | 9,71 |
| P10_CT3_B1 | 23,15 | 24 | 24 | 24 | 44 | 10,55 | -2,85 | -3,77 | 10,93 |
| P10_CT3_B2 | 23,23 | 24 | 24 | 24 | 48 | 10,55 | -4,35 | -5,44 | 11,41 |
| P10_CT3_B3 | 18,31 | 24 | 24 | 24 | 18 | 10,55 | -0,58 | -2,97 | 10,57 |
| P10_CT4_B1 | 15,36 | 19 | 24 | 24 | 10 | 8,45 | -2,12 | -3,41 | 8,71 |
| P10_CT4_B2 | 17,91 | 23 | 24 | 24 | 24 | 8,45 | -3,54 | -4,72 | 9,16 |
| P10_CT4_B3 | 9,18 | 7 | 22,1 | 24 | 1 | 8,45 | -0,13 | -2,89 | 8,45 |
| P15_CT0_B1 | 1 | 1 | 1 | 30 | 0 | 2,49 | -0,83 | -1,21 | 2,62 |
| P15_CT0_B2 | 1 | 1 | 1 | 30 | 0 | 2,49 | 0,99 | 0,24 | 2,68 |
| P15_CT0_B3 | 1 | 1 | 1 | 30 | 0 | 2,49 | -0,34 | -0,92 | 2,51 |
| P15_CT1_B1 | 1 | 1 | 1 | 30 | 0 | 3,04 | -1,40 | -1,56 | 3,35 |
| P15_CT1_B2 | 1 | 1 | 1 | 30 | 0 | 3,04 | 1,54 | 0,06 | 3,41 |
| P15_CT1_B3 | 1 | 1 | 1 | 30 | 0 | 3,04 | -0,85 | -0,98 | 3,16 |
| P15_CT2_B1 | 1 | 1 | 1 | 30 | 0 | 2,52 | -1,20 | -1,48 | 2,79 |
| P15_CT2_B2 | 1 | 1 | 1 | 30 | 0 | 2,52 | 1,36 | 0,15 | 2,86 |
| P15_CT2_B3 | 1 | 1 | 1 | 30 | 0 | 2,52 | -0,65 | -1,01 | 2,60 |
| P15_CT3_B1 | 1 | 1 | 1 | 30 | 0 | 2,2 | -1,65 | -1,93 | 2,75 |
| P15_CT3_B2 | 1 | 1 | 1 | 30 | 0 | 2,2 | 1,84 | 0,13 | 2,87 |
| P15_CT3_B3 | 1 | 1 | 1 | 30 | 0 | 2,2 | -0,96 | -1,26 | 2,40 |

Table B.2: **LFBT = last fraction below threshold. Gamma index metrics results for all lung patients. Mean = mean LFBT. Max = maximum LFBT. Med = median last fraction between threshold. 90th = 90th percentile of LFBT. #frac BT = number of simulations in which no single fraction reaches the threshold (100 simulations total). LR and AP motion have been corrected for gantry rotation. SI is not affected by gantry rotation. 2D_motion =$\sqrt{SI^2 + LR^2}$. presc. fx = number of prescribed fractions**

| pt_id | mean | median | 90th | presc. fx | #frac BT | SI [mm] | LR [mm] | AP [mm] | 2D motion |
|---|---|---|---|---|---|---|---|---|---|
| P01_CT0_B1 | 1 | 1 | 1 | 17 | 0 | 3,78 | 1,46 | 1,61 | 4,05 |
| P01_CT0_B2 | 1 | 1 | 1 | 17 | 0 | 3,78 | 1,94 | 1,02 | 4,25 |
| P01_CT1_B1 | 1,14 | 1 | 1,1 | 17 | 0 | 4,77 | 1,49 | 1,73 | 5,00 |
| P01_CT1_B2 | 1,08 | 1 | 1 | 17 | 0 | 4,77 | 2,01 | 1,12 | 5,18 |
| P02_CT0_B1 | 1 | 1 | 1 | 10 | 0 | 3,31 | 0,79 | 1,45 | 3,40 |
| P02_CT0_B2 | 1 | 1 | 1 | 10 | 0 | 3,31 | 1,98 | 2,02 | 3,85 |
| P02_CT0_B3 | 1 | 1 | 1 | 10 | 0 | 3,31 | 3,08 | -0,12 | 4,52 |
| P02_CT0_B4 | 1 | 1 | 1 | 10 | 0 | 3,31 | 2,80 | -1,30 | 4,33 |
| P02_CT1_B1 | 1 | 1 | 1 | 10 | 0 | 2,44 | 2,08 | 2,43 | 3,21 |
| P02_CT1_B2 | 1,02 | 1 | 1 | 10 | 0 | 2,44 | 3,79 | 2,78 | 4,51 |
| P02_CT1_B3 | 1,16 | 1 | 2 | 10 | 0 | 2,44 | 4,89 | -0,89 | 5,47 |
| P02_CT1_B4 | 1,03 | 1 | 1 | 10 | 0 | 2,44 | 4,07 | -2,29 | 4,75 |
| P03_CT0_B1 | 3,15 | 2 | 7,2 | 15 | 0 | 7,46 | 3,88 | 2,99 | 8,41 |
| P03_CT0_B2 | 2,13 | 1 | 4,1 | 15 | 0 | 7,46 | 4,69 | 1,50 | 8,81 |
| P03_CT1_B1 | 1,04 | 1 | 1 | 15 | 0 | 3,90 | 2,79 | 2,56 | 4,79 |
| P03_CT1_B2 | 1,07 | 1 | 1 | 15 | 0 | 3,90 | 3,52 | 1,47 | 5,25 |
| P16_CT0_B1 | 1,01 | 1 | 1 | 18 | 0 | 2,84 | 2,59 | 1,99 | 3,85 |
| P16_CT0_B2 | 1 | 1 | 1 | 18 | 0 | 2,84 | 3,14 | 0,99 | 4,23 |
| P16_CT1_B1 | 1,51 | 1 | 3 | 18 | 0 | 5,47 | 2,24 | 2,71 | 5,91 |
| P16_CT1_B2 | 1,42 | 1 | 2 | 18 | 0 | 5,47 | 3,06 | 1,79 | 6,27 |
| P16_CT2_B1 | 12,18 | 14,5 | 18 | 18 | 11 | 11,22 | 4,29 | 3,07 | 12,01 |
| P16_CT2_B2 | 10,45 | 10,5 | 18 | 18 | 4 | 11,22 | 5,11 | 1,44 | 12,33 |
| P17_CT0_B1 | 1,08 | 1 | 1 | 15 | 0 | 4,88 | 2,08 | 3,72 | 5,31 |
| P17_CT0_B2 | 1,21 | 1 | 2 | 15 | 0 | 4,88 | 4,19 | 3,09 | 6,43 |
| P17_CT0_B3 | 1,58 | 1 | 3 | 15 | 0 | 4,88 | 5,17 | 0,09 | 7,11 |
| P17_CT1_B1 | 1 | 1 | 1 | 15 | 0 | 3,71 | 2,29 | 3,26 | 4,36 |
| P17_CT1_B2 | 1,08 | 1 | 1 | 15 | 0 | 3,71 | 4,05 | 2,44 | 5,49 |
| P17_CT1_B3 | 1,2 | 1 | 1,1 | 15 | 0 | 3,71 | 4,73 | -0,25 | 6,01 |
| P18_CT0_B1 | 1 | 1 | 1 | 15 | 0 | 1,76 | 1,96 | 0,41 | 2,63 |
| P18_CT0_B2 | 1 | 1 | 1 | 15 | 0 | 1,76 | 1,98 | -0,29 | 2,65 |
| P18_CT1_B1 | 1 | 1 | 1 | 15 | 0 | 2,45 | 2,74 | 1,59 | 3,68 |
| P18_CT1_B2 | 1 | 1 | 1 | 15 | 0 | 2,45 | 3,12 | 0,43 | 3,97 |

Table B.3: **LFBT = last fraction below threshold. Gamma index metrics results for all lymphoma patients. Mean = mean LFBT. Max = maximum LFBT. Med = median last fraction between threshold. 90th = 90th percentile of LFBT. #frac BT = number of simulations in which no single fraction reaches the threshold (100 simulations total). LR and AP motion have been corrected for gantry rotation. SI is not affected by gantry rotation. 2D_motion $=\sqrt{SI^2 + LR^2}$. presc. fx = number of prescribed fractions**

## Correlation between tumor motion and Gamma index metrics

Figure B.6 shows the correlation between the three primary Gamma index metrics and the 2D tumor motion for all types of tumor.A very clear and strong correlation between primarily the tumor motion and the mean LFBT can be seen, but also between the two other metrics and the tumor motion.

Figure B.4 and B.5 show the correlation between CTV LR and SI motion with respect to the Gamma index metrics, respectively. While SI motion has a strong correlation with the Gamma index metrics that is similar to the 2D motion, there is no correlation between LR tumor motion and the Gamma index Metrics. This suggests that the SI tumor motion is the most important motion direction in interplay robustness calculation, like is often assumed in literature.

Figure B.7 shows the correlation between the 2D tumor motion and the Gamma index metrics. This is essentially the same figure as figure 3.6 but with a sigmoid fitted line instead of a linear one.
The sigmoid line is defined as

$$y = \frac{L}{1 + \exp(-k(x - x_0))} + b \tag{B.1}$$

where L equals the maximum value of y, k represents the steepness of the curve, $x_0$ determines the inflection or transition point, and b is the y-intercept curve.

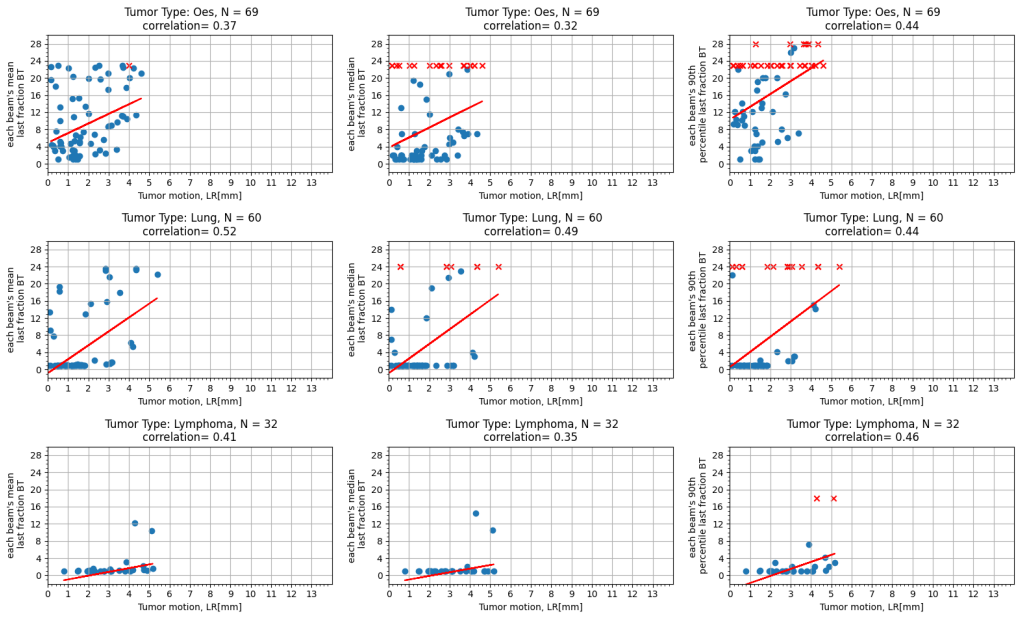


Figure B.4: **Correlation between only the LR tumor motion of the beams and the Gamma index metrics.**

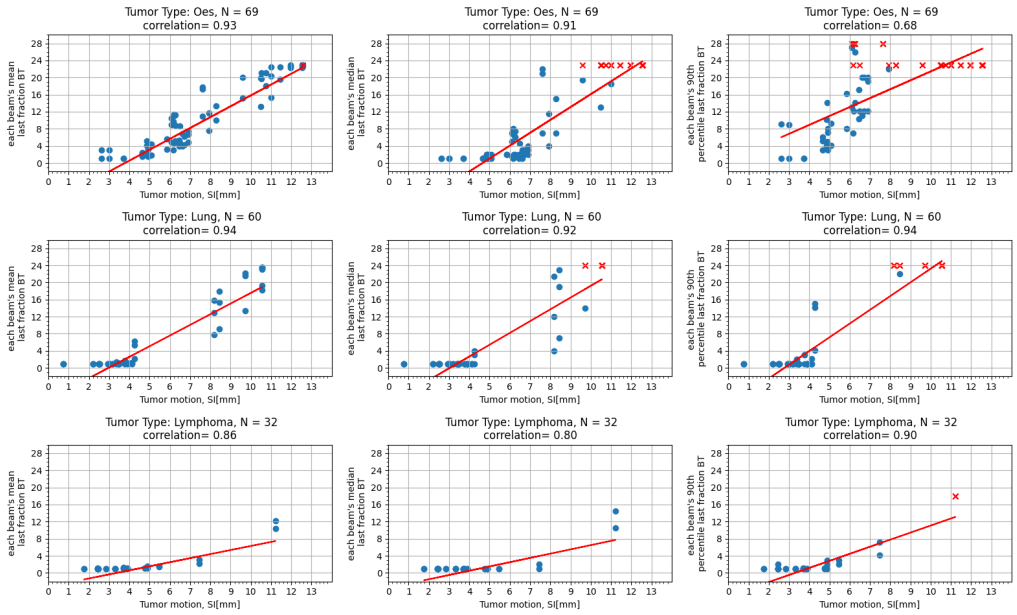


Figure B.5: **Correlation between only the SI tumor motion of the beams and the Gamma index metrics.**

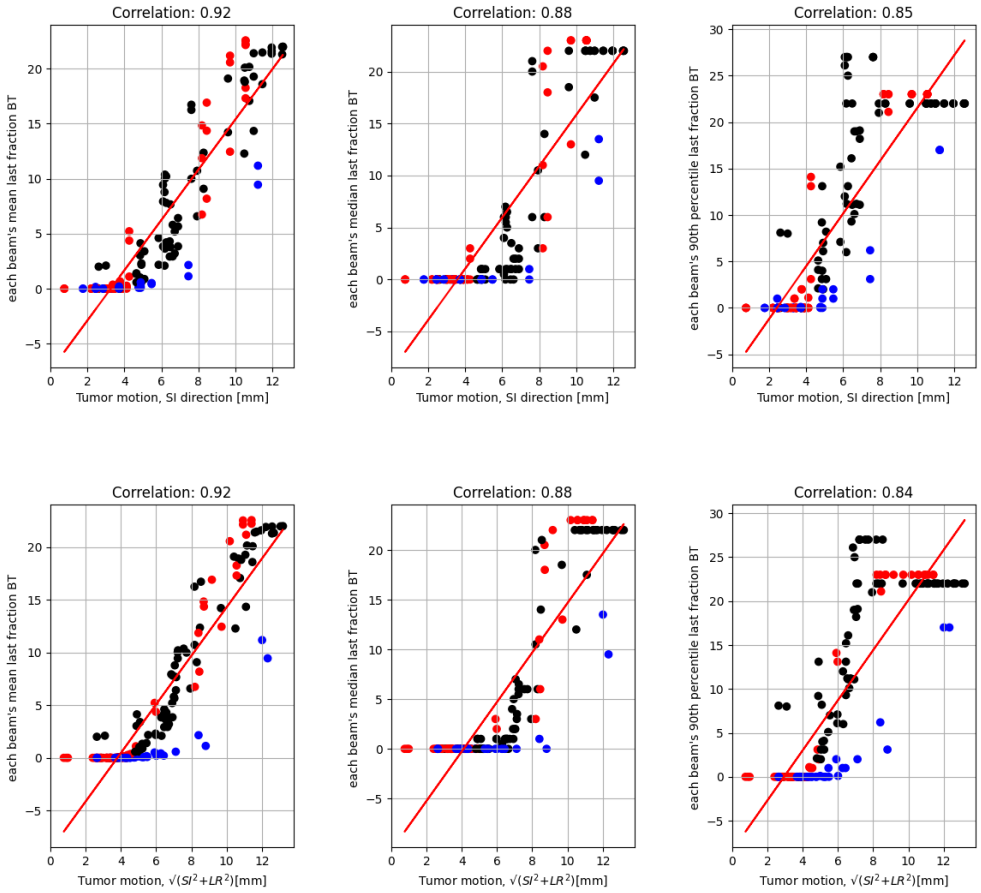


Figure B.6: **Correlation between the two types of motion (uni-dimensional and two dimensional) and the three Gamma index metrics described in section 3.1.4 Clinical evaluation.**
**BT = below threshold, 95%. Red= lung, black = esophagus, blue = lymphoma. N= 161 in all. Note that the LR motion has been corrected for gantry rotation.**

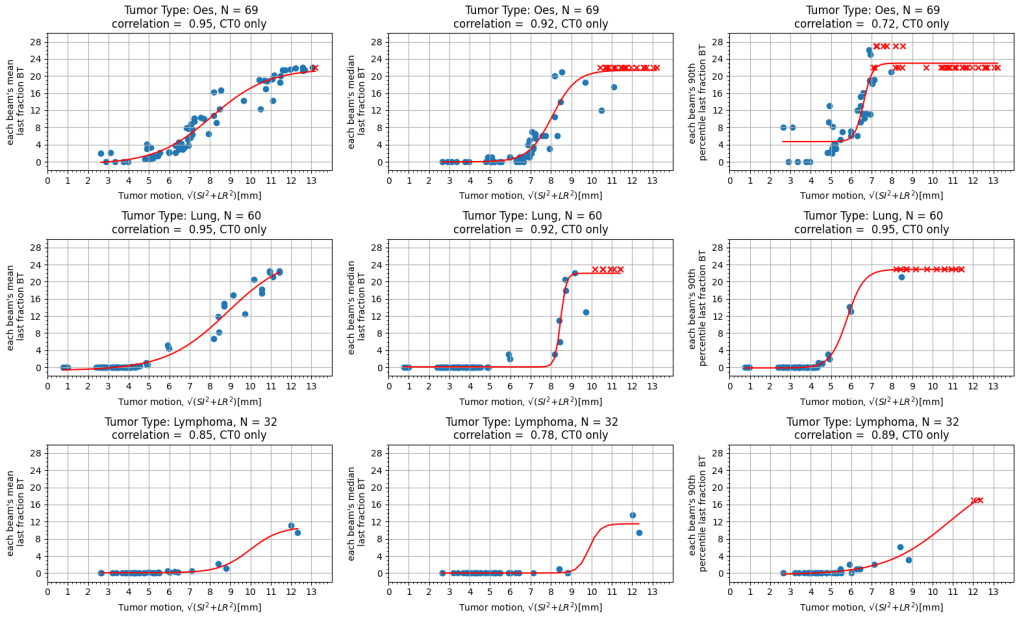


Figure B.7: **Correlation between 2D tumor motion of all three tumor types and the three primary Gamma index metrics. Each data point depicts one of the 161 beams. The red X's show the beams where the corresponding metric is equal to the number of fractions that have been prescribed in that patient's treatment plan. The same data as figure 3.6, but with a sigmoid fitting curve instead of a linear.**

## Other results

The patient- and beam data also contained the dates the 4D-CTs were taken and consequently, the time between planning 4D-CT called CT0, and the later 4D-CTs. If this data is graphed against the change Gamma index metrics, the effect of different tumor motion on the same treatment plan can be visualized. [1]

### Time since planning CT vs change in Gamma index metrics

Figure B.8 shows the correlation between the Gamma index metrics throughout 4D-CTs that are taken after the planning 4D-CT. For all the 4D-CTs that are taken later, the difference in Gamma index metrics as compared to the planning 4D-CT (CT0) are calculated and plotted against the time between the planning and later 4D-CT.

Since many of the beams have metrics that are 1 in all 4D-CTs (See Table B.3 for example), figure B.8b shows the same data but all the values where the change in Gamma index metric = 1 are removes.

The number of data points that are either above or below a $\Delta$metric of 0 is shown above the plot.

This data shows that in most of the simulations, the Gamma index metrics increase as time progresses. For example, in 74% of the beams, the 90th percentile last fraction below threshold, which is the main determinant metric as explained in section 3.1.4 Clinical evaluation, increases when compared to the same metric in the planning CT.

### Time since planning CT vs change in tumor motion amplitude

In order to assess the change in tumor motion amplitude in 4D-CTs that were taken after the initial planning 4D-CT (CT0), the number of days between CT0 and the later 4D-CTs was extracted from Raystation. This is depicted on the X-axis in figure B.9 . The Y-axis shows the tumor motion change in SI, LR, AP, 2D, and 3D direction, respectively, between CT0 and the later 4D-CTs.

The data shows there is a small decrease in LR and AP motion as time progresses.

### Ratio between SI and LR motion

Figure B.10 shows the ratio between the real esophagus and lung cancer patients' SI and LR motion. Even though the mean and median values are larger than a ratio of 2, the most common value (modus) is around two. This is similar to the ratio picked in section 4.1 Artificial amplitude.

### Correlation between Gamma index metrics and tumor motion

There is a strong correlation between the tumor motion and all four Gamma index metrics (see figure 3.6, and B.6 [70].

Figure 3.6 shows the three Gamma index metrics plotted against the 2D motion of the CTV in each beam's corresponding 4D-CT.

[1] Remember that between a patient's CT0 and CT1, the only factor that changes is the tumor motion amplitude in SI and LR direction. The starting breathing phase of each fraction simulation is random every time. The simulated dose measurement is the same. All simulation parameters are the same.

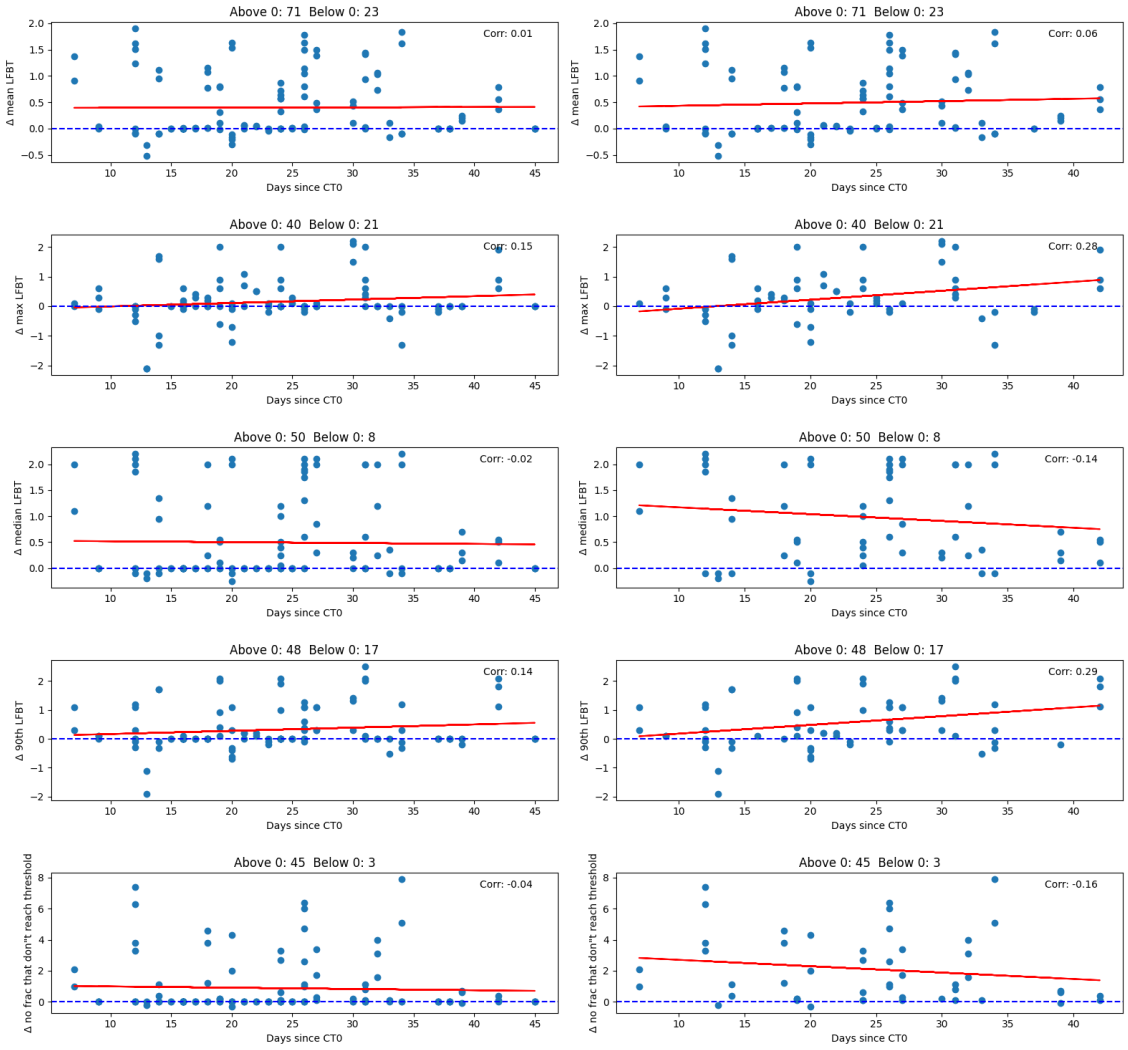


(a) (b)

Figure B.8: **Graphs show the difference between the Gamma index metrics of the first 4D-CT (CT0), on which the treatment planning was based, and the 4D-CTs taken later during the treatment. Title shows the number of beams in which the Gamma index metric increase or decrease in later 4D-CTs. LFBT = last fraction below threshold.**
**(a) Zeros remained. (b) Zeros removed.**

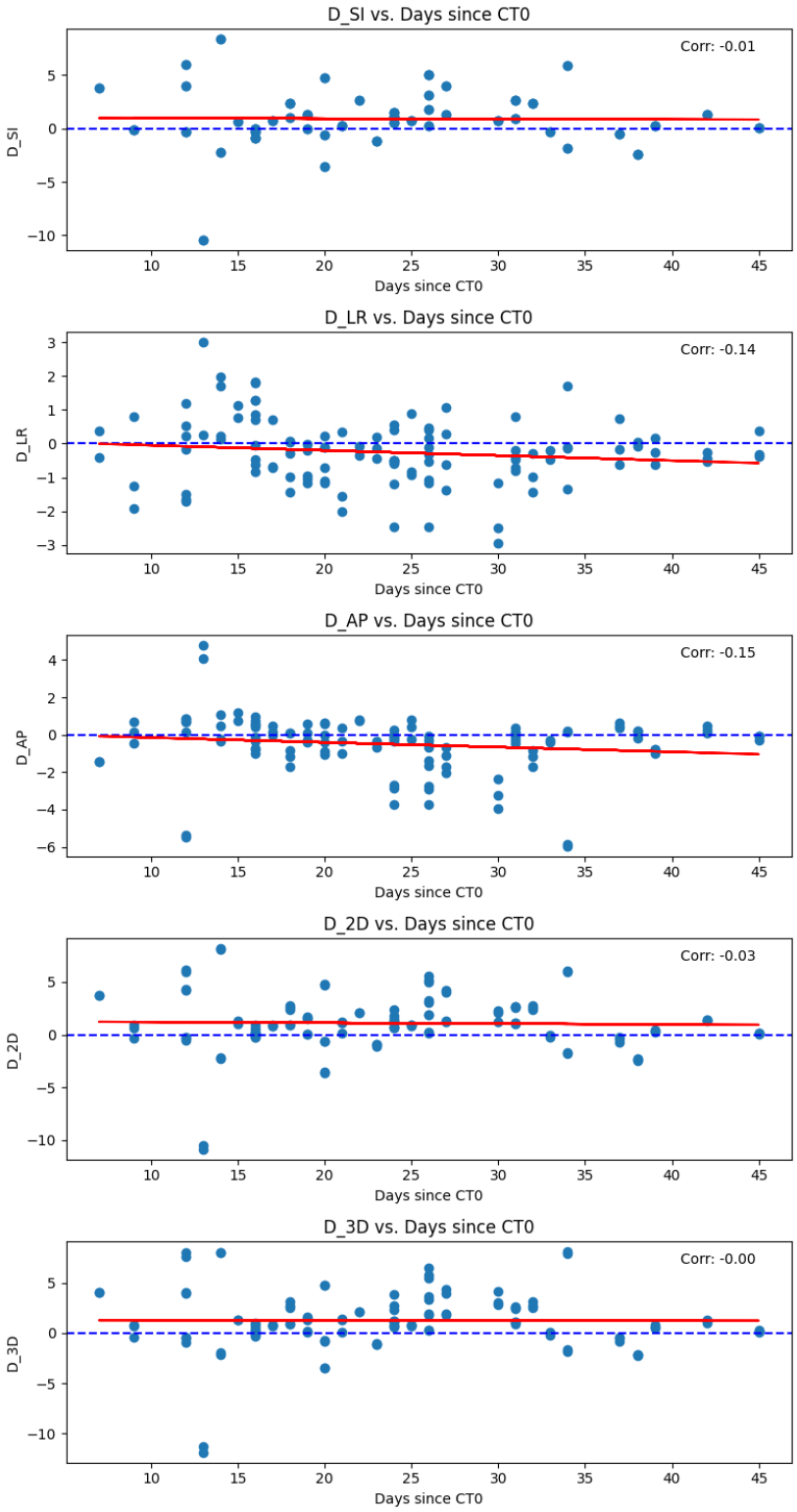




Figure B.9: **Relationship between the change in tumor motion amplitude in multiple directions as time progresses and new 4D-CTs are taken. Y-axis is in mm. D_SI stands for change in SI tumor motion.**

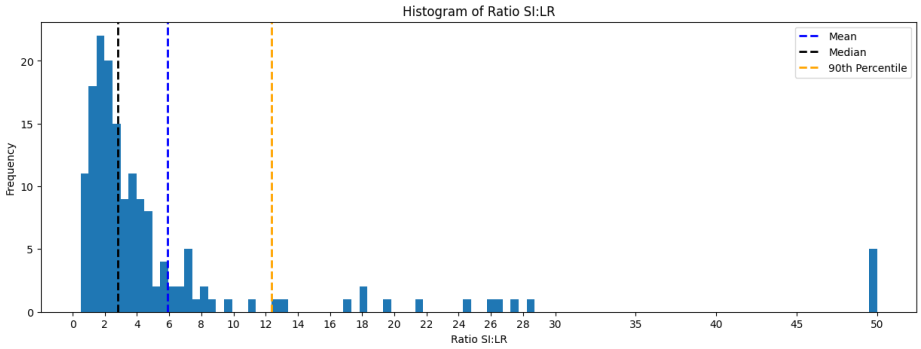


Figure B.10: **The Ratio between the real patients' SI and LR motion. The LR motion has already been corrected for beam rotation. To handle values above the threshold of 50, they have been capped and grouped into the bin corresponding to the value of 50. Similar data to figure 4.5.**

## 100 fractions

Figure B.11 shows the correlation between the 2D tumor motion amplitude and the three primary Gamma index metrics. In this simulation, each treatment is simulated with 100 fractions, instead of the regular number of prescribed fractions (ranging from 10 to 28). It shows that if the number of fractions is taken beyond the clinically prescribed number, tumor motion amplitude and Gamma index metrics are still strongly correlated.

Looking at the two data points around 12 mm amplitude in the bottom left graph, lymphoma patients' mean LFBT, notice a difference with the same data points in figure 3.6. If the number of fractions is equal to the clinically prescribed value (10-18 in lymphoma patients), the mean LFBT is around 12 fractions. However, if the number of fractions goes up to 100, the mean LFBT is 22 and 41 for those two beams. This can be explained by the fact that if, in one simulation, the LFBT is above the number of prescribed fractions, the LFBT will still be capped at the number of prescribed fractions. If from 100 simulations, 99 have an LFBT at the maximum possible value (the number of prescribed fractions), and one simulation has an LFBT smaller than the maximum possible value, the mean LFBT is still below the maximum value. [2]

[2]Mean([15, 15, 15, 15, 15, 15, 15, 15, 15, 1]) =14.2. This shows that only if all the simulations have an LFBT equal to the number of prescribed fractions the mean LFBT can be equal to the number of prescribed fractions.

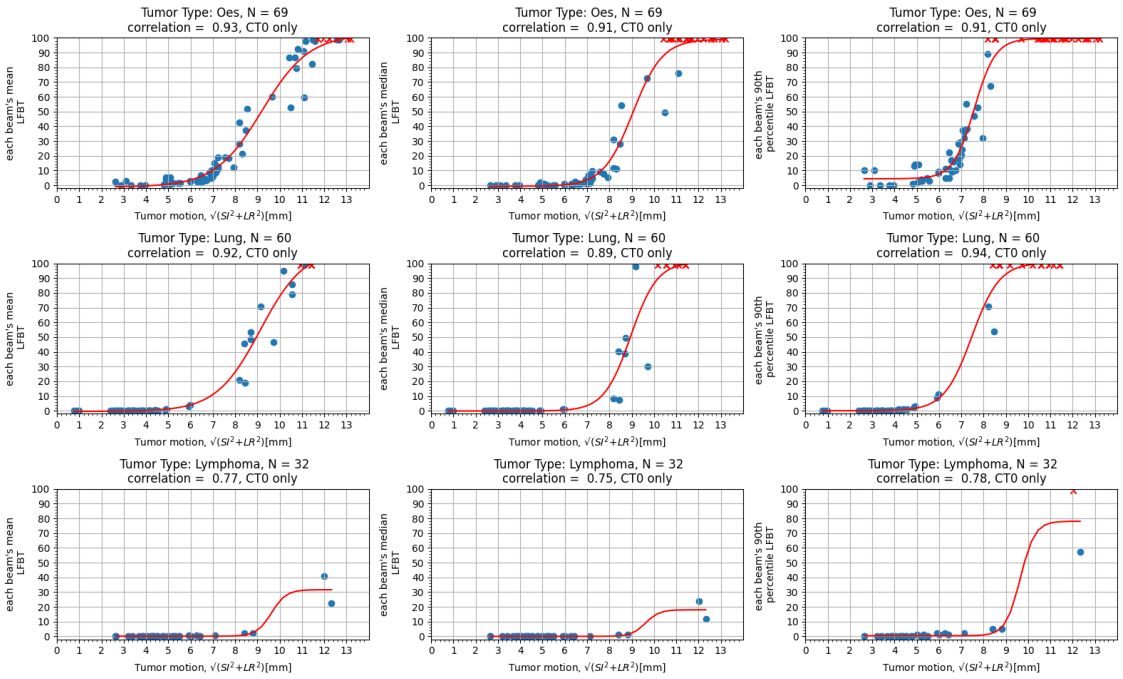


Figure B.11: **Correlation between Gamma index metrics and 2D tumor motion amplitude, simulated with 100 fractions. Each data point depicts one of the 161 beams. The red X's show the beams where the corresponding metric is equal to the number of fractions prescribed in that patient's treatment plan.**

# Appendix C

# Obsolete Approaches

The following sections contain explanations of methods that were abandoned: The center of mass (COM) method, percentile movement, and voxel tracking. They will be shortly explained in the following sections.

## Center of mass motion

The goal of this method was to track the locations of the geometrical center of mass of the CTV and assume the entire CTV moves similarly.

Of all the phases of each 4D-CT, the geometrical center or center of mass of all ten phases of the CTV was created in RayStation using the ROI center point specification method. All coordinates of these points are recorded. Next, these coordinates are normalized. This means for all ten X-coordinates of one 4D-CT, the mean of the X coordinates is subtracted to make their mean 0. The same method is applied to the Y and Z coordinates.

Subsequently, the 10 coordinates were interpolated to accommodate 40ms timesteps, similar to the results of the MatriXX detector array. Finally, these coordinates were stored in a .json file.

The validation of this method is described in C.3 Validation center of mass method.

## Percentile movement

Another option is to track the motion of all the CTV voxels between consecutive phases. Currently, the *respiratory_amplitude* script by Dr. Y. Wang applies this method to measure the motion of the tumor between the breath-in and breath-out phases. From this data, a distribution of the magnitude of voxel motion in one of the three directions can be made. For an example image of this, see figure C.3 and C.4. Next, a certain percentile of motion can be decided to represent the entire CTV motion in that specific phase. If all the motion between all ten phases is combined, a representation of CTV motion based on voxel motion can be made. It is important to note that this certain percentile of motion is not always the same voxel and so not always the same part of the tumor.

The steps taken to calculate the percentile movement are as follows:

- Check if CTV is present in at least one phase. When necessary, the triangle mesh was converted to regular contours.
- If the CTV is not present in all phases, apply contour propagation to copy it to all phases.
- Perform deformable registration is performed from 0% to 10%, 10% to 20%, etc
- Extract voxelwise displacement between all ten phases (see figure C.3 and C.4).
- Add the 50th percentile of this voxelwise displacement together in order to get one path with ten steps. Repeat for other percentiles.
- To this 3D tumor path, rotation is applied according to section 3.1.3 and Equation 3.1.

If the voxels of a CTV move in the negative direction on one of their axis, almost all the voxel motion will be negative as well. In that case, the 10th percentile should be taken rather than the 90th percentile. A percentile is always considered from lowest to highest, so the correct motion is not considered if the motion is primarily in the negative direction. For this reason, if the absolute value of the tenth percentile is higher than the absolute value of the 90th percentile, the 10th percentile will be considered as the 90th percentile For an example case, see figure C.3.

the same method of normalization and interpolation, as described in C Center of mass motion, was performed for these data.

The validation of this method is described in C.3 Validation of percentile method.

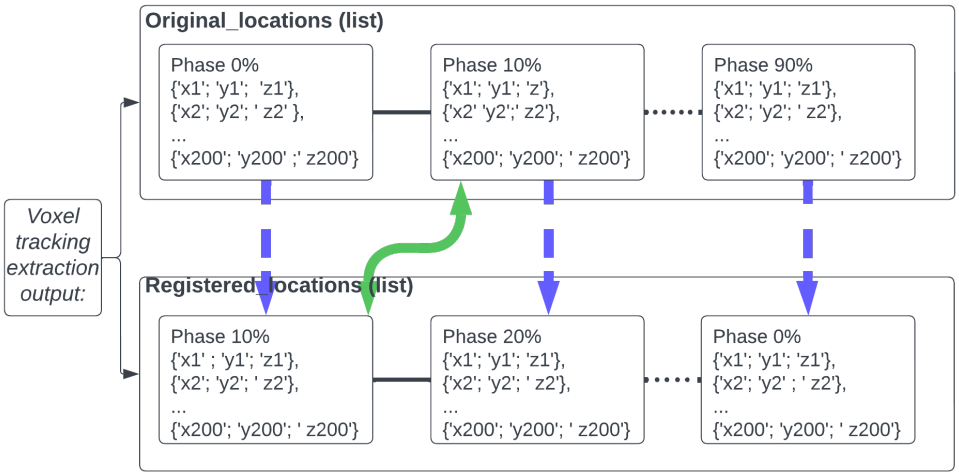


Figure C.1: **A diagram of the voxel tracking extraction output. The blue dashed lines depict the result of the deformable registration: according to the hybrid deformable registration, the original voxel coordinates in phase 0% are moved to the voxel coordinates of phase 10% in the list registered_locations. The green solid line shows which groups of coordinates hypothetically indicate the same voxel: the original_locations show the voxel coordinates in the CTV in phase 10%, delineated in RayStation and confirmed by a radiotherapist - oncologist and registered_locations list the voxel coordinates of the previous phase, based on the deformable registration.**

## Voxel tracking

An attempt was made to use tracking the location of individual voxels during the ten breathing phases.

With RayStation's integrated hybrid deformable registration features, it is feasible to identify the precise x, y, and z coordinates of a voxel in one phase and its subsequent location in the following phase as determined by the deformable registration process. This is performed for all the voxels in all ten breathing phases of the 4D-CT, resulting in every single voxel's trajectory as the patient breathes.

For an overview of the data extraction step in this method, see figure C.1.

- In *voxel _tracking_extraction.py*, two list are extracted:
  - *original_locations*, which contains all the x, y, and z coordinates of all voxels of the CTV in all ten phases.
  - *registered_locations*, which contains all the coordinates where the voxels in *original_locations* are registered to, based on phase-by-phase deformable registration.
- *voxel _tracking_processing.py*. In this script, processing steps are performed.

- Compare lists: For each of the coordinates in the registered_locations, it checks which of all the voxels in original_locations is closest to it. This step can be very computationally expensive.
- Find new locations: This creates a list that, for each of the voxels in the 0% phase, yields the x, y and z coordinates in all phases.
- The path length of all voxel trajectories is calculated, starting from the voxels in the 0% phase. The path lengths and trajectories are stored as .JSON files.

The output of the voxel tracking pipeline consisted of the following data 4D-CT [1] :

- A list with the coordinates of all voxels in each of the ten phases.
- A list with the coordinates where the voxels in the previous phase deform to.
- A list with for each of the voxels, the voxel index of the voxel it registers closest to in the next phase.
- Coordinates of the theoretical path trajectory for each of the voxels in the 0% phase.
  - Resulting from this: plots of one voxel and its trajectory through all ten phases (see figure C.7)
- Path lengths of each voxel's path.
  - Histograms of the path lengths of the voxel trajectories in each beam (See figure C.6)

The output data could be very large; The CTV in P01_CT0_B1, for example, consisted of 17.000 voxels in each phase. As a result, calculating which of the voxels in the next phase is closest to the voxel's registered location resulted in 17.000 * 17.000 = 289.000.000 distance comparisons for each of the ten phases. Calculation time could reach anywhere from 10 minutes to 1 hour per 4D-CT.

One important note needs to be made in advance regarding convergence. First, the size of the CTV is not always equal between all phases of the same 4D-CT. In *voxel_tracking_processing.py*, the original coordinates are compared to the registered coordinates one by one. If the first list has four voxels and the second list has six voxels, the last two voxels of the second list will inevitably be matched to the voxels of the first list that already have a corresponding voxel from the second list.

Secondly, it is possible that two voxels in the *registered_location* list are very close to the same voxel in the *original_location*. While all coordinates in the original list are in step sizes of [3, 1, 1] in [SI, LR, AP] direction, registered coordinates are not uniformly distributed.

The validation of this method is described in section C.3 Voxel tracking validation.

[1] Note that the 3D path of each voxel is independent of beam angle. After each voxel's path has been constructed, the path could be rotated to make it beam-specific.

## C.1 Results old methods

The validation of both the COM, percentile motion, and voxel tracking methods can be found in Appendix C.3, C.3 and C.3.

After the methods were validated, they were applied to the patient data. However, we quickly realized the resulting tumor motion was not a realistic tumor motion.

### COM method

Figure C.2 shows some examples of the center of mass motion. In some cases, the motion looks like it intuitively would be correct. However, the amplitude in both directions is extremely small; Only one of the examples has an amplitude in one direction larger than 1mm. All the other amplitudes are below 0.8mm. The tumor motion amplitudes from the *respiratory_amplitude* script (Table A.2) shows the amplitude that is clinically used in Holland PTC. The amplitudes in figure C.2 is up to 8 times lower than the ones reported in Table A.2. Due to this difference, the steps are considered too small to be considered correct by the author.

A possible explanation arises from the fact that the center of mass effectively averages out the diverse tumor locations and, consequently the associated motion as well.

### Percentile motion

Figure C.3 and C.4 show examples of histograms of the data discussed in section C Percentile movement. Figure C.3 depicts the voxelwise tumor motion from one patient going from the full inhale to the full exhale phase.

Figure C.4 depicts the voxelwise tumor motion from one patient going from the 0% phase to the 10% phase.

Figure C.5 shows some examples of different tumor motion paths using the percentile motion method, section C. (c) shows a result that might intuitively be expected. (a) also has a motion that intuitively looks correct, except for the shaky part in the middle.

Unfortunately, many of the results were similar to (b) and (d), with unrealistic tumor trajectories.

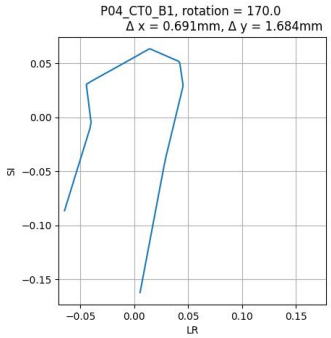


(a) Image 1

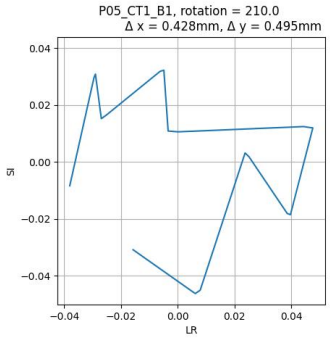


(b) Image 2

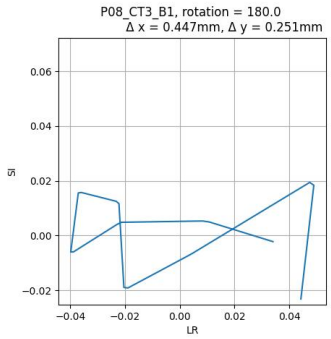


(c) Image 3

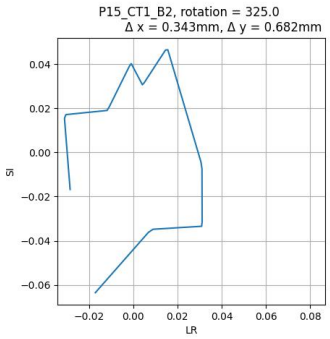


(d) Image 4

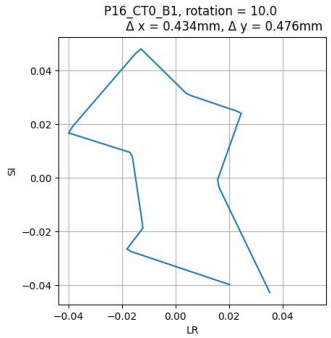


(e) Image 5

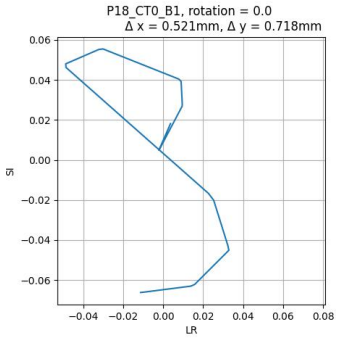


(f) Image 6

Figure C.2: **A few plots of the center of mass(COM) coordinates, out of a total of 155. The intuitive accuracy of the samples varies.**
**The paths have already been corrected for beam rotation, so this is the path of the COM, as 'seen' through by the gantry.**

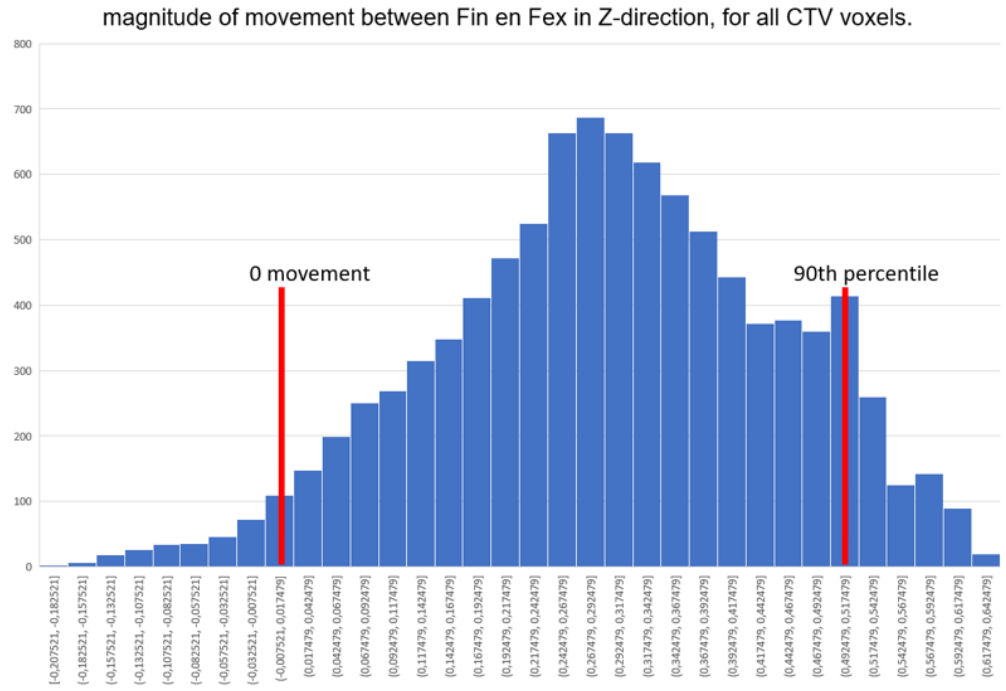


Figure C.3: **Histograms of the movement in SI direction. The X-axis is the movement of the voxels, in cm. ...**

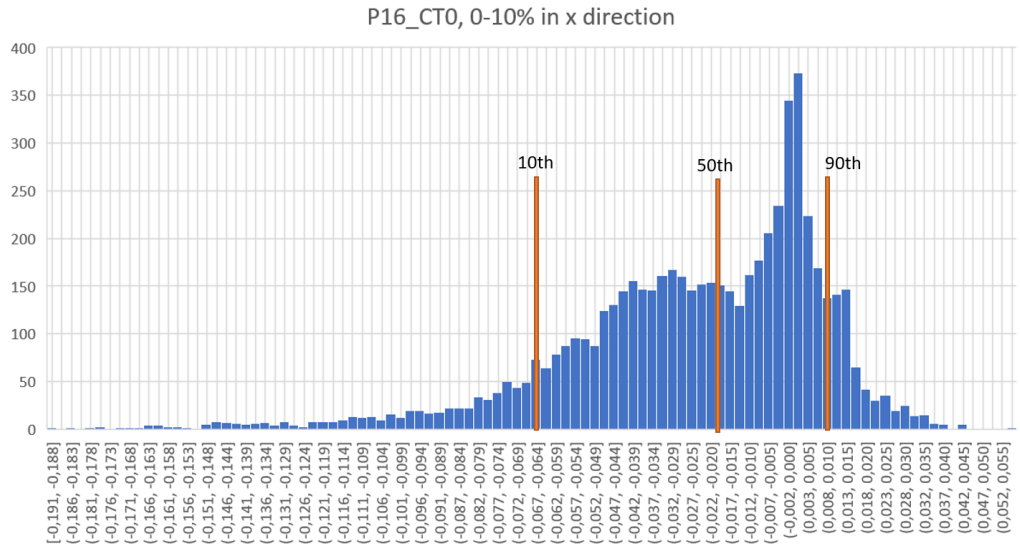


Figure C.4: **Percentile motion: Example of the motion distribution of voxels, primarily in the negative direction. Notice that the 0 motion is at the peak and is very close to the 90th percentile and that the majority of motion is in the negative direction.**

## Voxel tracking

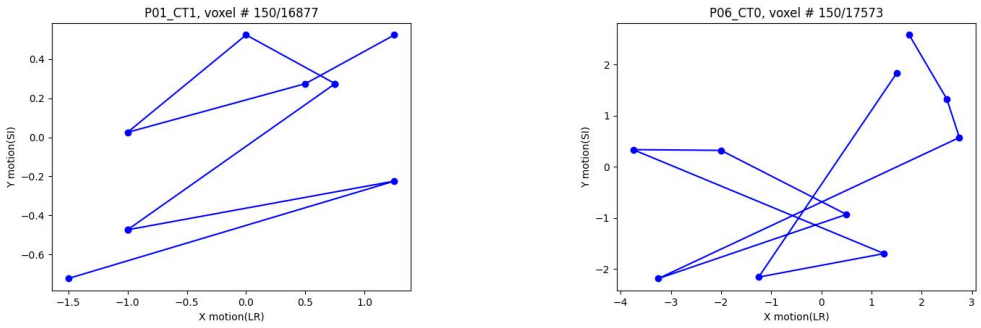


(a) (b)

Figure C.7: **Path trajectories of two of the same 4D-CTs as depicted in Figure C.6. It is obvious that this does not represent realistic voxel motion. All plots showed chaotic, seemingly random behaviour. All units are in cm.**

See figure C.6 for examples of the histograms of the voxel trajectory path lengths that result from the voxel tracking method. The large spike at length =0, especially in (b), corresponds to a large group of voxels that only were assigned a path of one voxel, so not something that can be considered correct.

Figure C.7 shows voxel trajectories of the 150th voxel (randomly picked) of the same 4D-CTs as in figure C.6 (a) and (b). It is clear that this does not constitute a realistic tumor motion path. All voxels showed this kind of random behavior.

Due to time constraints on my thesis, the decision was made to abandon this method after many attempts to solve the issues.

## C.2 Discussion old methods

### Center of Mass

Multiple articles from the literature study (section 1.8 ) claimed to base tumor motion on the center of mass of either the CTV or the GTV. However, all of them simplified tumor motion to either SI [71]–[73] or SI and LR [74] tumor motion. None of the articles mention using the data to create a 3-dimensional path of the center of mass (COM) of either the GTV or CTV.

Besides the chaotic motion of some of the tumor motion paths that result from this method, the amplitude (maximum position in SI direction - minimum position in SI direction, etc) that resulted from this method is a factor 5-10 smaller than what results from the *respiratory amplitude* script.

One problem in this comparison is that it is difficult to determine what the actual tumor motion amplitude is. In the *respiratory amplitude* script, the distance traveled by all voxels of the CTV between the full-in and full expiratory breathing phase is recorded. The 90th percentile of this collection is taken. This way, the largest possible amplitude is picked while excluding the 10 percent most mobile voxels, which might be outliers.

When considering the center of mass (COM) for tracking CTV movement, the focus is often on the tumor's largest portion. If this region is less mobile than the surrounding CTV areas, a 'dampened' motion trajectory may result.

The shapes of some of the images in figure C.2 seem intuitively correct if the two ends are connected (Image 1, for example). However, in many, there are irregular spikes and motions that do not seem to fit what is to be expected. While intuition is not something that should guide scientific decisions, it might indicate that the center of mass is not the best method to represent tumor motion.

While

### Percentile motion

After validation, the results from the percentile motion method still yielded unrealistic results. One reason could be that it is possible a different part of the tumor is tracked between every phase. This problem is largely tackled by the voxel tracking method.

### Voxel tracking

The voxel tracking method is considered an upgrade of the percentile motion method by the author. It was based on the same type of data but removed the problem of being unable to track the same part of the tumor.
The examples in figure C.7 indicate there is most likely an error in the script that is used to extract the voxels' trajectories. In the (very large) files that contained the lists with all voxels' coordinates through the phases, there were occasionally many voxels that only had a path of one position, the starting position in phase 0%. This corresponds to the large spike at voxel trajectory length at 0 cm in figure C.6.

Since the deadline of my thesis came closer and I still found no solution to the unrealistic, chaotic tumor trajectory C.7, I decided to discard this method. However, I do think this is the method that still holds the most potential.

### C.2.1 Advantages and disadvantages

The main advantage of the COM method is its simplicity. It only depends on the delineations of the target volume in the different breathing phases. This makes it a straightforward and efficient approach for simulation target motion. However, the tumor motion can 'dampen' the COM motion, for example, if one part of the CTV moves more than another part. This problem could be mitigated by using the COM of the GTV rather than the CTV. The GTV has a smaller margin, so might better model the fluctuations of tumor motion during breathing

Using a completed and validated method of voxel tracking, it could be possible to choose which parts of the tumor you want to focus on. it would be possible to select, for example, a voxel in the lymph nodes and see the motion of that part. A downside is its complexity and computational time. calculating the ten locations (3D coordinates) of every voxel could take up to 30 minutes. I made no use of GPU clusters, so that might greatly increase computational time since the calculations consist of many simple comparisons ($17.000^2 = 289$ million for P01_CT0_B1). Also, this process might be simplified. The current script compares every CTV coordinate in the 0% phase to every registered coordinate in the 10% phase, which is obviously redundant.

## C.3 Validation

### Validation center of mass method

In order to validate the method with which the center of mass is extracted, a fake structure has been created. In each of the ten phases, a cuboid is created with sizes 1 by 1,2 by 1 cm (LR, SI, PA direction). See Figure C.8. It can be seen that the block in phase 7, 8 and 9 are moved relative to the other blocks. See Table C.1 for the coordinates of the centers of mass of the blocks. The same methods that are applied to the patients' CTVs have been applied to this fake structure. The maximum distance in SI, PA and LR direction has been checked on the CT images, calculated manually based on the COM coordinates and calculated by the script that generates the figures and performs the rotation.

The modeled CTV motion of this fake structure can be seen in Figure C.9. The SI and LR motion in the figures' captions is the same as the calculated and measured motion. Since the Matrixx detector array only measures in 2D, the decision was made to ignore the depth movement, away from the gantry, of the CTV. For this reason the depth of the CTV cubes, that is clearly visible in Figure C.8, is not visible in Figure C.9.

Since the amplitude of the fake structure outputted by the scripts correspond to the measured and calculated amplitude, and the motion is as to be expected, I consider the method validated.

| phase | LR | SI | PA |
|---|---|---|---|
| 0% | 7,5 | -52,73 | 34,5 |
| 10% | 3,5 | -52,73 | 34,5 |
| 20% | 3,5 | -49,13 | 34,5 |
| 30% | 7,5 | -49,13 | 34,5 |
| 40% | 11,5 | -49,13 | 34,5 |
| 50% | 15,5 | -49,13 | 34,5 |
| 60% | 19,5 | -49,13 | 34,5 |
| 70% | 19,5 | -52,73 | 36,7 |
| 80% | 15,5 | -52,73 | 36,7 |
| 90% | 11,5 | -52,73 | 36,7 |

Table C.1: **The coordinates of the center of mass of the ten blocks. The distance is in cm.**

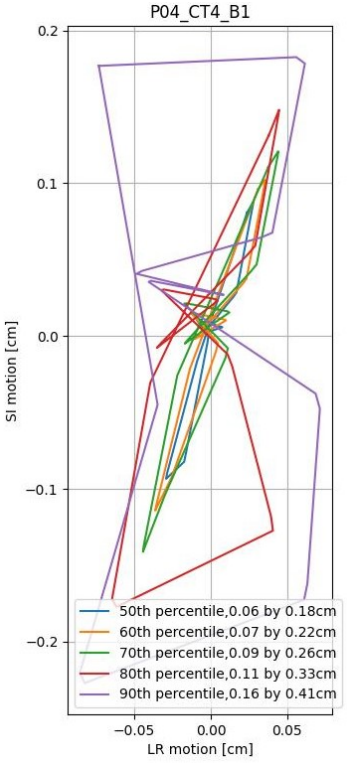


(a)

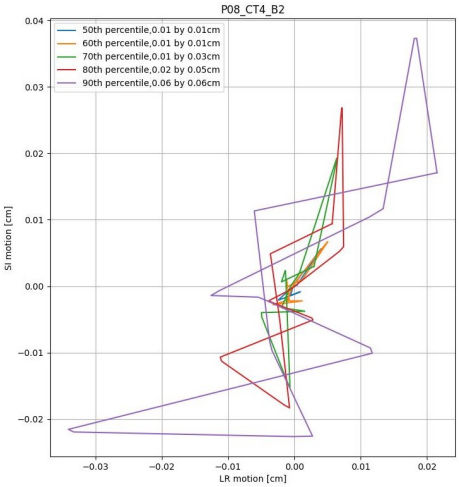


(b)

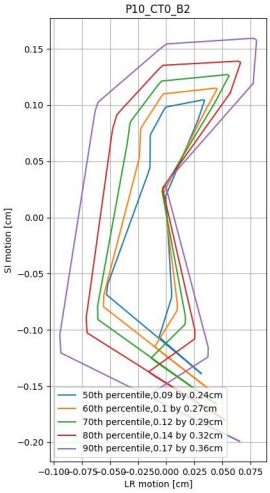


(c)

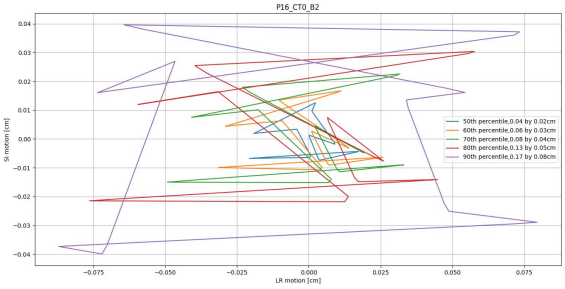


(d)

Figure C.5: **For each of the picked percentiles (except the 100th), shows the tumor path. The distance in the label is the maximum amplitude in the LR and SI directions, respectively**

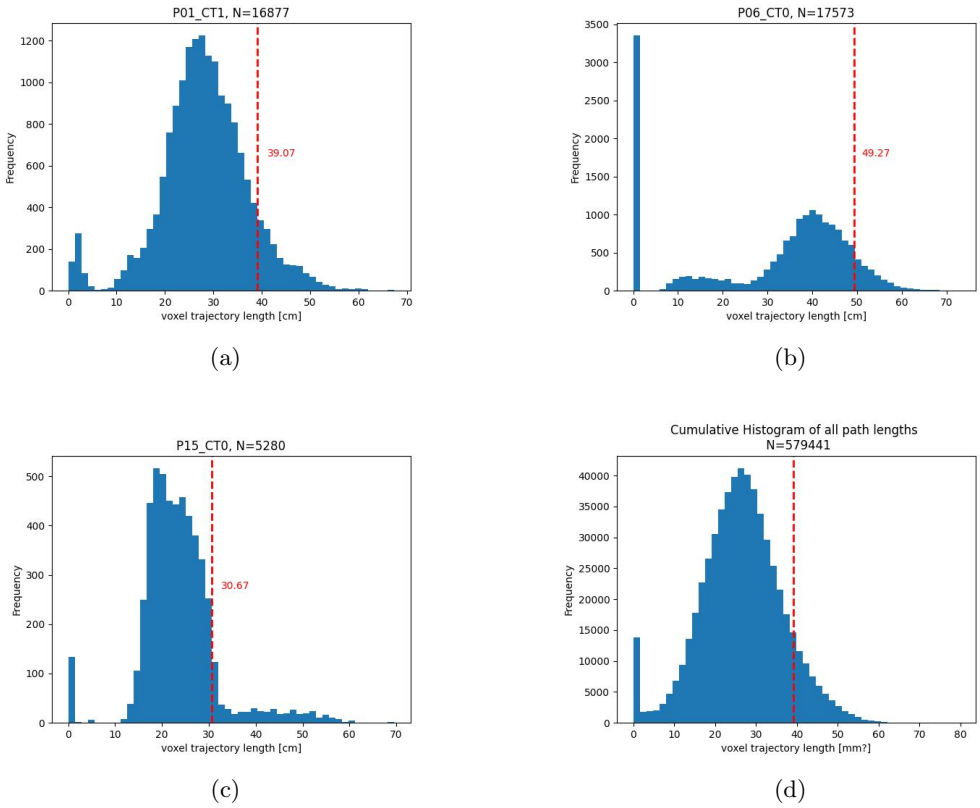


Figure C.6: **Histograms of three random 4D-CT voxel trajectories, (a-c) and the cumulative histogram of all 63 4D-CTs (d). The red dashed line depicts the 90th percentile. All units are in cm.**

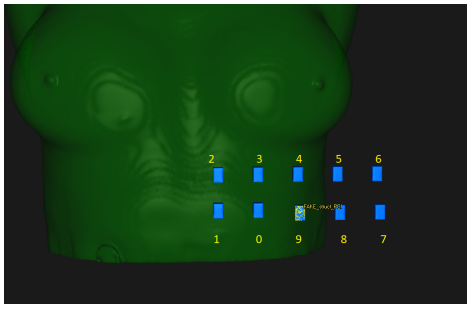


(a) Front view, 0°. The numbers correspond to the phase in which the block is placed (0 for 0%, 1 for 10% etc).

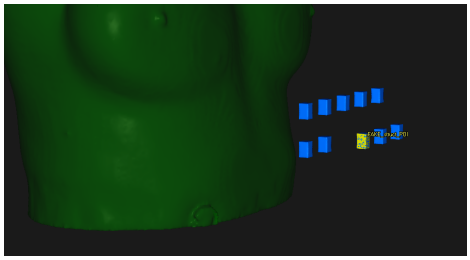

(b) 45°

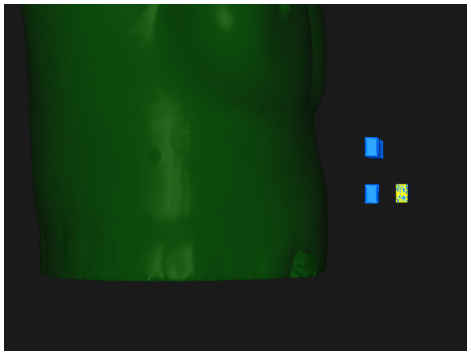

(c) 90°

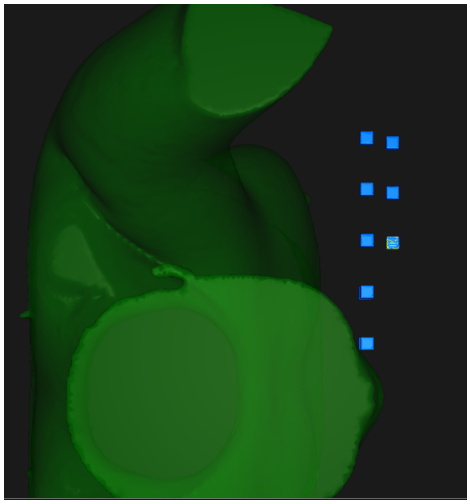

(d) top view

Figure C.8: **The fake structure created in order to validate the center of mass method of movement extraction. Each block is a fake CTV in one of the ten phases. The blue structure is the fake ITV. The view in (a), (b) and (c) correspond to the gantry view if it had rotated to that angle.**

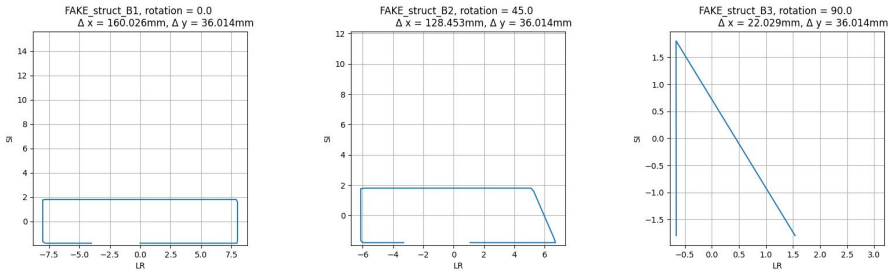


(a) (b) (c)

Figure C.9: **The modeled CTV motion from Figure C.8 (a), (b) and (c), as yielded from the scripts used to model the COM motion.**

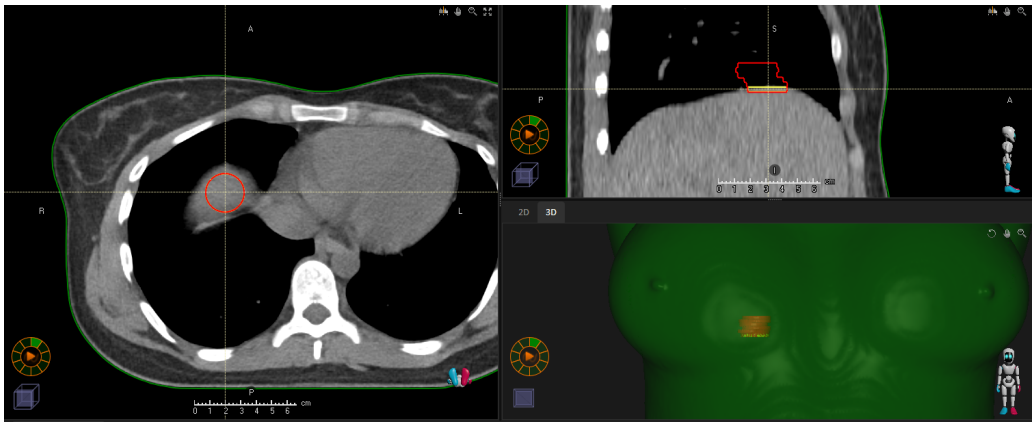

Figure C.10: **The yellow shape is the artificial CTV (most superior part of the liver) in one phase. The red shape is the ITV, the union of all the ten CTVs.**

# Validation of percentile method

Validation of the method of tumor motion extraction is not as straightforward as the validation of the center of mass method. While the center of mass and its coordinates are easily definable, finding a certain percentile of the motion of all CTV voxels is not straightforward or intuitive. This is especially difficult because extracting voxel motion requires deformable registration between the phases. The standard deformable registration in RayStation *uses a combination of image intensity information and anatomical information* [56]. This means registration is based on the Hounsfield units of the tissue inside the contour and not just on the contour shape and position, as is the case in COM motion extraction.

## Real structure movement

In order to validate the voxel motion method, a structure needed to be picked that moves in an easy do distinguishable direction. This way, the intuitive and measurable motion of the structure can easily be compared to the outcome of the voxel motion method, which is somewhat opaque. For this structure, the top of patient 1's liver was chosen. This is a structure that primarily and distinctly moves in the superior-inferior direction. This structure can be seen in Figure C.10. The method described in section 3.1.1 Tumor motion data preparation was applied to this CTV.

The distribution of the voxel motion in SI direction in each phase can be seen in Figure C.11. The motion distribution in the LR and AP direction was magnitudes smaller for this CTV. The liver top motion that is derived from the 4DCT is unvarying during a phase and the phase's mean motion seems to follow a predictable pattern. These results indicate that this motion representation is a good representation of the liver top's motion during breathing.

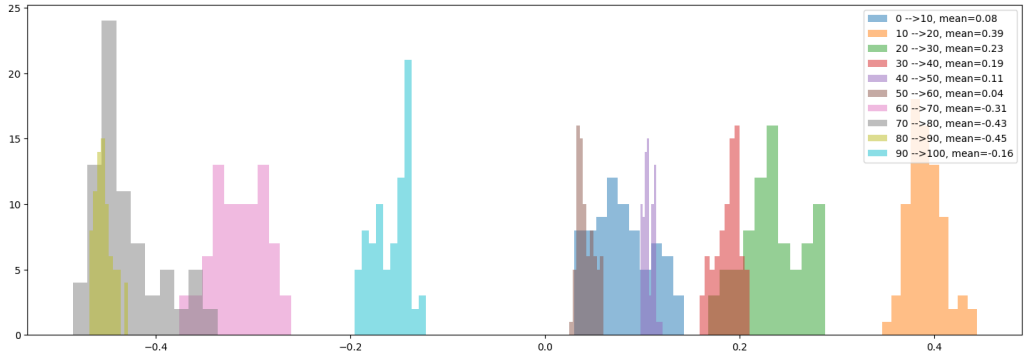


Figure C.11: **The voxel motion distribution in superior-inferior (SI) direction of the artificial liver top CTV of Figure C.10. It can be seen that in each phase, there is a clear direction and uniform amplitude.**

## Voxel tracking validation

For the validation of the voxel tracking, I created two structures that are easy to visualize (figure C.12).

All the steps that are described in section C are performed on the validation structures. The list *registered_locations* was created by copying the *original_locations* list and shifting all the breathing phases' coordinates on phase to the left. This way, the 0% voxel coordinates register to the exact location of the 10% voxel coordinates, which is what would happen in an ideal situation.

After applying all the steps, the trajectory, path length and trajectory plots are checked. The trajectory and trajectory plots (c) and (d) in figure C.12) were as expected and planned. The path length (10 and 10) step size for (a) and (b) respectively) also matched.

This lead to my conclusion that the methods are correct.

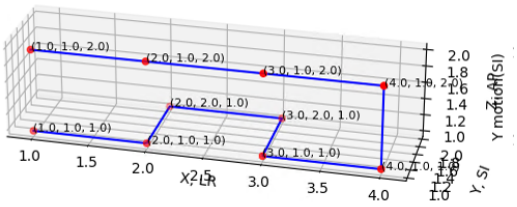


(a) The first validation shape, called stairs. All step sizes are 1.

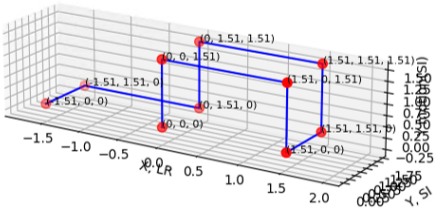


(b) The second validation shape The step size (1.51 in this example) was a random number between 1 and 2.

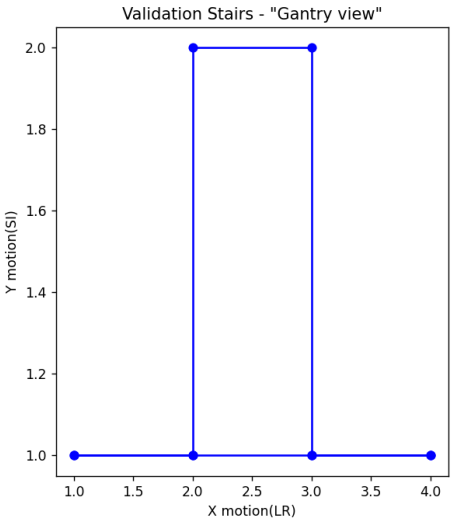


(c)

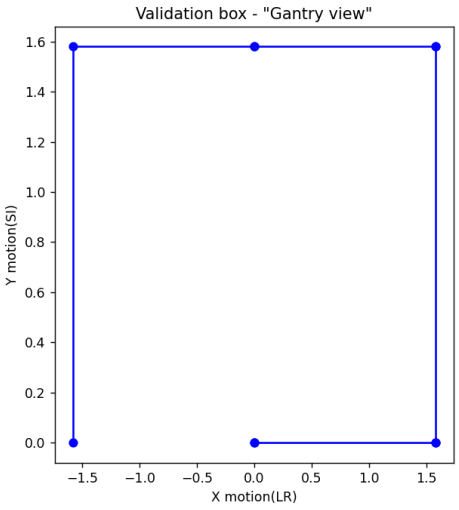


(d)

Figure C.12: **Two shapes were created. A fake original_locations.json file was created. The JSON file for (a) contained 2 coordinates in each 'breathing phase': the one depicted in (a) and one with an offset of +1 in all three directions (starting bottom left [2, 2, 2]; [3, 2, 2]; ...).**
**The JSON file for (b) contained 10 coordinates. All had the same start location (0,0,0) but a different step size (between 1 and 2), that was constant for every step in a set of coordinates.**
**(c) and (d) show the tumor motion that resulted from the voxel tracking method. It shows the shape in (a) and (b) from a top view.**

# Appendix D

# Beam compensation calculation example

This section is related to section 6.5 Single beam vs multi beam analysis in the Discussion. It provides some example calculations to show how to calculate whether different beams can compensate for each other's dosimetric errors to yield a treatment plan that is robust against the interplay effect.

Remember that the Gamma pass rate tells which percentage of the reference points meet the acceptance criteria (of 2%/2mm in Holland PTC [67]). The Gamma index is a score that is given to every reference point. It shows how much the reference point's dose differs from the planned dose in that area.

Assume a patient receives 60 Gy per fraction with three beams. Holland PTC's internal guidelines [75] states that for lung patients, the dose delivered by one individual beam can contribute no more than 175% of the 'equally shared dose', or 35Gy (and 12.5 Gy for both other beams).[1]. If all beams delivered the same dose, each beam would deliver 20 Gy to the entire volume. If $B_1$ delivers 35Gy (175% of 20 Gy), $B_2$ and $B_3$ both deliver 12.5 Gy. In this case, one beam delivers the maximum dose. If we also assume that this primary beam has dosimetric deviations, this is something that could be considered the worst-case scenario.
For this example, we'll ignore the distance to agreement aspect of the Gamma index calculation, and assume that the difference between the reference dose distribution and measured dose distribution is only in the dose difference.

The cumulative Gamma index of a single dosimetric position needs to be $\leq 1$ for the position to pass the interplay robustness test.

The Gamma index of the combined beams at one position, denoted as $\Gamma_\Sigma$, is calculated based on the individual beam's Gamma index values, $\Gamma_1$, $\Gamma_2$, and $\Gamma_3$, and their corresponding weights (the fraction of the dose each beam delivers), $w_1$, $w_2$, and $w_3$, respectively:

$$\Gamma_\Sigma = \frac{\Gamma_1}{w_1} + \frac{\Gamma_2}{w_2} + \frac{\Gamma_3}{w_3} \tag{D.1}$$

[1] This value is 150% for both lymphoma and esophagus patients.

If we assume $w_1$ = 35 Gy/60 Gy = $0.58\overline{3}$, $w_2 = w_3$ = 12.5 Gy/60 Gy =$0.208\overline{3}$, $\Gamma_\Sigma$ =1 (Total Gamma threshold the maximum value within acceptable bounds) and $\Gamma_2 = \Gamma_3$ (both secondary beams are equal and have the same Gamma index value) and fill this in in formula D.1, we get:

$$1 = \frac{\Gamma_1}{0.58\overline{3}} + 2 \cdot \frac{\Gamma_2}{0.208\overline{3}} \tag{D.2}$$

Simplifying yields:

$$\Gamma_1 = 0.58\overline{3} - 5.6 \cdot \Gamma_2 \tag{D.3}$$

When $B_2$ and $B_3$ both have a Gamma index of 0 (perfect beams, no dose difference between planned and measured dose distribution at that specific position), it means that the Gamma index of $B_1$ can be 0.5833 and the cumulative Gamma index would still be sufficient (equal to or smaller than 1). A Gamma index of 0.5833 with acceptance criteria of 2%/2mm means that the primary beam in this treatment plan can deviate $0.5833 \cdot 2\%$ = 1.166% of the intended dose (of 35Gy), or 0.41 Gy, and the specific point would still meet acceptance criteria.

We can also inverse the comparison. If the primary beam ($B_1$) has a perfect Gamma index of 0, it means that both $B_2$ and $B_3$ can have a Gamma index of 0.104 and the plan would be considered robust against the interplay effect.

# Appendix E

# Different robustness criteria

In this chapter, I will shortly explain the differences between the two different types of interplay robustness criteria. One is used by Holland PTC clinical physicists, while the other one is devised by the author.

From section 3.1.5 Gamma index metrics, so the method created by the author:

**Last fraction below threshold** An important value that's at the basis of each of these custom metrics is the ***last fraction below threshold*** (LFBT).
The Gamma pass rate (a score between 0 and 100%) is a score that indicates how much two dose distributions 'match'. In the context of this thesis, it is used to compare the static dose measurement to the simulated moving dose measurement. The dose distribution of the second fraction is equal to the first fraction's simulation plus the second fraction's simulation, etc. The Gamma pass rate of each of the simulations is calculated.

Generally, the more fractions are simulated, the more the Gamma pass rate tends to increase toward 100%. In each simulation, if the Gamma pass rate starts below the threshold (95%) at fraction one and is above this value after the last fraction, the last fraction where the Gamma pass rate was below this value is recorded. This value is defined as the last fraction below threshold, the LFBT.

**Clinical evaluation criteria** The Gamma pass rate of a patient's treatment plan is required to meet the criteria of 95% at the end of the patient's treatment scheme. For this reason, a treatment beam is considered robust against the interplay effect if the 90th percentile LFBT is equal to or smaller than the number of prescribed fractions. This means that in 90 out of 100 simulations, the fractionation scheme reached the threshold before the end of the patient's treatment.

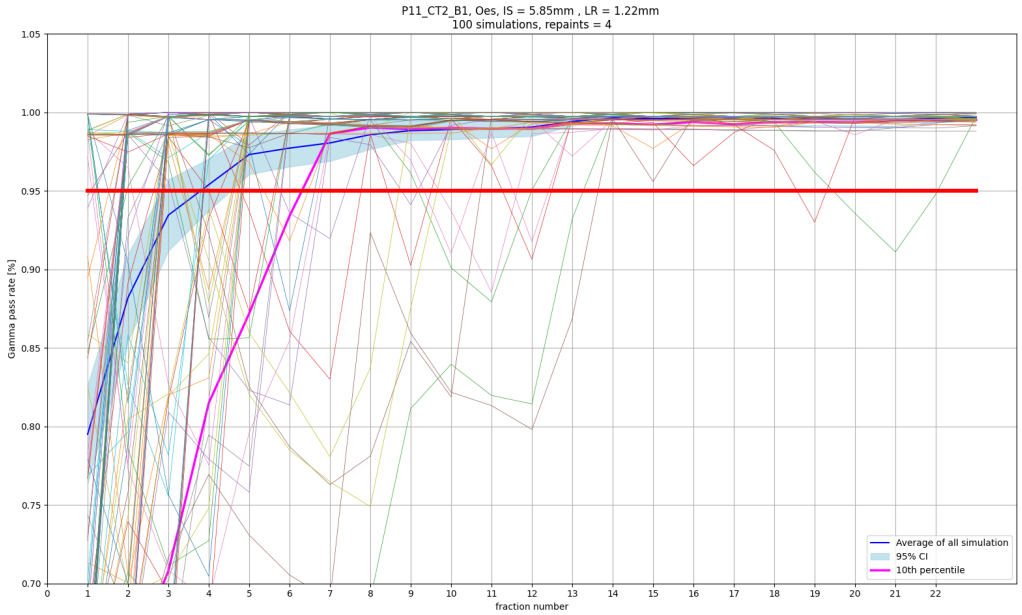


Figure E.1: **Example of the Gamma index metrics, explained in section 3.1.5 Gamma index metrics. For each beam, a simulation with several fractions was performed (thin lines). For each treatment simulation, the last fraction with a Gamma pass rate below the threshold of 95% was recorded.**
**The same data as figure 3.5, but with the clinical physicists' method included. The tenth percentile worst Gamma pass rate per fraction (the pink line) was originally included in the author's method but was later discarded for redundancy because it did not contribute to any results or conclusions.**

The criterion used by the department of clinical physics is different.
A number of treatment deliveries are simulated. Next, the tenth percentile of the Gamma pass rate after each fraction is calculated. This results in a line (the pink line in figure E.1) that represents the tenth percentile 'worst' treatment. The fraction at which this line passes the threshold of 95% Gamma pass rate is the required number of fractions for the treatment beam to be considered robust (approximately 6.5 in figure E.1).

Figure E.2 compares the LFBT as calculated using both different methods for all 161 treatment beams. Not that for many of the beams, both values were equal to 0, so they are not clearly visible in the graph. The correlation is very high ($r > 0.99$). The slope (1.003) and intercept (0.4) show that the author's method results in an average LFBT that is higher by 0.4 fractions compared to the clinical physicists' methods. This difference was not deemed clinically relevant, so the decision was made to continue using the author's method.

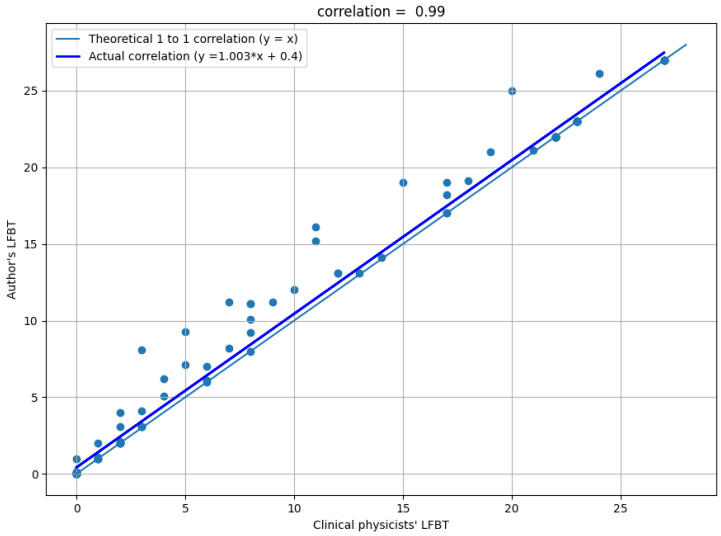


Figure E.2: **Comparing the two different last fraction below threshold values. LFBT = last fraction below threshold. N= 161.**

# Appendix F

# ELST

A previous Technical Medicine intern at Holland PTC, J. Paramasamy, has worked extensively on beam parameters and their effect on the interplay effect. One of these was the Energy Layer Switching Time, or ELST [48]. The ELST is the time the gantry needs to switch between different iso-dose layers. It is an inherent property of a treatment plan. It is captured by the MatriXX PT during QA. Paramasamy showed the average ELST was around 0.8 seconds in 3 patients whose MatriXX measurements she had available. Since this is a relatively large part of the entire beam delivery, it is important to take this value and its possible variation into account.

An attempt was made to extract the ELST from the treatment plans that were available for this thesis. The ELST shows as a number of consecutive empty frames in which the MatriXX measures no dose (frame 00697 and onwards in figure 1.8). This was done by extracting the maximum value for each of the frames in a beam measurement. A histogram can be seen in figure F.1 showing the maximum value in mGy that the MatriXX measures. in the first figure, a prominent spike is visible at the maximum value of 0 mGy, indicating frames during which the MatriXX received no dose. This data could be used to determine in how many frames the beam was turned off (barring the frames and the start and end of the measurements that are also empty). An attempt was made to find a threshold that could, for every beam measurement, determine the cut-off point that indicated the moment a beam was 'on' or 'off'. Finding a method that worked universally for all measured beams turned out to be harder than anticipated. One reason might be the fact that I focussed on the maximum value in a frame. The idea was that if the maximum value was greater than a certain value, the beam must be on. However, there might still be background noise available in the 'off' frames. If this changes day by day, finding a universal method for this threshold might be difficult.

Figure F.2 shows an example where the results may be deemed realistic. Figure F.3, however, shows an attempt which shows that results are sometimes very variable.

The goal was to capture the variation in ELST and incorporate this randomness into the interplay simulation script. An attempt would also be made to find patient or beam factors that influenced the ELST in order to make the ELST as representative as possible.

However, the process turned out to be more complex than expected. Secondly, it would be difficult to change the empty frames in the sequence in a representative yet

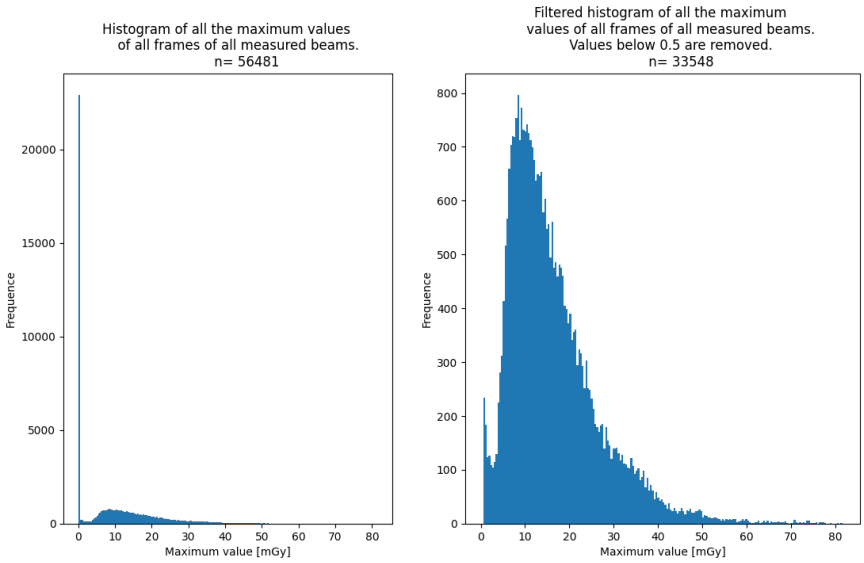


Figure F.1: **Histograms of the maximum detector array element energy (in mGy) of all the frames of all the beam measurements. The left image shows that in about half of all the 56481 frames, no or negligibly low energy is measured.**

random way. For these reasons, the decision was made to stop this part of the project.

The code is available in my folders, so if anyone is planning on continuing this part of the project, feel free to contact me so I can help with understanding.

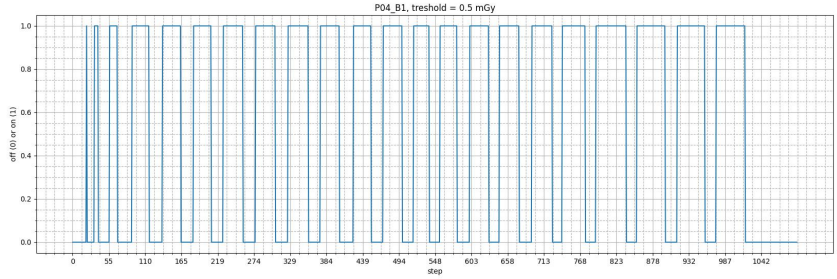


Figure F.2: **'On' and 'off' switching of the proton beam in one patient's beam measurement, based on the maximum value in each of the MatriXX PT's frames. It is clear the beam is alternatingly on or off. The steps refer to the frame number, each step corresponding to a measurement of 40ms.**

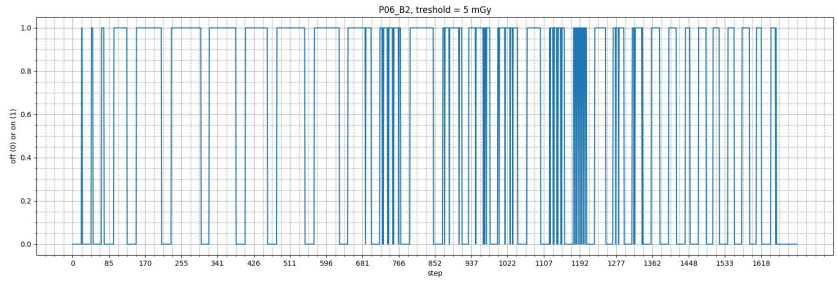


Figure F.3: **On' and 'off' switching of the proton beam in one patient's beam measurement. This example was chosen to show that finding a threshold for the switch between 'on' and 'off' is difficult, for example, around 1192 frames. If different threshold values were chosen, the chaotic parts would be at a different location.**

# Bibliography


[1] *Cancer, world health organisation*, Available at https://www.who.int/news-room/fact-sheets/detail/cancer, Sep. 2021. [Online]. Available: https://www.who.int/news-room/fact-sheets/detail/cancer.

[2] A. McIntyre and A. K. Ganti, "Lung cancer-a global perspective," *Journal of Surgical Oncology*, vol. 115, no. 5, pp. 550–554, Apr. 2017. DOI: 10.1002/jso.24532.

[3] integraal kankercentrum Nederland, *Incidentie longkanker*, Available at https://iknl.nl/kankersoorten/longkanker/registratie/incidentie, 2020.

[4] M. Plus, *Lung cancer - non-small cell: Medlineplus medical encyclopedia*, 2015. [Online]. Available: https://medlineplus.gov/ency/article/007194.htm.

[5] R. kanker.nl, *Overlevingscijfers van niet-kleincellige longkanker*, ASvailable at https://www.kanker.nl/kankersoorten/longkanker/algemeen/overlevingscijfers-van-niet-kleincellige-longkanker, Oct. 2020.

[6] F. M. Specialisten, *Richtlijn niet-kleincellig longcarcinoom, stadium iii-nsclc*, Available at https://richtlijnendatabase.nl/richtlijn/niet_kleincellig_longcarcinoom/startpagina_-_niet-kleincellig_longcarcinoom.html, Jul. 2015. [Online]. Available: https://richtlijnendatabase.nl/richtlijn/niet_kleincellig_longcarcinoom/startpagina_-_niet-kleincellig_longcarcinoom.html.

[7] A. Sheha, R. Z. Elia, and N. M. F. H. Ghoneim, "The added value of18f-fdg pet/ct in staging non-small cell lung cancer," *Egyptian Journal of Radiology and Nuclear Medicine*, vol. 50, no. 1, Dec. 2019. DOI: https://doi.org/10.1186/s43055-019-0081-0.

[8] landelijk platform voor radiotherapie bij longtumoren, *Landelijk Indicatie Protocol Protonen Therapie longcarcinoom*. Jun. 2019.

[9] L. platform voor radiotherapie bij longtumoren (LPRL) and L. P. P. (LPPT), *Landelijk Indicatie Protocol Protonen Therapie Longcarcinoom*. Jun. 2019, Available at https://nvro.nl/publicaties/rapporten.

[10] E. C. Smyth, J. Lagergren, R. C. Fitzgerald, *et al.*, "Oesophageal cancer," *Nature Reviews Disease Primers*, vol. 3, no. 1, Jul. 2017. DOI: https://doi.org/10.1038/nrdp.2017.48.

[11] X. Wang, B. Hobbs, S. J. Gandhi, C. T. Muijs, J. A. Langendijk, and S. H. Lin, "Current status and application of proton therapy for esophageal cancer," *Radiotherapy and Oncology*, vol. 164, pp. 27–36, Nov. 2021. DOI: https://doi.org/10.1016/j.radonc.2021.09.004. [Online]. Available: https://www.sciencedirect.com/science/article/pii/S0167814021067244?via%5C%3Dihub.

[12] I. K. N. (IKNL), *Overlevingscijfers van slokdarmkanker*, Feb. 2022. [Online]. Available: https://www.kanker.nl/kankersoorten/slokdarmkanker/algemeen/overlevingscijfers-van-slokdarmkanker.

[13] F. M. Specialisten, *Oesofaguscarcinoom richtlijn*. [Online]. Available: https://richtlijnendatabase.nl/richtlijn/oesofaguscarcinoom/oesofaguscarcinoom_-_startpagina.html.

[14] J. Lv, X.-F. Cao, B. Zhu, L. Ji, L. Tao, and D.-D. Wang, "Effect of neoadjuvant chemoradiotherapy on prognosis and surgery for esophageal carcinoma," *World Journal of Gastroenterology*, vol. 15, no. 39, p. 4962, 2009. DOI: https://doi.org/10.3748/wjg.15.4962.

[15] P. van Hagen, M. Hulshof, J. van Lanschot, *et al.*, "Preoperative chemoradiotherapy for esophageal or junctional cancer," *New England Journal of Medicine*, vol. 366, no. 22, pp. 2074–2084, May 2012. DOI: https://doi.org/10.1056/nejmoa1112088.

[16] Amsterdam UMC Oesophaguscardiaresectie met buismaagreconstructie, Apr. 2023. [Online]. Available: https://www.amsterdamumc.nl/nl/chirurgie/patienteninformatie/oesophaguscardiaresectie-met-buismaagreconstructie-met-intrathoracale-anastomose-slokdarmoperatie-met-buismaagreconstructie-met-nieuwe-verbinding-in-de-borstholte.htm.

[17] S. H. Lin, B. P. Hobbs, V. Verma, *et al.*, "Randomized phase iib trial of proton beam therapy versus intensity-modulated radiation therapy for locally advanced esophageal cancer," *Journal of Clinical Oncology*, vol. 38, no. 14, pp. 1569–1579, May 2020. DOI: https://doi.org/10.1200/JCO.19.02503. [Online]. Available: https://www.ncbi.nlm.nih.gov/pmc/articles/PMC7213588/.

[18] S. H. Lin, K. W. Merrell, J. Shen, *et al.*, "Multi-institutional analysis of radiation modality use and postoperative outcomes of neoadjuvant chemoradiation for esophageal cancer," *Radiotherapy and Oncology*, vol. 123, no. 3, pp. 376–381, Jun. 2017. DOI: https://doi.org/10.1016/j.radonc.2017.04.013. [Online]. Available: https://www.sciencedirect.com/science/article/pii/S0167814017301548.

[19] I. K. Nederland, *Overlevingscijfers van hodgkinlymfoom — kanker.nl*, Feb. 2022. [Online]. Available: https://www.kanker.nl/kankersoorten/hodgkinlymfoom/algemeen/overlevingscijfers-van-hodgkinlymfoom.

[20] N. C. institute, *Regional lymph nodes — seer training*. [Online]. Available: https://training.seer.cancer.gov/lymphoma/anatomy/lymph-nodes.html.

[21] Mar. 2022. [Online]. Available: https://www.mayoclinic.org/diseases-conditions/hodgkins-lymphoma/symptoms-causes/syc-20352646#:~:text=People%5C%20who%5C%20have%5C%20had%5C%20illnesses.

[22] A. C. Society, *Hodgkin lymphoma risk factors — risk factors for hodgkin disease*, May 2018. [Online]. Available: https://www.cancer.org/cancer/types/hodgkin-lymphoma/causes-risks-prevention/risk-factors.html.

[23] S. H.-O. voor Volwassenen Nederland (HOVON), *Richtlijn hodgkin lymfoom bij volwassenen*, Nov. 2019. [Online]. Available: https://hovon.nl/_asset/_public/TreatmentGuidelines/TreatmentGuidelines_Lymphoma/richtlijn_hodgkin_lymfoom_hovon_2019_v1.pdf.

[25] M. de Semoni, M. Fischetti, E. Gioscio, *et al.*, "Fred: A fast monte carlo code on gpu for quality control in particle therapy," vol. 1548, no. 1, pp. 012 020–012 020, May 2020. DOI: https://doi.org/10.1088/1742-6596/1548/1/012020.

[26] M. Engelsman, M. Schwarz, and L. Dong, "Physics controversies in proton therapy," *Seminars in Radiation Oncology*, vol. 23, no. 2, pp. 88–96, Apr. 2013. DOI: https://doi.org/10.1016/j.semradonc.2012.11.003.

[27] T. P. Diwanji, P. Mohindra, M. Vyfhuis, *et al.*, "Advances in radiotherapy techniques and delivery for non-small cell lung cancer: Benefits of intensity-modulated radiation therapy, proton therapy, and stereotactic body radiation therapy," *Translational Lung Cancer Research*, vol. 6, no. 2, pp. 131–147, Apr. 2017. DOI: https://doi.org/10.21037/tlcr.2017.04.04.

[28] M. Krämer and M. Durante, "Ion beam transport calculations and treatment plans in particle therapy," *The European Physical Journal D*, vol. 60, no. 1, pp. 195–202, Mar. 2010. DOI: https://doi.org/10.1140/epjd/e2010-00077-8.

[29] Z. Liao, J. J. Lee, R. Komaki, *et al.*, "Bayesian adaptive randomization trial of passive scattering proton therapy and intensity-modulated photon radiotherapy for locally advanced non–small-cell lung cancer," *Journal of Clinical Oncology*, vol. 36, no. 18, pp. 1813–1822, Jun. 2018. DOI: https://doi.org/10.1200/jco.2017.74.0720.

[30] L. Pan, D. Lei, W. Wang, Y. Luo, and D. Wang, "Heart dose linked with cardiac events and overall survival in lung cancer radiotherapy," *Medicine*, vol. 99, no. 38, e21964, Sep. 2020. DOI: 10.1097/md.0000000000021964.

[31] T. F. DeLaney, T. I. Yock, and H. Paganetti, "Assessing second cancer risk after primary cancer treatment with photon or proton radiotherapy," *Cancer*, vol. 126, no. 15, pp. 3397–3399, May 2020. DOI: 10.1002/cncr.32936.

[32] T. Depuydt, A. Van Esch, and D. P. Huyskens, "A quantitative evaluation of imrt dose distributions: Refinement and clinical assessment of the gamma evaluation," *Radiotherapy and Oncology*, vol. 62, no. 3, pp. 309–319, Mar. 2002. DOI: 10.1016/s0167-8140(01)00497-2.

[33] D. A. Low, W. B. Harms, S. Mutic, and J. A. Purdy, "A technique for the quantitative evaluation of dose distributions," *Medical Physics*, vol. 25, no. 5, pp. 656–661, May 1998. DOI: 10.1118/1.598248.

[34] B. Price and R. C. Cancer, *Imrt 2.0 — physics session 10 — qa for imrt on youtube*, Available at https://www.youtube.com/watch?v=SmDNiAC1gO4, Dec. 2020.

[36] M. Hussein, C. Clark, and A. Nisbet, "Challenges in calculation of the gamma index in radiotherapy – towards good practice," *Physica Medica*, vol. 36, pp. 1–11, Apr. 2017. DOI: 10.1016/j.ejmp.2017.03.001.

[37] T. Kataria, K. Sharma, V. Subramani, K. P. Karrthick, and S. S. Bisht, "Homogeneity index: An objective tool for assessment of conformal radiation treatments," *Journal of Medical Physics / Association of Medical Physicists of India*, vol. 37, no. 4, pp. 207–213, 2012, Available at https://www.ncbi.nlm.nih.gov/pmc/articles/PMC3532749/. DOI: 10.4103/0971-6203.103606.

[38] S. Rana and A. B. Rosenfeld, "Investigating volumetric repainting to mitigate interplay effect on 4d robustly optimized lung cancer plans in pencil beam scanning proton therapy," *Journal of Applied Clinical Medical Physics*, vol. 22, no. 3, pp. 107–118, Feb. 2021. DOI: 10.1002/acm2.13183.

[39] ICRU, *ICRU REPORT 50: prescribing, recording, and reporting photon beam therapy*. Sep. 1993. [Online]. Available: https://www.icru.org/report/prescribing-recording-and-reporting-photon-beam-therapy-report-50/.

[40] H. Arimura, Y. Shibayama, M. Haekal, and Z. Jin, "Computer-assisted target volume determination," Jan. 2017. DOI: https://doi.org/10.1007/978-981-10-2945-5_5.

[42] H. Paganetti, *Proton therapy physics*. Crc Press, Taylor and Francis Group, 2012, ISBN: 9781138626508.

[43] L. A. den Otter, R. M. Anakotta, M. Weessies, *et al.*, "Investigation of inter-fraction target motion variations in the context of pencil beam scanned proton therapy in non-small cell lung cancer patients," *Medical Physics*, vol. 47, no. 9, pp. 3835–3844, Jul. 2020. DOI: https://doi.org/10.1002/mp.14345.

[44] J.-P. Bissonnette, K. N. Franks, T. G. Purdie, *et al.*, "Quantifying interfraction and intrafraction tumor motion in lung stereotactic body radiotherapy using respiration-correlated cone beam computed tomography," *International Journal of Radiation Oncology*Biology*Physics*, vol. 75, no. 3, pp. 688–695, Nov. 2009. DOI: https://doi.org/10.1016/j.ijrobp.2008.11.066.

[45] Y. Seppenwoolde, H. Shirato, K. Kitamura, *et al.*, "Precise and real-time measurement of 3d tumor motion in lung due to breathing and heartbeat, measured during radiotherapy," *International Journal of Radiation Oncology*Biology*Physics*, vol. 53, no. 4, pp. 822–834, Jul. 2002. DOI: 10.1016/s0360-3016(02)02803-1.

[46] L. Knybel, J. Cvek, L. Molenda, N. Stieberova, and D. Feltl, "Analysis of lung tumor motion in a large sample: Patterns and factors influencing precise delineation of internal target volume," *International Journal of Radiation Oncology*Biology*Physics*, vol. 96, no. 4, pp. 751–758, Nov. 2016. DOI: 10.1016/j.ijrobp.2016.08.008.

[47] T. Pfeiler, D. Ahmad Khalil, M. Ayadi, C. Bäumer, and O. Blanck, "Motion effects in proton treatments of hepatocellular carcinoma—4d robustly optimised pencil beam scanning plans versus double scattering plans," *Physics in Medicine and Biology*, vol. 63, no. 23, p. 235 006, Nov. 2018. DOI: https://doi.org/10.1088/1361-6560/aaecfc.

[49] M. Schwarz, "Treatment planning in proton therapy," *The European Physical Journal Plus*, vol. 126, no. 7, Jul. 2011. DOI: https://doi.org/10.1140/epjp/i2011-11067-y.

[50] C. Bert, S. O. Grözinger, and E. Rietzel, "Quantification of interplay effects of scanned particle beams and moving targets," *Physics in Medicine and Biology*, vol. 53, no. 9, pp. 2253–2265, Apr. 2008. DOI: https://doi.org/10.1088/0031-9155/53/9/003.

[51] A. E. Lujan, E. W. Larsen, J. M. Balter, and R. K. Ten Haken, "A method for incorporating organ motion due to breathing into 3d dose calculations," *Medical Physics*, vol. 26, no. 5, pp. 715–720, May 1999. DOI: 10.1118/1.598577.

[52] R. George, S. S. Vedam, T. D. Chung, V. Ramakrishnan, and P. J. Keall, "The application of the sinusoidal model to lung cancer patient respiratory motion," *Medical Physics*, vol. 32, no. 9, pp. 2850–2861, Sep. 2005. DOI: 10.1118/1.2001220. [Online]. Available: https://pubmed.ncbi.nlm.nih.gov/16266099/.

[53] O. Pastor-Serrano, S. Habraken, D. Lathouwers, M. Hoogeman, D. Schaart, and Z. Perkó, "How should we model and evaluate breathing interplay effects in impt?" *Physics in Medicine and Biology*, vol. 66, no. 23, Nov. 2021. DOI: 10.1088/1361-6560/ac383f. [Online]. Available: https://pubmed.ncbi.nlm.nih.gov/34757958/.

[54] M. Engelsman and C. Bert, "Proton therapy physics 14.4 dealing with motion," in *Proton Therapy Physics*. Boca Raton, Fl: Crc Press, Taylor and Francis Group, 2012.

[55] C. Bert, A. Gemmel, N. Saito, and E. Rietzel, "Gated irradiation with scanned particle beams," *International Journal of Radiation Oncology*Biology*Physics*, vol. 73, no. 4, pp. 1270–1275, Mar. 2009. DOI: https://doi.org/10.1016/j.ijrobp.2008.11.014.

[56] raySearch laboratories, *raystation 10B RayPhysics Manual*. Stockholm, Sweden, Dec. 2020.

[59] iba dosimetry GmbH, *MatriXX PT User's Guide*. Aug. 2013.

[61] K. Dolde, Y. Zhang, N. Chaudhri, *et al.*, "4dmri-based investigation on the interplay effect for pencil beam scanning proton therapy of pancreatic cancer patients," *Radiation Oncology*, vol. 14, no. 1, Feb. 2019. DOI: 10.1186/s13014-019-1231-2. [Online]. Available: https://www.ncbi.nlm.nih.gov/pmc/articles/PMC6367829/pdf/13014_2019_Article_1231.pdf.

[62] J. H. Phua and K. W. Ang, "Interplay effect in lung cancer proton therapy," *Journal of Xiangya Medicine*, vol. 3, pp. 43–43, Dec. 2018. DOI: 10.21037/jxym.2018.11.04.

[64] S. Spautz, A. Jakobi, A. Meijers, *et al.*, "Experimental validation of 4d log file-based proton dose reconstruction for interplay assessment considering amplitude-sorted 4dcts," *Medical Physics*, vol. 49, no. 6, pp. 3538–3549, Jun. 2022. DOI: 10.1002/mp.15625. [Online]. Available: https://pubmed.ncbi.nlm.nih.gov/35342943/.

[65] P. Munck af Rosenschöld, M. C. Aznar, D. E. Nygaard, *et al.*, "A treatment planning study of the potential of geometrical tracking for intensity modulated proton therapy of lung cancer," *Acta Oncologica (Stockholm, Sweden)*, vol. 49, no. 7, pp. 1141–1148, Oct. 2010. DOI: 10.3109/0284186X.2010.500620. [Online]. Available: https://pubmed.ncbi.nlm.nih.gov/20831506/.

[68] A. A. Loginova, D. A. Tovmasian, D. A. Kokoncev, S. M. Varzar, and A. P. Chernyaev, "Studying the angular sensitivity of the matrixx detector array for the dosimetric verification of treatment plans with intensity modulation," vol. 76, no. 5, pp. 384–391, Sep. 2021. DOI: https://doi.org/10.3103/s0027134921050118.

[69] H. Li, L. Dong, L. Zhang, J. N. Yang, M. T. Gillin, and X. R. Zhu, "Toward a better understanding of the gamma index: Investigation of parameters with a surface-based distance methoda)," *Medical Physics*, vol. 38, no. 12, pp. 6730–6741, Nov. 2011. DOI: https://doi.org/10.1118/1.3659707.

[70] the BMJ, *11. correlation and regression — the bmj*, https://www.bmj.com/about-bmj/resources-readers/publications/statistics-square-one/11-correlation-and-regression, 2019.

[71] A. Jakobi, R. Perrin, A. Knopf, and C. Richter, "Feasibility of proton pencil beam scanning treatment of free-breathing lung cancer patients," *Acta Oncologica (Stockholm, Sweden)*, vol. 57, no. 2, pp. 203–210, Feb. 2018. DOI: 10.1080/0284186X.2017.1355107. [Online]. Available: https://pubmed.ncbi.nlm.nih.gov/28760089/.

[72] A. Schatti, M. Zakova, D. Meer, and A. J. Lomax, "The effectiveness of combined gating and re-scanning for treating mobile targets with proton spot scanning. an experimental and simulation-based investigation," *Physics in Medicine and Biology*, vol. 59, no. 14, pp. 3813–3828, Jun. 2014. DOI: 10.1088/0031-9155/59/14/3813.

[73] K. M. Kraus, E. Heath, and U. Oelfke, "Dosimetric consequences of tumour motion due to respiration for a scanned proton beam," *Physics in Medicine and Biology*, vol. 56, no. 20, pp. 6563–6581, Sep. 2011. DOI: 10.1088/0031-9155/56/20/003.

[74] S. Ulrich, W. Cao, R. Mohan, and M. Bangert, "Impact of respiratory motion on variable relative biological effectiveness in 4d-dose distributions of proton therapy," *Acta Oncologica*, vol. 56, no. 11, pp. 1420–1427, Aug. 2017. DOI: 10.1080/0284186x.2017.1354131.

# HollandPTC internal documents (unpublished)


[24] S. Hutschemaekers and tumorwerkgroep mediastinale lymfomen, *Behandelrichtlijn voor protonentherapie hodgkin lymfoom*, Jan. 2022.

[35] P. van Beers, *Gantry - protocol patient qa*, K. Spruijt and M. Hoogeman, Eds., May 2022.

[41] M. Kroesen, *Hollandptc behandelrichtlijn voor protonentherapie longcarcinoom (holland ptc internal document)*, May 2022.

[48] J. Paramasamy, *Master thesis: impact of variations in patient and beam parameters of proton therapy using PBS*. Jun. 2022, Available at https://repository.tudelft.nl/islandora/object/uuid:f2539d85-dd78-4ff3-a95a-eb1776906357.

[57] R. de Jong, *Improving interplay robustness*, K. Spruijt and M. Hoogeman, Eds. Nov. 2020.

[58] A. Ibrahimi, *The Interplay Effect*, K. Spruijt and M. Hoogeman, Eds. 2020, Available at https://repository.tudelft.nl/islandora/object/uuid%3A34e200d1-f744-4685-b4d0-2cfa2efce158.

[60] P. van Beers, K. Spruijt, and K. de Nijs, *Gantry - protocol patiënt qa*, May 2022.

[63] J. Jacobs, *Werkinstructie dosisplanning repainting (internal document)*, K. Spruijt and A. L. Wolf, Eds., Sep. 2022.

[66] K. Spruijt and Y. Wang, *Manual matrixx interplay simulations*, Feb. 2023.

[67] E. van Weerd, J. Jacobs, and P. Cambria Lopes, *Werkinstructie dosisplanning oesophagus (Holland PTC internal document)*. Holland PTC, Sep. 2022.

[75] E. Van Weerd and J. Jacobs, *Dpl werkinstructie dosisplanning long*, Aug. 2022.